Development and Characterization of Nano-Hydroxyapatite - Collagen - Chitosan Scaffolds for Bone Regeneration

D i s s e r t a t i o n

zur Erlangung des akademischen Grades

Doctor rerum naturalium (Dr. rer. nat.)

vorgelegt der

Naturwissenschaftlichen Fakultät I
Biowissenschaften

der Martin-Luther-Universität Halle-Wittenberg

von

Herrn Hagen Nitzsche

geb. am 28.09.1980 in Bautzen

Gutachter /in

1. Professor Dr. rer. nat. habil. Karsten Mäder
2. Professor Dr. rer. nat. habil. Thomas Groth
3. Professor Dr. rer. nat. habil. Michaela Schulz-Siegmund

Halle (Saale), 13.07.2010 (Tag der öffentlichen Verteidigung)

„Die Wissenschaft schreitet schnell voran, weil man das Wissen früherer Wissenschaftler benutzen kann. Unsere menschliche Qualität jedoch können wir von niemandem übernehmen und deshalb entwickelt sich der Mensch nicht. Das schafft die beunruhigende Situation von kleinen Kindern, die mit tödlichen Waffen spielen.“ (Kodo Sawaki)

TABLE OF CONTENTS

LIST OF ABBREVIATIONS AND SYMBOLS V

PART I – GENERAL INTRODUCTION AND CRITERIA REGARDING THE SOURCE MATERIALS 1

Chapter 1 – General introduction 1

1.1 Tissue Engineering 1

1.2 Fundamentals about bone structure and regeneration 2

1.3 Theoretical considerations about the source materials 8

1.4 Keynotes on scaffolds properties and analytical challenges 11

1.5 Thesis objectives 13

1.6 Frequently & generally applied materials and methods 14

Chapter 2 – Characterization of source materials and preparation of a biomimetic composite material 16

2.1 Introduction 16

2.2 Materials and Methods 17

2.2.1 Zeta potential measurements of the polyelectrolyte interaction between collagen and chitosan 17

2.2.2 Preparation of a biomimetic hydroxyapatite-collagen composite material 18

2.2.3 X-ray diffraction (XRD) 19

2.2.4 Thermogravimetry (TGA) 19

2.3 Results and Discussion 20

2.3.1 Zeta potential measurements of the polyelectrolyte interaction between collagen and chitosan 20

2.3.2 Preparation of a biomimetic hydroxyapatite-collagen composite material 23

2.3.3 X-ray diffraction (XRD) 26

2.3.4 Thermogravimetry (TGA) 26

2.4 Conclusion and Outlook 29

PART II – SCAFFOLD FABRICATION 30

Chapter 3 – Fabrication of cylindrical scaffolds composed of hydroxyapatite, collagen and chitosan 30

3.1 Introduction 30

3.2 Materials and Methods 31

3.2.1 Fabrication of cylindrical hydroxyapatite-collagen-chitosan scaffolds 31
3.2.2 Hydroxyapatite-collagen-chitosan scaffolds with enzymatical crosslinked collagen 32

3.3 Results and Discussion 33

3.3.1 Fabrication of cylindrical hydroxyapatite-collagen-chitosan scaffolds 33
3.3.2 Hydroxyapatite-collagen-chitosan scaffolds with enzymatical crosslinked collagen 37

3.4 Conclusion and Outlook 39

Chapter 4 – Alternative approaches towards scaffold fabrication 40

4.1 Introduction 40

4.2 Materials and Methods 41

4.2.1 Coating of polyglycolic acid meshes 41
4.2.2 Preliminary experiments for scaffold fabrication with the GeSiM Nano-Plotter™ 42

4.3 Results and Discussion 45

4.3.1 Coating of polyglycolic acid meshes 45
4.3.2 Preliminary experiments for scaffold fabrication with the GeSiM Nano-Plotter™ 46

4.4 Conclusion and Outlook 49

PART III – SCAFFOLD CHARACTERIZATION 50

Chapter 5 – Characterization of the size of the mineral constituent inside the scaffolds 50

5.1 Introduction 50

5.2 Materials and Methods 51

5.2.1 Fabrication of blank samples 51
5.2.2 Small angle x-ray scattering (SAXS) 51
5.2.3 Transmission electron microscopy (TEM) 52
5.2.4 Environmental scanning electron microscopy (ESEM) 52
5.2.5 Atomic force microscopy (AFM) 53
5.2.6 MR Imaging of the distribution of the hydroxyapatite 53

5.3 Results and Discussion 53

5.3.1 Small angle x-ray scattering (SAXS) 53
5.3.2 Transmission electron microscopy (TEM) 56
5.3.3 Environmental scanning electron microscopy (ESEM) 57
5.3.4 Atomic force microscopy (AFM) 59
5.3.5 MR Imaging of the distribution of the hydroxyapatite 59

5.4 Conclusion and Outlook 61

Chapter 6 – Characterization of physical scaffold properties 63

6.1 Introduction 63

6.2 Materials and Methods 64

6.2.1 Mechanical testing 64
6.2.2 Mercury intrusion porosimetry 66
6.2.3 Environmental scanning electron microscopy (ESEM) 67
6.2.4 Mass transport measurements by MRI 67

6.3 Results and Discussion 70

6.3.1 Mechanical testing 70
6.3.2 Mercury intrusion porosimetry 76
6.3.3 Environmental scanning electron microscopy (ESEM) 77
6.3.4 Mass transport measurements by MRI 78

6.4 Conclusion and Outlook 85

PART IV – IN VITRO EXPERIMENTS OF SCAFFOLDS COLONIZED WITH CELLS 87

Chapter 7 – Cells cultured on cylindrical hydroxyapatite-collagen-chitosan scaffolds 87

7.1 Introduction 87

7.2 Materials and Methods 88

7.2.1 Culture of MG63 cells 88
7.2.2 Labeling of MG63 cells with superparamagnetic iron oxide nanoparticles 88
7.2.3 Colonization of the cylindrical hydroxyapatite-collagen-chitosan scaffolds with MG63 cells 88
7.2.4 Staining, light microscopy and histology 89
7.2.5 Transmission electron microscopy (TEM) 89
7.2.6 Confocal laser scanning microscopy (CLSM) 90
7.2.7 Magnetic resonance imaging (MRI) 90

7.3 Results and Discussion 91

7.3.1 Labeling of MG63 cells with superparamagnetic iron oxide nanoparticles and evaluation of the labeling efficiency 91
7.3.2 Evaluation of the colonization of the cylindrical hydroxy-apatite-collagen-chitosan scaffolds with MG63 cells 93

7.4 Conclusion and Outlook 97

Chapter 8 – Cells cultured on the coated polyglycolic acid meshes 99

8.1 Introduction 99

8.2 Materials and Methods 100

8.2.1 Cell compatibility evaluation with primary chondrocytes and osteoblasts 100
8.2.2 Histological staining 101
8.3 Results and Discussion 101
8.3.1 Cell compatibility evaluation with primary chondrocytes and osteoblasts 101
8.3.2 Histological staining 104
8.4 Conclusion and Outlook 106

PART V – SUMMARY 108

Chapter 9 – Summary 108
9.1 English version 108
9.2 German version 111

LITERATURE 115

APPENDIX VI

ACKNOWLEDGEMENT VII

PUBLICATIONS IX

CURRICULUM VITAE XI

EPILOGUE XII

SELBSTÄNDIGKEITSERKLÄRUNG XV

LIST OF ABBREVIATIONS AND SYMBOLS

AFM	Atomic force microscopy
BSE	Back scattering electron
DHT	Dehydrothermal treatment
ESEM	Environmental scanning electron microscopy
GAG	Glucosaminoglycans
HA	Hydroxyapatite
HES	Hydroxyethyl starch
I	Intensity
IEP	Isoelectric point
PGA	Polyglycolic acid
PLGA	Poly (lactic-co-glycolic acid)
q	Scattering vector
R_g	Radius of gyration
SAXS	Small angle X-ray scattering
SPIO´s	Superparamagnetic iron oxide nanoparticles
TG	Transglutaminase
TGA	Thermogravimetry
WST	Water soluble tetrazolium
XRD	X-ray diffraction

PART I – GENERAL INTRODUCTION AND CRITERIA REGARDING THE SOURCE MATERIALS

Chapter 1 – General introduction

1.1 Tissue Engineering

A forward-looking and sustainable tendency in the treatment of medical conditions is the elimination of the cause of the disease. This is not a new approach at all. One famous example, which had an enormous impact on the success of medical treatments, was the discovery of antibiotics and their use for the cure of infections. To a high extent such developments are the fruit of discoveries in science. The incessant progression in the understanding of the basic building blocks of life and the mechanisms of vital functions even down till an atomic resolution opens the door for numerous advancements. What might have begun with the substitution of regulating molecules like for example insulin, proceeds with the application of cells or tissues secreting those molecules and ends up with the replacement of whole organs. This is exactly the point where tissue engineering joined. As interdisciplinary medical and scientific subject, it is aimed to generate therapies more close to the natural paradigm, avoiding the traditional replacement approaches. By C.T. Laurencin, tissue engineering is defined as "the application of biological, chemical, and engineering principles toward the repair, restoration, or regeneration of living tissues using biomaterials, cells, and factors alone or in combination" [1]. It is widely accepted that the fundamental idea emerged during a conversation between J. Vacanti and R. Langer in the mid-1980s, which are accordingly considered as the founding fathers of tissue engineering [2]. Their basic concept is still the fundament of most approaches in this area. It is comprised of specific cells, a matrix as carrier for the cells, often referred to as scaffold, and bioactive substances to stimulate a desired development [3].

Although tissue engineering is often reported to be still in its infancy, there are several examples for the success of clinical trials to the point of products already established in the medical practice [2]. One example related to the topic of this work is InductOs® (Wyeth). It is merchandised as a medical device for the treatment of

intervertebral disc degeneration and acute tibia fractures. It consists of a collagen sponge, a powder mixture and water for injection. Beside several pharmaceutical excipients, the powder mixture contains bone morphogenetic protein 2. This growth factor attracts undifferentiated cells to migrate into the defect site and to differentiate into bone forming cells. A second related example is Bioseed®-OralBone (Biotissue technologies, Freiburg, Germany). Salgado et al. even called it the first commercialized tissue-engineered bone graft. It comprises of cells taken from the patient, proliferated in autologous serum and seeded on a three-dimensional biodegradable matrix. The prefabricated constructs have already been implanted in the defect sites of human jaw-bones and yield successful tissue regeneration [4].

1.2 Fundamentals about bone structure and regeneration

Composition and structure of natural bone

The fundamental relevance of bone for the human existence was comprehensively and tellingly expressed by A. L. Boskey as follows: “Bone protects the internal organs of the body, facilitates locomotion and mechanical functions, and serves as a source of calcium and magnesium ions for mineral homeostasis” [5]. To cope with all this functions bone possesses a highly organized structure in several scales of magnitude. As there is a huge amount of details known about the structure of bone, just a short review is given in the introduction of the present work. From the chemist’s point of view, bone is a composite material made up of an organic constituent, mainly the protein collagen and an inorganic counterpart, mainly the calcium phosphate hydroxyapatite. Like in other tissues, several triple helical collagen molecules are associated to form fibrils. Hydroxyapatite crystallites are located within small gaps between the collagen molecules (Fig. 1.1) [6-9]. Independent which of the different types of bone is considered, at this nanoscale size range they have similar structure. From the perspective of a biologist, three cell types are primarily important for the maintenance of vital bone, the osteoblasts, the osteoclasts and the osteocytes (Fig. 1.2). Osteoblasts deposit a stable matrix that is able to mineralize. Subsequently they often remain inside and mature to osteocytes whose main functions are the regulation of the blood-calcium level and the functional adaptation of bones [10,11]. The osteoclasts are multinucleated cells able to degrade the mineralized bone matrix. By attachment to the bone surface, they generate a local acidic microenvironment for the dissolution of the mineral phase. Additionally, they secrete

proteolytic enzymes into the resorption lacunae for the degradation of the extracellular matrix (Fig. 1.1). Subsequently, the emerged void is mostly filled with new bone matrix by osteoblasts. In healthy bone, there is a complex interplay between the different cell types to assure a permanent progression of the remodelling and modulation of the bone constitution as response to the occurring stress and impact force to meet the requirements of daily life [10,12].

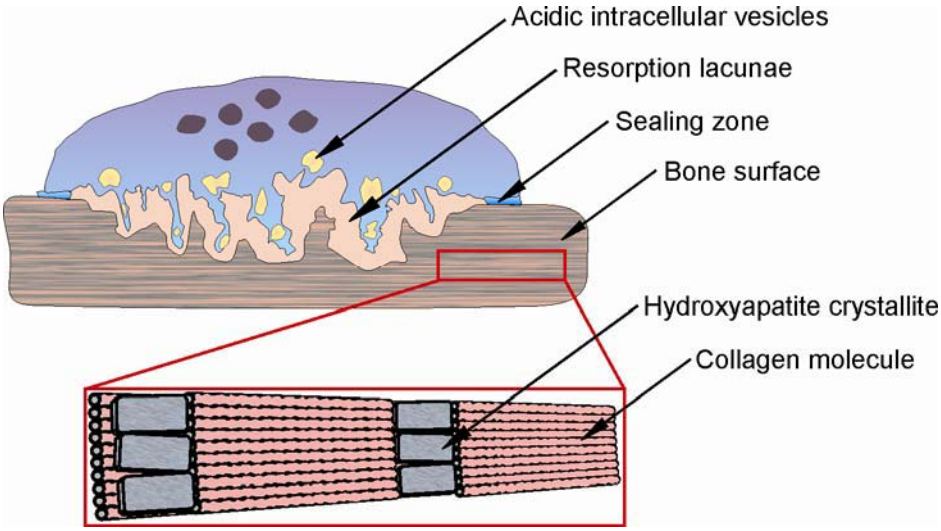

Fig. 1.1 Schematic drawing of an osteoclast on the bone surface (top), and of the bone structure at the nanoscale (bottom)

At the macroscopic range two types of bone are distinguished. In general, it is the morphological appearance that makes the differentiation very easy, but an accurate classification can only be realized by microscopy methods. Cancellous bone possesses a porous, sponge like structure and cortical bone is a more dense material mainly found at the shaft of long bones [13]. On the microstructural level the matrix of cancellous bone exhibits an interconnecting framework structure, where the single connections are called trabecula. In contrast, cortical bone possesses different forms of appearance. During growth or injury healing, the fast deposited and less organized type evolves first. It is called woven bone. Due to the more randomly oriented disposition of the mineralized matrix it is the weaker form [11]. Subsequently, main parts are replaced by the more structured and stronger lamellar bone. In this type, the mineralized collagen fibrils, associated in fibres, are densely packed in planar arrangements, called lamellae. They are concentric wrapped around a blood vessel carrying hole, the haversian channel. Adjacent lamellae are aligned in a way that their collagen fibres run perpendicular towards each other.

Osteocytes are embedded in between those layers, which together build up one osteon. Intermediate blood vessels generate a three-dimensional network by connecting different haversian channels. The osteons are placed in parallel to the long dimension of the bone [11,13]. The outer surface of most bones is covered by a membrane, called periosteum, whereas the inner surface is separated from the bone marrow by the endosteum.

The entirety of the various levels of the bone structure ranging from the single mineralized collagen fibril over lamellae, osteons, trabelulae to cortical and cancellous bone as well as the biologic ability of adaptation account for the outstanding properties of this unique material.

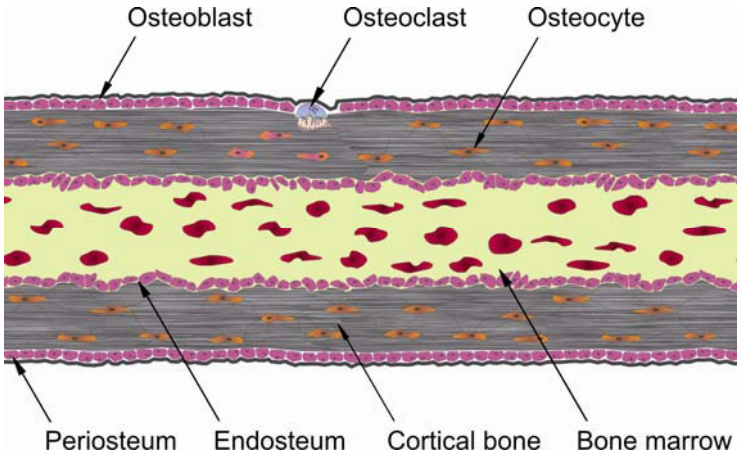

Fig. 1.2 Schematic drawing of bone at the microscopic level

Bone regeneration

The general ability of natural bone defect repair as well as the way of its progression is strongly dependent on the size and the extent of the failure. In this regard, the integrity of the periosteum plays a key role. It is composed of fibroblasts and progenitor cells. The second account for the regeneration capacity of the bone. They are also called mesenchymal cambial layer cells and possess the ability to differentiate into other cell types [14].

If a bone defect occurs and the periosteum remains intact, there is usually a high capacity for self-healing. After the inflammatory phase, the progenitor cells differentiate into osteoblastic cells. Woven bone develops, which is subsequently remodelled into compact bone. This process is called intramembraneous ossification. It is an integral part of skeletogenesis but also takes place in the reparation of small defects with intact periosteum and sufficient blood supply [15-17].

If the periosteum is damaged, another self-healing mechanism takes place, called endochondral ossification. For the explanation of the complex mechanisms it is classified into four stages, a. the inflammatory phase, b. the reparative phase one, c. the reparative phase two and d. the remodelling phase. In the following a short review will be given about the different stages. A schematic illustration of each phase is shown in figure 1.3.

a. Early fracture and the inflammatory phase

Directly after the tissue injury, a blood clot is formed to close the wound. Macrophages and osteoclasts degrade and remove the debris. Cells of the immune system enter the location and a granuloma tissue is formed offering structural support. In the meantime various signalling molecules are released from the different cells as well as from the disintegrated extracellular matrix, aimed to initiate the further progression. Additionally, the vascularization of the new tissue begins enabling nutrition and further cell invasion [18].

b. Reparative phase one – soft callus formation

The progenitor cells differentiate into chondrocytes and build up a cartilaginous matrix mainly composed of collagen type II but also containing a lot of other functional non-collagenous proteins. Finally, the chondrocytes exit their cell cycle, become hypertrophic and change the pattern of protein expression [16,18].

c. Reparative phase two – hard callus formation

As the onset of bone development the cartilage template starts to mineralize. At this step, the chondrocytes induce further vascularization, because the development and maintenance of a bony tissue requires higher oxygen levels than cartilage. Osteoblasts and osteoclasts enter the hard callus region through the blood vessels [15,18,19]. Additional to the mechanical support, the cartilage template serves as space holder to prevent the encroachment of fibroblasts. A sufficient osteoblast to fibroblast ratio is important to prevent the penetration of soft tissue [7,20,21].

d. Remodelling phase

In this stage the mineralized cartilage is replaced by the more organized bony structure. During the osteoclastic degradation of the unorganized matrix, noncollagenous signalling proteins are released. Those stimulate osteoblasts to

secrete a new mineralizing extracellular matrix mainly composed of collagen type I [16,18].

The described self-healing processes are limited to a certain size. If the so called critical size is exceeded, human bone is not able to regenerate spontaneously [22].
Implantation and transplantation technologies have lead to an enormous improvement in the medical treatment of such bone failures. Although mainly used, the grafting procedures have different drawbacks [23]. This resulted in the development of alternative approaches like the two examples given in part 1.1 and in the sequel of this work.
Furthermore, the four frequently used terms osteoconduction, osteoinduction, osseointegration and osteogenicity have to be defined.
Osteoconduction is the ability to serve as a barrier to prevent the penetration of foreign tissue into the defect site. Often additional properties like the favouring of cell attachment, proliferation and migration in the structure and the capacity for mass transfer and vascularisation are factored into this term as well [1,12,20,24].
Osteoinduction is the stimulation of mesenchymal stem cells or other osteoprogenitor cells to differentiate towards the osteoblast lineage. Often, it is directly related to the application of growth factors, but in general, osteoinduction describes the effect of various bioactive molecules to stimulate cell migration and osteogenesis [1,12,20,24].
A material is referred to as osteogenic when it supports osteoblasts in producing mineral for the calcification of a collagenous matrix [1].
The term osseointegration is used for an implant which is tolerated inside the body and which is incorporated into the tissue with direct microscopic contact to the living bone [1,12].

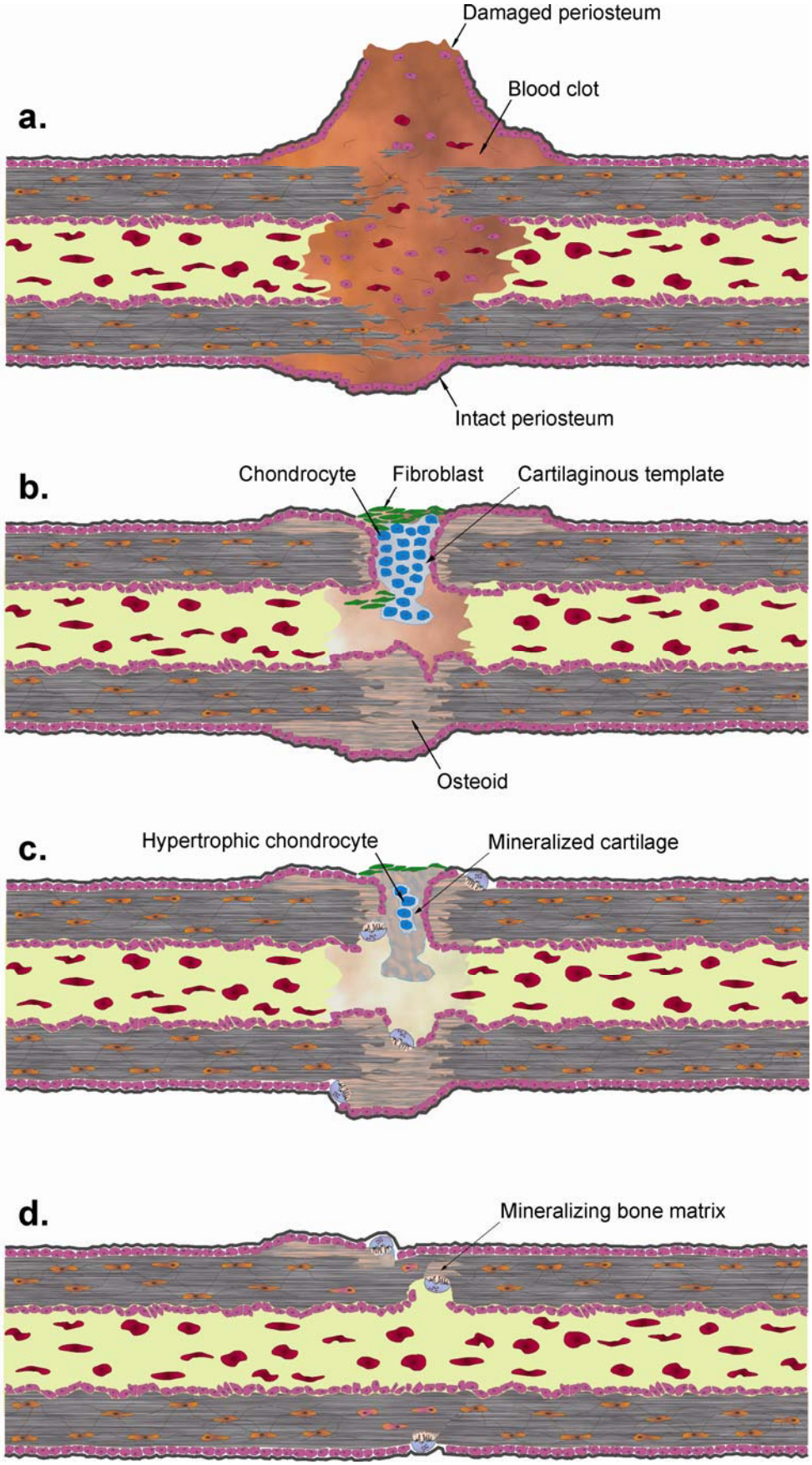

Fig. 1.3 Schematic drawings of the different stages of natural bone healing, Inflammatory phase (a), reparative phase one (b), reparative phase two (c) and remodelling phase (d)

1.3 Theoretical considerations about the source materials

The implantation of biodegradable scaffolds is a common strategy for bone reconstruction. For the development of a suitable construct, particular attention should be drawn to the choice of the used source materials. A comprehensive knowledge about their properties is essential for the systematic engineering of products with those intended applications. Commonly used scaffold materials for bone and cartilage regeneration are (1) poly(α-hydroxy acids), (2) collagen and (3) calcium phosphates, mainly hydroxyapatite. The single use of each of them has shown to yield undesirable properties. Additionally, (4) chitosan is attracting more and more interest in the biomedical field.

This part of the general introduction is aimed to shortly review the mentioned materials for their potential to contribute as component of a biodegradable scaffold for bone tissue engineering.

(1) Poly(α-hydroxy acids)

Poly(α-hydroxy acids) like polyglycolic acid (PGA), polylactic acid (PLA) and the copolymer of both (PLGA) are preferentially applied due to their mechanical properties. Additionally, modifications of composition and molecular weight facilitate some control over the velocity of the polymer degradation [1,25]. Furthermore, scaffold matrices composed of Poly(α-hydroxy acids) can retain embedded growth factors and thereby serve as a controlled drug delivery system to stimulate osteogenesis [25]. Thus, the important goal that the extent of new bone formation will be simultaneously accompanied by the biodegradation of the scaffold appears to be feasible. The main drawback of the Poly(α-hydroxy acids) is related to the formation of acidic degradation products, because a reduced local pH-value accelerates the polymer degradation rate and induces local inflammation [23,26-28]. A second disadvantage is the hydrophobic surface of such constructs which is not favourable for cell attachment, complicating cell seeding procedures [6,29].

In consequence, one concern of the present study was to develop innovative fabrication technologies to reduce or avoid poly(α-hydroxy acids) inside the resulting scaffolds or to modify existing constructs composed of PGA to attenuate the mentioned drawbacks.

(2) Collagen

Collagen, one main constituent of human cartilage and bones, is an already established material for implantable scaffolds in clinical use. It is well known for some favourable properties regarding bone tissue engineering, like excellent biocompatibility and biodegradability and, due to the amino-acid sequence Arg-Gly-Asp (RGD sequence), the facilitation of cell attachment and enhancement of the differentiation and proliferation of osteoblasts [12,22,27,30]. Furthermore, it is known to possess osteoconductive properties [31]. However, after the application, collagen sponges are fast decomposed or degraded and have insufficient mechanical stability [32]. These disadvantages are improvable by different crosslinking methods, but residues of chemical crosslinkers in the material can reduce the biocompatibility of the implant [9,27]. A second mentioned constraint is the tendency towards denaturation and consequently extensive limitations of the feasible processing parameters to ensure the integrity of the protein [31,33]. But a denaturation is not necessarily disadvantageous. In contrast, it was shown to enhance RGD-dependent cell adhesion and is suggested to provide a signalling effect on distinct cells, what could stimulate the tissue regeneration [34]. In the present study several fabrication conditions are considered to alter the structure or lead to an entire or partly denaturation of the collagen. Whether intact or altered the protein component inside the fabricated constructs is continuously designated as collagen regarding to its origin.

As implication for the present study collagen is contained in all the developed formulations because of its essential properties. The combination with other components (chitosan and poly(α-hydroxy acids)) and the application of non-chemical crosslinking techniques (dehydrothermal treatment and enzymatic crosslinking) were used to improve the constructs towards more resistance against degradation and bearing load.

(3) Hydroxyapatite

The inorganic component of vertebrate bone is often referred to as hydroxyapatite. But there is a distinct difference between bone mineralites and pure geologic hydroxyapatite, which has the chemical formula $Ca_{10}(PO_4)_6(OH)_2$. Due to the inclusion and/or surface adsorption of trace ions like e.g. carbonate, fluoride, chloride, magnesium, sodium or potassium, the inorganic constituent of most

mineralized hard tissues is an impure analogue of hydroxyapatite [5,9,12,13,35,36]. Nevertheless, in the present work no distinction is made. Irrespective of the purity, the inorganic component is designated as hydroxyapatite.
By weight, it is the main component of human bone and a biocompatible material known for its ability to enhance osteoblast proliferation and differentiation [27,29,36]. In addition, it is known to be osteoconductive [37-39]. Monolithic hydroxyapatite implants in the form of dense or porous blocks provide strong mechanical properties, but their application is disputed due to the limitations of their biodegradability [8]. Even particles of large magnitude are supposed to cause increased inflammatory response [27]. A grain size on the nanometer-level was shown to be important especially for the homogeneous resorption by osteoclasts [7,9,35,36,40]. Several techniques, often divided in solid state methods and wet chemical methods, were reported for the fabrication of nanometer-sized hydroxyapatite [27,29].

In consequence, one goal of the present study was to fabricate a composite material containing nanometer-sized hydroxyapatite and incorporate it into a porous polymeric construct of sufficient mechanical stability.

(4) Chitosan

Chitosan is a biocompatible and biodegradable polymer. Especially due to the wide availability of chitin, the raw material for its production, it is attracting more and more interest in the biomaterials field [12,41-43]. For mimicking or supporting the natural healing process of bone lesions, chitosan appears to be well suited [8,41]. In endochondral bone formation, a cartilaginous matrix is filling the defect volume before the remodelling into bone takes place [16]. Hence, it is not only the osteogenic-, the osteoconductive- or the osteoinducing property, but also the chemical alikeness to some cartilage-specific glucosaminoglycans (GAGs) which makes chitosan an ideal polymer for bone tissue engineering [6,8,41,42]. Furthermore, it has haemostatic and antimicrobial features, two considerable advantages for the implantation into damaged tissue [42]. Chitosan is also described to have inhibitory effect on fibroblasts while stimulating osteoblast activity [6]. This property makes it convenient to prevent the encroachment of surrounding tissues into the defect site, because fibroblasts might be the first cells filling large bone or cartilage defects, what is supposed to constrain osteogenesis [20,44]. In addition, the polycationic nature facilitates cell adhesion and electrostatic interactions with anionic

compounds like GAGs or several proteins [42]. Of particular interest for the present study is the interaction with collagen leading to a complex formation. It is supposed to increase the mechanical strength and to hinder the enzymatic degradation of collagen scaffolds [25,45]. Furthermore, the extent of chitosan biodegradation can be regulated by the use of material differing in the degree of deacetylation and molecular weight [42,46].

Because of these favourable properties, the corollary for the present study was to employ chitosan in almost all the formulations.

1.4 Keynotes on scaffold properties and analytical challenges

In the first instance, the scaffold serves as space-holder to prevent the encroachment of surrounding, non osseous tissues. To be suitable beyond, such a matrix has to be sterile, biocompatible, porous and also biodegradable to not restrict the remodelling of the natural bone [20]. Appropriate to the defect site, tailored mechanical properties and degradation rates should exactly come along with the kinetics of new tissue formation. Most of the mentioned properties are subject-matter of the following chapters of this work and will be discussed in detail.

A combination of scaffolds with growth factors as well as with osteoblastic precursor cells is often used to support the remodelling process of these three-dimensional matrices into bone tissue [14,20]. The scaffolds used in most experimental approaches are of small volume. This is disadvantageous but has a cogent reason. In healthy bone tissue, the distance between blood capillaries and cells is never exceeding 200 µm [20]. This circumstance has to be considered for scaffold implantation to prevent cells from deficiencies in oxygen and nutrient supply as well as from problems in metabolite removal. Advantages enhancing the mass transport are achieved by means of scaffolds with large interconnected pores and attempts of prevascularisation [28,47]. As already mentioned before, bone reconstruction is in first place necessary above a critical defect size. Hence, it is obvious that functioning large sized scaffold systems are required.

Further systematic development necessitates advanced analytical tools, especially imaging modalities suitable for monitoring processes inside the scaffolds in vitro and in vivo. The conventional method for characterization of the constructs is histology. The main drawback of this method is the destruction of the sample, precluding further

proceeding of the experiment with the same sample [48-51]. Alternatively, some noninvasive optical imaging techniques are providing continuous analytics of one sample. The fate of cells seeded on scaffolds can be monitored by fluorescent dyes penetrating into the matrix [52]. But with increasing size of the constructs, the analysis of processes inside becomes more complicated. Due to interference with autofluorescence and its limited penetration depth, the use of fluorescence techniques is restricted to small or thin samples, especially for optically opaque scaffolds and in vivo experiments [48,53]. Single-photon emission computed tomography and positron emission tomography are noninvasive and have high penetration depth, but both use radioactive labels, which can affect living cells adversely [54]. Magnetic resonance imaging (MRI) possesses none of the three discussed drawbacks and represents an already established technique in clinical diagnostics. Recent publications show progress in the field of regenerative medicine using MRI. The studies are predominantly about cell tracking experiments and monitor the fate of transplanted stem cells in vivo [55-60]. Only a few can be found which deal with the characterization of scaffolds. For example, approaches for the determination of the porosity of biodegradable matrices were reported [61,62]. Peptan et al. showed that the osteogenic differentiation of bone marrow stromal cells on scaffolds is evaluable by MRI [49]. The mineral deposition in scaffolds associated with bone formation was examined using magnetic resonance microscopy [48,51]. In vivo experiments analyzing an implanted demineralised bone matrix were carried out by Hartman et al. [63]. Fluid transport measured by MR flow imaging was performed by the group of Bechtold [62,64]. Several groups have investigated important properties of constructs for cartilage repair, for example the content of negatively charged glucosaminoglycans, the perfusion or alterations resulting from mechanical stress [50,65,66]. Cell tracking experiments on collagen scaffolds were reported by Terrovitis et al. [67].

All these studies are carried out by standard or high resolution MRI or by magnetic resonance microscopy with field strengths ranging from 1.5 to 11.7 T using super-conducting magnets [48-51,55,57,61-68].

Apparently, the method has still not reached the state to be used as standard laboratory practice equipment, especially for in vitro experiments. The reasons are mainly high investment and maintenance costs of superconducting MRI devices and

very strong gradients for sufficient spatial resolution or the need of special designed coils for the excitation and detection of small samples [63].

The recently developed benchtop-MRI (BT-MRI) equipment is much more affordable due to a low static magnetic field strength of 0.5 T, a small pole shoe gap of 30 mm, a small gradient coil gap and therefore a high gradient strength ensuring a spatial in plane resolution better than 0.35 mm and the absence of a helium cooling system (Fig 1.4) [69,70].

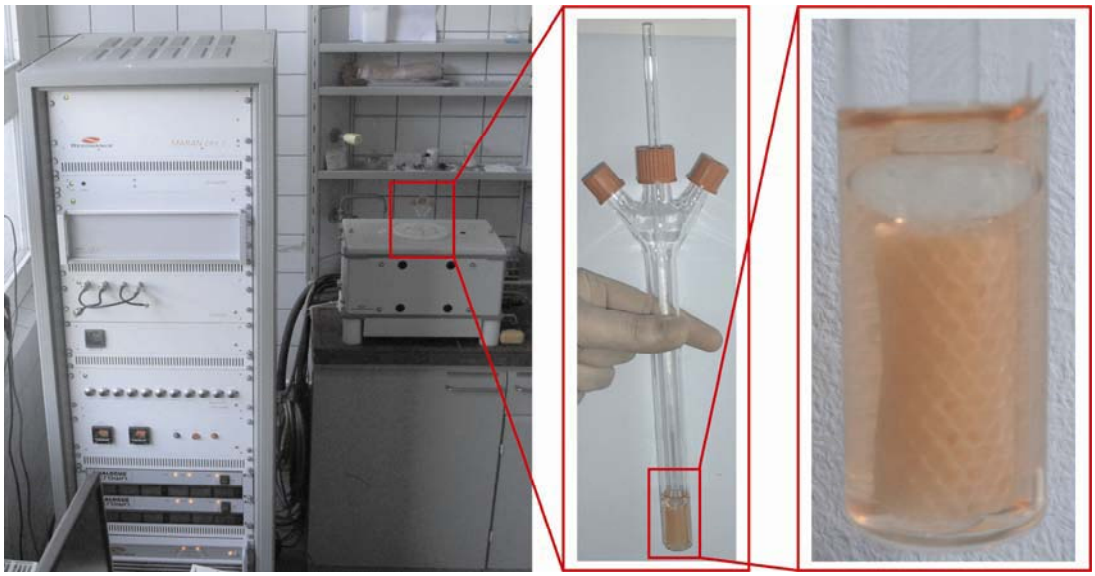

Fig. 1.4 Photograph of the benchtop NMR spectrometer MARAN DRX2 and enlarged the colonized scaffold fixed in the test tube for MR imaging

1.5 Thesis objectives

This thesis is aimed at two main objectives,

(1) The development and characterization of biocompatible, high porous, biodegradable and mechanical stable scaffolds for bone tissue engineering. A special composition was chosen in order to mimic the matrix which is build up during the natural self-healing process of small bone lesions. Therefore, most of the constructs contain nano-hydroxyapatite, collagen and chitosan. Particular attention was paid to the particle size and the polymeric embedding of the nano-hydroxyapatite. Additionally, different approaches were made for improvements of the mechanical scaffold properties.

and

(2) The establishment of the new method of benchtop MRI towards a noninvasive analytical assessment of scaffolds for tissue engineering constructs. For that reason,

three suitable applications have been evaluated. First, the hydroxyapatite distribution inside a scaffold was imaged. Second, information on the velocity of mass transfer between the matrix and the surrounding medium was obtained. And third, the location of iron labeled cells seeded and cultured on the scaffold was investigated. The experiments for the third application were partly combined with the following first steps of a biocompatibility evaluation.
To achieve those objectives, a tight operating schedule had to be kept. Therefore, at the beginning of the work, the complete attention was focussed on the practical realization of the scaffold fabrication strategy. Two exceptions were made in order to analyze properties of the source materials. The zeta potential of collagen, chitosan and blends of both were measured and the hydroxyapatite-collagen composite material was analyzed for its composition by TGA.

1.6 Frequently & generally applied materials and methods

All chemicals used were at least reagent grade and purchased from Sigma (Taufkirchen, Germany) or Roth (Karlsruhe, Germany) unless otherwise stated. The water mentioned in the descriptions of experiments always refers to purified water. Frequently applied materials and methods are listed below.

List of frequently applied materials

Chitosan
(ChitoClear™ FG95 TM1369, Primex ehf, Iceland), white or slight yellowish powder

Collagen dispersion
(Lohmann & Rauscher GmbH & Co. KG, Germany), aqueous dispersion containing 1 % of equine collagen type I and 0.5 % of hydrogen peroxide

Phosphate buffer, conserved
(0.13 M KH_2PO_4 and 0.54 M $Na_2HPO_4 \cdot 2H_2O$ and 0.017 M NaN_3 dissolved in water)

Polyglycolic acid meshes
(Safil®, B. Braun Melsungen AG, Germany),

- fine-meshed with a pore size of 0.75 mm, (ReNe FSM 000419 W1 PT-29)
- coarse-meshed with a pore size of 1.4 mm, (ReNe F 041103 W1 PT-200)

TRIS-buffer pH 8.0
(0.15 M NaCl, 0.025 M Tris(hydroxymethyl)-aminomethan, 0.001 M $CaCl_2$ dissolved in water, pH 8 was adjusted using 1 M HCl or NaOH solution)

List of frequently applied methods

Impinging light microscopy
Stereo microscope (Olympus SZX9, Olympus Deutschland GmbH, Germany)

Image analysis software
Analysis auto (Version 5.0, Olympus Deutschland GmbH, Germany)

Light microscopy
Light microscope (Olympus Highlight 3100, Olympus Deutschland GmbH, Germany)

Lyophilisation
Christ® Alpha 2-4 (Christ® LOC-1m) (Martin Christ Gefriertrocknungsanlagen GmbH, Germany) equipped with a chemistry-HYBRID™ pump RC5 (Vacuubrand GmbH & Co. KG, Germany)
Lyophilisation was performed for at least 10 hours. Inside the drying chamber a temperature of -30 °C and a pressure of (0.37 ± 0.10) mbar were set. The ice condenser was set to -80 °C.

Magnetic resonance imaging (MRI)
1H NMR imaging experiments were performed on the benchtop NMR spectrometer MARAN DRX2 (Oxford Instruments, GB) with an operating frequency of 20 MHz and static magnetic field strength (B_0) of 0.5 T. The scaffolds, incubated in different media, were fixed in a test tube with a sample holder (Fig. 1.4). For any incubation before and also during the experiments the samples were maintained at a temperature of (37.0 ± 0.5) °C. Three slices of 3 mm thickness were selected perpendicular to the main magnetic field. The recovery time (TR) was set to 300 ms and the echo time (TE) to 9.4 ms. Obtained images are composed of 128 × 128 pixels on a field of view (FOV) of 40 × 40 mm. For cell free experiments, the scaffolds were incubated in phosphate buffer pH 7.4 containing 0.1 % of sodium azide as a preservative.

Chapter 2 – Characterization of source materials and preparation of a biomimetic composite material

2.1 Introduction

The unique properties of natural bone are based on the highly structured constitution on several orders of magnitude, which are infeasible with current technologies. For example, the simple mixing of hydroxyapatite and collagen leads to products with very weak mechanical stability and problems arise from different biodegradation velocity of the two components [29,32,71]. Sophisticated fabrication techniques were shown to be able to combine hydroxyapatite and collagen with at least a nanostructure similar to bone [9,12,29,32,36,71,72]. One of the wet chemical methods, often called biomimetic approach has also been applied in the present study. The main principle is the precipitation of hydroxyapatite in alkaline aqueous medium in the presence of collagen, which is reported to result in nano-sized hydroxyapatite crystals [9,29,71-76]. Several authors suggest a process directing function of the organic matrix regulating not only size, but also shape and organization of the hydroxyapatite crystals [5,29,32,77]. The exact mechanism is still under debate [36]. It is suggested that carboxyl groups on the collagen surface promote calcium ion accumulation and serve as nucleation sites.

Therefore, and for several other reasons the zeta potential of materials used in tissue engineering is an important parameter to be characterized, what is summarized in the following subitems:

(1) Andrade et al. reported that the negative surface charge of collagen is important for the formation of hydroxyapatite on its surface [78]. For such polyampholytes this parameter relies strongly on the pH-value of the aqueous surroundings. Thus, in the present study the zeta potential was observed pH-value dependent to gain knowledge about the variability of the surface charge and to define the isoelectric point (IEP) of the utilized collagen.

(2) The stability of a composite scaffold against mechanical stress and degradation is substantially influenced by the bonding force between the different components [29]. The interaction of collagen with chitosan is caused by their charged character. Consequently, zeta potential measurements offer one analytical method for systematic optimization tasks.

(3) Additionally, surface properties like the zeta potential have strong impact on the interfacial reactions between the biomaterial and the surrounding tissue [79].

In the present study, two different experimental approaches were accomplished to study the pH-value dependent charge properties of collagen and chitosan and the interaction between both. All experiments were focused on the electrokinetic behaviour in an aqueous environment. Regarding the pure source materials, no further characterization was performed.

In the course of this work the fabricated hydroxyapatite-collagen composite is used as a source material, therefore the analytics about its qualitative and quantitative composition are described in this chapter. For this purpose, x-ray diffraction and thermogravimetry were used. The particle size of hydroxyapatite in the produced composite material was investigated thoroughly. The results are given in chapter 5.

2.2 Materials and Methods

2.2.1 Zeta potential measurements of the polyelectrolyte interaction between collagen and chitosan

The measurements were performed at 20 °C with a Zetasizer nano® (Malvern Instruments Ltd., UK). The measured electrophoretic mobility was converted into an apparent zeta potential using the Helmholtz-Smoluchowski equation [80]. The obtained relative values are sufficient for the discussion of tendencies but should not be taken as an absolute measure of the zeta potential.

pH-titrations of collagen, chitosan and blends of both

Stock solutions of collagen and chitosan were prepared containing 0.05 % (w/v) of the particular compound in 1 % aqueous acetic acid solution. Blends were obtained by mixing the stock solutions in the volume ratios collagen to chitosan 70:30, 80:20, 90:10, and 95:5. The blends and samples of the pure stock solutions were stirred for 2 h at 50 °C. Respectively, 10 ml of a sample was filled into the equipment vessel. For the titration 0.25 M solutions of HCl and NaOH were used to set the pH-value. By increments of 0.3 pH units, the zeta potential was measured in the range from pH 3 to 9. For each sample at least two separate preparations and measurements were performed.

Titration of collagen through stepwise addition of chitosan

Stock solutions of collagen and chitosan were made with 0.1 % (w/v) of the particular compound in 0.2 % aqueous acetic acid solution. Water and 0.25 M NaOH were used to prepare dilutions of different pH-values, containing 0.05 % of collagen or chitosan. All solutions were stirred for 2 h at 50 °C. The chitosan solution was respectively used to be stepwise added during the titration into the collagen dispersion. The sampling for zeta potential measurements was done for a range of mass ratios between chitosan and collagen from 0:100 to 30:70 in the titration medium.

The titrations were carried out in three separate experimental procedures just varying in the pH-value of the applied collagen dispersion and chitosan solution. In the first, both provide a pH-value of 3.6±0.2, in the second of 5.0±0.2 and in the third of 7.0±0.2.

2.2.2 Preparation of a biomimetic hydroxyapatite-collagen composite material

For the fabrication of a biomimetic hydroxyapatite-collagen composite material, the methods of Itoh and Hu were modified (Fig. 1.5) [73,75]. Two aqueous precursors were prepared. For the first, 12.5 g of the collagen dispersion were weighed in a graduated cylinder. After the addition of 20 ml of a 0.15 M phosphoric acid solution, the dispersion was filled up to a volume of 50 ml with deionised water. The second precursor was 50 ml of a 5 mM solution of calcium chloride in deionised water. Over a period of 1½ hours, a peristaltic pump (Tubing pump ISM834A, Ismatec SA, Switzerland) was used to drip both precursors simultaneously into the reaction vessel containing 20 ml of deionised water. The temperature of the system was set to (40 ± 5) °C. A pH-value of 8.3 ± 0.8 was maintained for 5 hours by a 0.3 M solution of sodium hydroxide using an automatic titration unit (Titrator DL21, Mettler Instruments AG, Germany) equipped with a standard glass electrode (electrode 84909, Bioblock Scientific AG, France). The resulting dispersion was agitated for at least 13 hours at (40 ± 2) °C in an end over end shaker and subsequently centrifuged at 800 rpm for 3 min (Labofuge 300, Heraeus - Kendro Laboratory Products GmbH, Germany). The centrifugate was washed with deionised water and centrifuged again under the same conditions. The washing step was repeated twice. For drying, the

precipitate was stored in a desiccator over phosphorus pentoxide under reduced pressure.

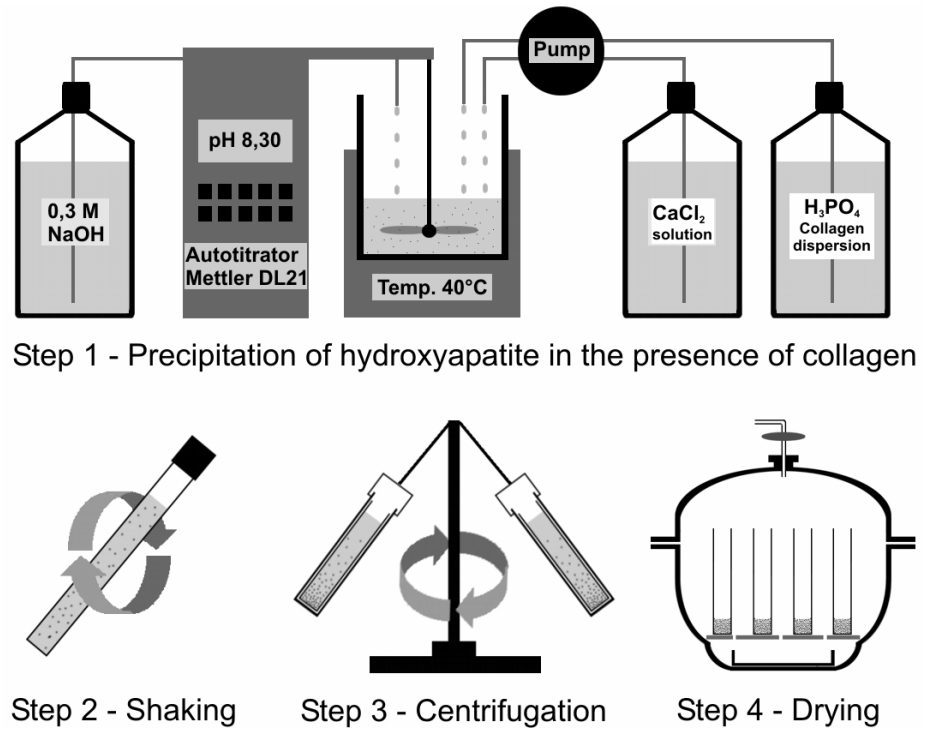

Fig. 1.5 Schematic drawing of the different steps of the hydroxyapatite-collagen composite material fabrication procedure

2.2.3 X-ray diffraction (XRD)

The powdered hydroxyapatite-collagen composite material was investigated with an X-ray powder diffractometer STADI MP (STOE, Germany). Under exposure to Co-$K_{\alpha 1}$ radiation, a diffraction range from 0 to 80° was scanned with a step size of 0.03° for 160 min. The resulting diffraction pattern was compared with one obtained from a hydroxyapatite reference.

2.2.4 Thermogravimetry (TGA)

The composition of the hydroxyapatite-collagen composite material was examined by thermo gravimetric analysis with the TG 209 instrument (Netzsch Gerätebau GmbH, Germany). A temperature range from 20 °C to 950 °C was scanned at a heating rate of 10 K/min under nitrogen atmosphere.

2.3 Results and Discussion

2.3.1 Zeta potential measurements of the polyelectrolyte interaction between collagen and chitosan

In the first experiments, pH titrations were carried out of dilutions of the single components or blends of those. The titration curves are shown in figure 1.6. For the pure collagen dispersion the average of three separate measurements gives a pH-value of 5.7 for the isoelectric point (IEP). This result is close to the isoelectric ranges of bovine collagen near 4.5 reported by Taravel & Domard and from pH-value 6-8 reported by Russell [46,81]. In agreement with Andrade et al. the measured value for the IEP of the applied collagen seems to be ideal for the fabrication of a collagen-hydroxyapatite composite material. The adjusted reaction condition, above pH 8, could provide a negative net charge of the collagen, what is supposed to attract calcium ions and subsequently cause the formation of hydroxyapatite on its surface [78]. In contrast, Kikuchi et al. reported that “the zeta potential of collagen becomes zero in the range of pH 7-9” [71]. Also Jiang et al. found the IEP of bovine collagen type I at a pH-value of 9.3 [82]. One reason for these contradictory results could be the application of different collagens, e.g. variations in the source or the extraction conditions as reported by Hattori et al. [83]. A second possible reason could be a different ionic environment. Specific adsorption of multivalent cations is a known reason for alterations of the IEP [84]. It was shown that the conformational stability as well as the IEP of collagen is strongly dependent on the type of salt and the ionic strength of the aqueous surrounding. Increased ionic strength by calcium chloride can shift the IEP of collagen to above pH 9 [85]. Hence, the result of Kikuchi et al. could possibly represent a charge compensation of the carboxyl groups by calcium ions as the beginning step of the mineralization process. Nevertheless, he described a biomimetic precipitation of hydroxyapatite at alkaline conditions and referred the carboxyl groups of the present collagen as the sites of the hydroxyapatite nucleation [71]. More detailed investigations on the inorganic-organic interface in the mineralization of natural bodies was described by Sato et al., also pointing on the important role of the carboxyl functions [86].

Chitosan possessed a higher magnitude in change of the zeta potential over the investigated pH range, whereas the differences in the surface charges between collagen and chitosan become smaller at higher pH-values.

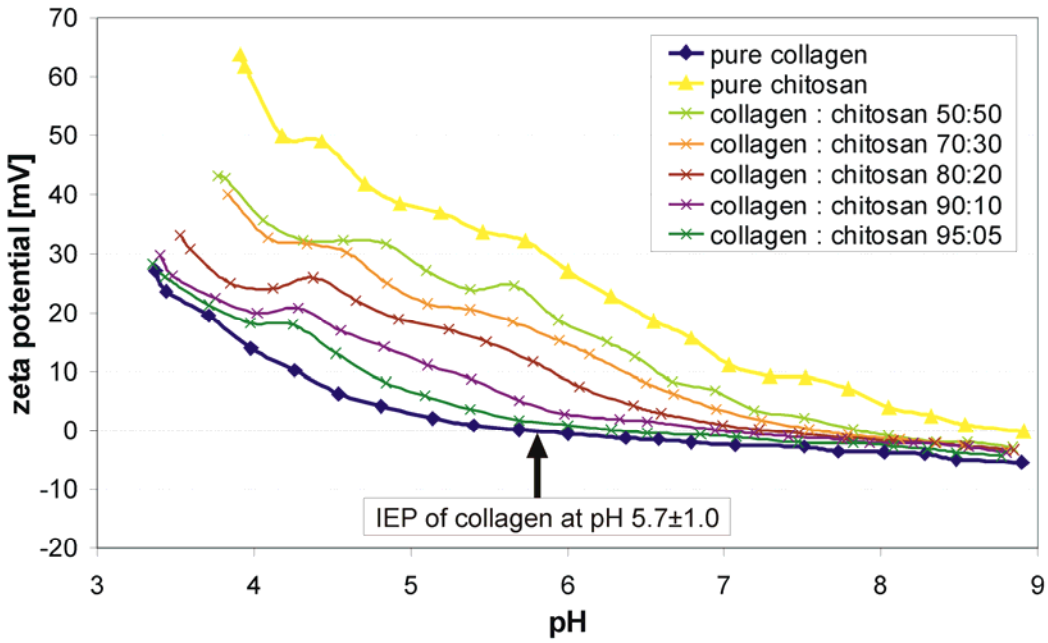

Fig. 1.6 pH-profile of the zeta potential of collagen and chitosan and different blends of both

Regarding aqueous mixtures of collagen and chitosan it is well known that occurring electrostatic interactions between positively charged amino groups and negatively charged carboxyl groups lead to a complex formation [46,87]. The titration curves of the different blends show that the measured zeta potential values of a 50:50 (w/w) mixture is more close to values obtained for the pure chitosan sample. A positive net charge is dominating over a broad pH range. Hence, the density of positive charges of chitosan seems to be much higher than the density of negative charges of collagen. A curve progression as the mean between the collagen curve and the chitosan curve is suggested to represent a stage of balance between the interacting charged functional groups of both entities. Such a mean curve progression was found to be in the range between mixtures of collagen and chitosan in the ratios of 70:30 or 80:20 (w/w). Taravel & Domard reported a theoretical weight proportion of 28.5 % of chitosan in such polyanion-polycation complexes for the assumption of a complete reaction of both components [88]. Like other researches, they found experimental results differing from this theoretical value [88,89]. Consequently, the conclusion was drawn that complete charge compensation cannot be obtained at any stoichiometric composition of the complex. They supposed the resulting lower content of chitosan to be caused by a competing gelation, what decreases the complex formation by the encapsulation of collagen [46]. However, with an excess of chitosan, higher contents can be achieved, but the interactions lead to hydrogen bonding complexes involving the denaturation of collagen [88]. In the present study,

such alterations of the collagen structure could be even intensified due to the elevated temperature of 50 °C. This might be one reason for the median zeta potential curve progressions of samples with the ratios of 70:30 or 80:20 (w/w) collagen to chitosan compared to the curve progression of the pure components. To confirm this hypothesis, further investigations with different analytics have to be carried out.

In the second experimental approach, the change of the zeta potential of the collagen dispersion by stepwise addition of chitosan was observed at three different pH stages. The results are shown in figure 1.7. The strongest influence of the chitosan content was found at pH 5. The surface charge of collagen was altered for about 20 mV in the investigated concentration range. This result corresponds well with the optimum value for the formation of the polyanion-polycation complex reported in the literature, which is declared to be up to pH 5.8 [88].
Compared to pH 5, a minor influence of the chitosan content on the zeta potential of the collagen dispersion was found for pH 3.6. For the investigated concentration range, a magnitude of around 10 mV was observed. This could be due to the fact that below the IEP of collagen more carboxylic groups are in the free acid form and not available for the ionic complex formation.

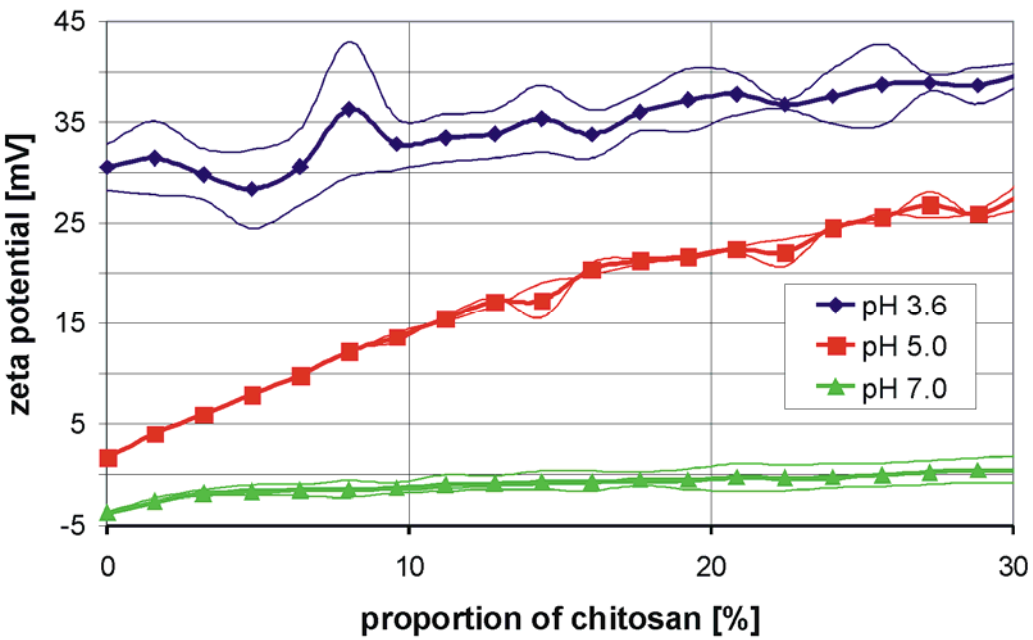

Fig. 1.7 Profile of the zeta potential of collagen at successive steps of chitosan addition for three different pH stages. The thick lines represent the average values of two measurements and the thin lines represent the values of the single measurements

The IEP is a macroscopic measure of all molecular charges. Hence, the positive net charge in these pH ranges does not mean that there are no negative ionic charges on the collagen surface at all [82]. Gupta et al. reported that polymers with a heterogeneous charge distribution on the surface can bear regions with the opposite charge than the net charge. He called this regions surface patches and accounts those for the interaction of gelatin with chitosan under conditions were both had the same kind of net charge [90]. Due to the alikeness of gelatine and collagen, it is suggestive that this is also relevant for the present study.

Although at pH 7 both biopolymers possess different kinds of net charge, a very low influence of the chitosan content on the zeta potential of the dispersion was found. One reason for this finding is the smaller difference in the surface charge at higher pH-values, as observed in the first experiment. A second reason could be the sample preparation with the addition of electrolytes in the form of sodium hydroxide for the pH adjustment, as it was reported that a high ionic strength can reduce the range of electrostatic interactions [85]. This assumption is supported by the observed conductivity variations between the different samples. A value of around 0.2 mS/cm was found for the samples of pH 3.6, whereas the samples of pH 5 possessed a conductivity of around 1.0 mS/cm and the samples of pH 7 of around 1.4 mS/cm.

Beyond that, this fact does anyway complicate the comparability of the results for the three different pH stages in the second experiment. For further experiments a conditioning of the ionic strength of the different samples for example with sodium chloride is recommended to achieve more comparable results.

2.3.2 Preparation of a biomimetic hydroxyapatite-collagen composite material

The fabrication of a substitute exactly mimicking the natural bone in all the scales of the structural hierarchies is not realizable at the time [12,32]. Therefore, the applied biomimetic approach was aimed to yield a composite material with at least the nanostructure similar to bone. Regarding the reaction parameters (nature and concentration of the precursors, temperature, pH-value and duration) several publications describe the hydroxyapatite crystallization proceeding along the direction of collagen fibrils under comparable conditions [27,71,73-75]. In biological tests of materials produced by these methods the integration into bone metabolism was demonstrated [9]. Additionally, the mineralization of collagen was shown to enhance the stiffness and the stability against enzymatic degradation [27,32]. Hence, the

differences in the biodegradability between the two components may somehow converge.

In the present study the most critical point for the reliable progression of the precipitation procedure was the pH-value stabilization. The pH electrode has to be rinsed with diluted acetic acid before and after the process. It is assumed that an adhesion of collagen or of the composite material on the glass surface and also on the diaphragm of the electrode occurred. If the washing step was skipped, the electrode was less sensitive at the end of the fabrication process. In consequence, wrong pH settings, lower rates of yield and a more brittle composite material emerged.

Quite a few publications exist about the use of alternative materials to serve as templates for the hydroxyapatite crystallization instead of collagen, for example chitosan-gelatine mixtures or polyamides [8,29]. Another strategy for biomimetic mineralization attempts is the incubation of polymeric matrices or surfaces in simulated body fluids. This approach has been used for the preparation of biomaterials as well as for studies of bio-mineralization processes elucidating the fundamental mechanisms [9,36,78,86]. Thereby it was discovered that the mineral deposition was significantly improved when there was already initial nano-sized hydroxyapatite incorporated in the scaffolds [23]. In contrast to the biomimetic approaches, Murugan and Ramakrishna applied a comparable aqueous precipitation method without any polymeric template but did also attain hydroxyapatite at the nanoscale [40]. With a mean particle size of 200 nm, they are slightly bigger than most of the reported sizes of hydroxyapatite particles produced by the biomimetic approaches or found in vertebrate bone [5,8,9,13,27,29,36,91].

As motivations for further experiments and for the optimization of the composite material, three different strategies were found in the literature, which should be considered:

(1) In the fabrication procedures described by Zhang et al. and by Cui et al., more attention is paid on assembly and maintenance of the triple helical structure of collagen within the mineralized matrix [9,72]. As a consequence for further efforts in this field, the state of the collagen has to be analyzed as well as its influence on the biological performance of the product. Correspondingly, the processing parameters, especially the temperature and the ionic strength could be modified to protect or alter the collagen structure.

(2) Recent publications show that scientists working in the field of biomineralization more and more question the sole role of collagen as the only organic component of bone responsible for the guidance of the hydroxyapatite crystallization [12,36,77,92,93]. Noncollagenous proteins like bone sialoprotein, osteonectin, osteopontin and osteocalcin are thought to promote or even initiate the mineralization due to their high density of aspartic acid and glutamic acid residues, which have a high affinity for calcium ions [12]. The present study was carried out in complete absence of noncollagenous proteins. In a comparable co-precipitation procedure Liao et al. added osteonectin into the collagen dispersion. Additional to hydroxyapatite particles in the nanometer range, the mineralized collagen fibers were arranged in bundled structures of up to 1100 nm in diameter. Thus, not only the mineralization but also the collagen self assembly can be improved by this strategy [93].
(3) As already mentioned in chapter 1, the mineral component of bone is not pure stoichiometric hydroxyapatite. Additional to the particle size in the nanometer range, the resulting imperfections in the crystal lattice of the biogenic hydroxyapatite could give reason for its better resorption by osteoclasts. By a sol-gel synthesis Kalita and Bhatt attempted advancement in this field, but the osteoclastic degradation of the resulting nanocrystalline hydroxyapatite powder doped with magnesium and zinc still needs to be evaluated [35]. For a further development of the biomimetic approach applied in the present study it could be beneficial if strategies are invented to insert such impurities into the hydroxyapatite-collagen composite material.

Beyond all this preparative concerns, in the basic research there is still a controversial issue about the fundamental mechanism how the natural collagen mineralization is initiated. The concept of an amorphous precursor was long time declined suggesting a traditional solution crystallization process also termed nucleation and growth mechanism, whereas results of recent research are suggesting the first again [12,36,77].
By now the strong impacts of the collagen template, the growth factors and the noncollagenous proteins are widely accepted, but there is no complete understanding about the regulatory mechanisms involved in the complex process of biomineralization in vivo [5]. The knowledge, that these biomolecules and also the pattern in which they were secreted are products of the intricate cell-tissue interplay highlights the difficulties or even the infeasibility of a full synthetic mimicry. It should be kept in mind that mimicry of the entire intact bone structure could be pathbreaking

for analytical approaches about biomineralization but it is not a requisite for the successful development of a regeneration supporting biomaterial.

2.3.3 X-ray diffraction (XRD)

The obtained diffraction pattern of the hydroxyapatite-collagen composite material shows all the peaks typical for hydroxyapatite (Fig. 1.8). The visible broadening of the diffraction peaks and the strong diffraction intensity close to 0 ° are indicative for a small grain size and low crystallinity of the hydroxyapatite [36,76].

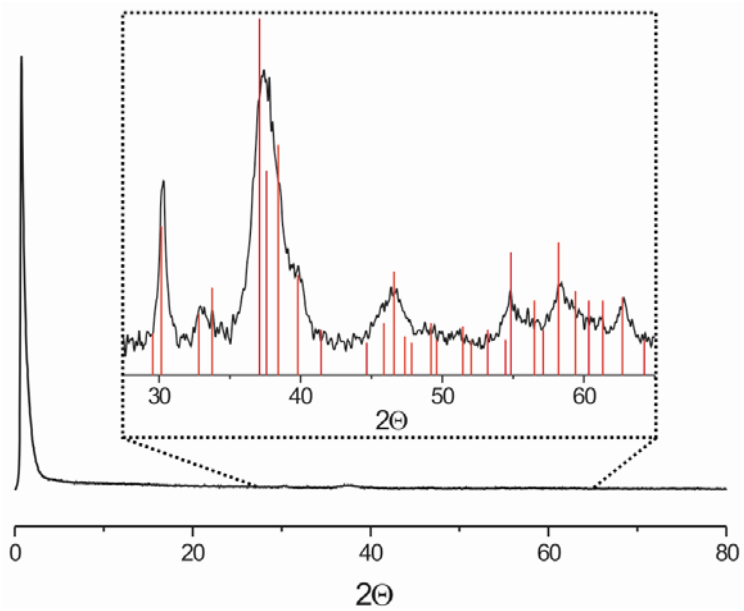

Fig. 1.8 XRD pattern of the hydroxyapatite-collagen composite material. The inset is focused on the 2Θ range between 37° and 65°. The red lines are the peaks for a pure crystalline hydroxyapatite reference.

2.3.4 Thermogravimetry (TGA)

In the present study, the conditions for the preparation of the composite material were exerted according to the methods described by Itoh and Hu [73,75]. The starting materials were chosen in a ratio that would result in a collagen to hydroxyapatite weight ratio of 20:80 for a complete retrieval. TGA was used to evaluate the effectively resulting quantitative composition of the hydroxyapatite-collagen composite material. Two main stages of weight loss were observed. The first is due to the evaporation of water showing the main mass loss around 60 °C (Fig. 1.9). The second is derived from the decomposition of collagen above 300 °C, what was proven by TGA of a pure collagen sample (Fig. 1.10). Above 600 °C, the remaining weight exhibits mostly the fraction of hydroxyapatite as the inorganic

constituent. Two main restrictions were identified limiting this broad classification of the weight loss stages. First, the initial amount of collagen was shown to be not completely transformed into volatile compounds below 600 °C. Second, the TGA of a pure hydroxyapatite sample revealed that certain mass fraction of hydroxyapatite is lost between 200 and 600 °C (Fig. 1.11).

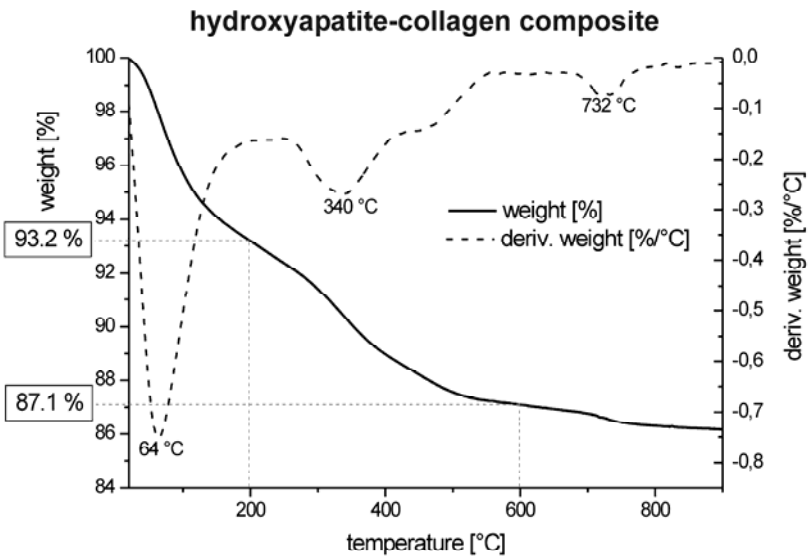

Fig. 1.9 Thermogram of the hydroxyapatite/collagen composite material is depicted as a black line. The main stages of mass turnover are better represented in the derivative of the weight percent shown as dashed line

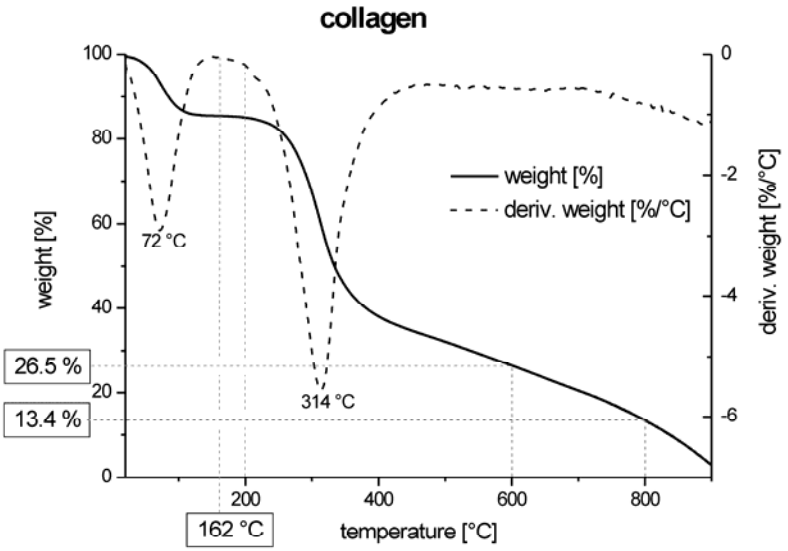

Fig. 1.10 Thermogram of a pure freeze dried collagen sample

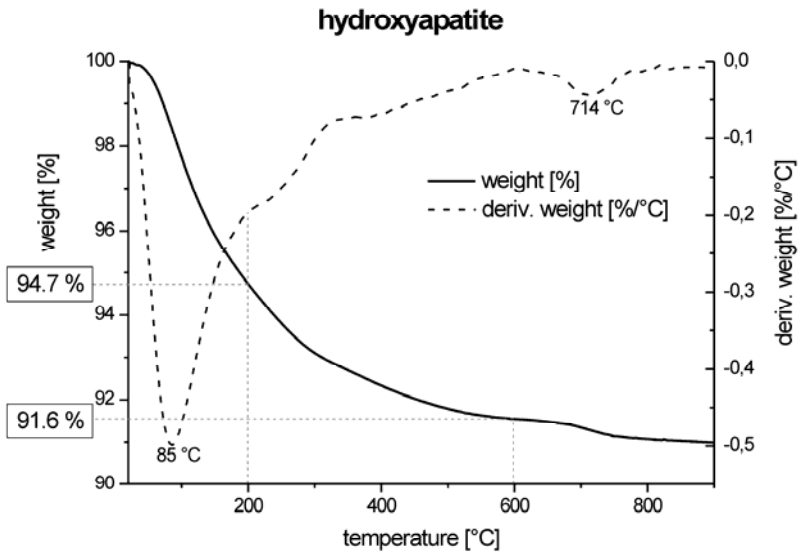

Fig. 1.11 Thermogram of a pure hydroxyapatite sample

The experimental data were used to calculate the composition of the hydroxyapatite-collagen composite in two different approaches. The “error estimation and data correction way” and the computer based “independent component analysis”.

For the first approach, the TGA data of the pure hydroxyapatite and the pure collagen were used to estimate the mass fractions mismatching the classification of the weight loss stages. Respectively, the data of the hydroxyapatite-collagen composite were corrected by the calculated proportions.

The second approach is called “independent component analysis” or “ratio method” and was reported by Koenig for the quantification of components from mixture spectra obtained by Fourier transform infrared spectroscopy. It is based on an algorithm derived from a spectral unmixing method using the spectra of the pure components for the calculation of the ratio of absorbances of the mixture [94].

The results of both approaches suggests that the composite contains less collagen and more hydroxyapatite than the theoretical content of 20 : 80, rather in the range of 10 : 90 with an additional water content of around 10 % by weight (Table 1.1). This result is in agreement with the findings of Kikuchi et al. [74]. A loss of collagen could be due to the very slight centrifugation step, compared to the fabrication conditions used by Zhang et al. [72]. Regarding the TGA, evaporation of stronger bound water and dehydroxylation of hydroxyapatite causes additional weight loss above 200 °C and also a complete combustion of collagen is not fully achieved below 800 °C [76,95]. Both are reasons for the limited accuracy of the classification of the weight

loss stages necessitating the mathematical estimation of the composition from the TGA results.

Table 1.1 Average and single results of the evaluation of the TGA data revealing the composition of the hydroxyapatite-collagen composite material

	Thermogravimetric analysis (TGA)				
	Experiment 1	Experiment 2	Experiment 3	Experiment 4	Average
Error estimation and data correction way					
c_{water} [%]	9.43	8.61	8.90	9.85	**9.2**
$c_{hydroxyapatite}$ [%]	82.50	81.87	81.45	79.96	**81.4**
$c_{collagen}$ [%]	8.06	9.52	9.66	10.19	**9.4**
Independent component analysis					
$c_{hydroxyapatite}$ [%]	94.12	93.36	92.94	91.40	**93.0**
$c_{collagen}$ [%]	4.62	6.17	6.44	7.30	**6.1**

2.4 Conclusion and Outlook

By the zeta potential measurements the IEP of collagen was assessed. In respect of the statements in the literature, it is suggested that the applied fabrication conditions were suitable for the biomimetic precipitation of hydroxyapatite. Additionally, the method was used to evaluate the interactions between collagen and chitosan. From the results, it is assumed that the strongest interaction between both components occurs around pH 5. It is weaker at lower and higher pH-values. In subitem 2.2.2 the fabrication of the hydroxyapatite-collagen composite material is described in detail. The identity of hydroxyapatite as the mineral constituent of the composite material was proved by XRD. By TGA it was shown that the ratio between collagen and hydroxyapatite is in the range of 10:90. The potential of improvements is revealed by control of the state of the collagen, the addition of special noncollagenous proteins and the incorporation of impurities into the inorganic phase.

PART II – SCAFFOLD FABRICATION

Chapter 3 – Fabrication of cylindrical scaffolds composed of hydroxyapatite, collagen and chitosan

3.1 Introduction

The following two chapters are focused on strategies of scaffold preparation. Fabrication technologies used in the present work are described in detail, the applicability is discussed, the results are presented, and alternatives are shortly reviewed and compared with the applied methods.

For several reasons, hydroxyapatite, collagen and chitosan are attractive materials for the fabrication of scaffolds aimed to support the healing of bone lesions. Miscellaneous aspects are reported in the general introduction part. Beyond the choice of the materials, further properties of a construct are important for its suitability as a tissue engineering scaffold for bone regeneration. The porosity and the stability are two challenging issues especially for the fabrication technology. Regarding the porosity, a high degree of interconnectivity and special pore sizes are required. The claim for stability is related to the mechanical properties like weight bearing ability on the one side and the resistance against enzymatic degradation and decomposition in physiological environment on the other side. The analytics of these properties and special requirements for a successful biological outcome are discussed more detailed in chapter 6.

In the fabrication strategy described in this chapter, a high porosity of the scaffolds was achieved through the freezing of diluted aqueous dispersions of the components and subsequent lyophilisation. This is a common method to produce porous matrices of chitosan or collagen [31,42,96]. Sufficient stability of such freeze dried sponges against mechanical stress and degradation in aqueous media is hard to achieve but it is often required for the application as a scaffold for bone tissue engineering [31,97]. In the present study, three different strategies were explored to enhance those properties, (i) the incorporation of a supporting PLA mesh, (ii) a low pressure – high temperature treatment and (iii) enzymatic collagen cross-linking.

In summary, the main goal of the fabrication was the homogenous embedding of the hydroxyapatite-collagen composite material into a mechanical stable and porous

polymeric matrix composed of chitosan and collagen. Such a construct is thought to mimic the mineralizing cartilage template known from the endochondral bone formation.

3.2 Materials and Methods

3.2.1 Fabrication of cylindrical hydroxyapatite-collagen-chitosan scaffolds

The methods described by Guo and Zhang were modified towards the incorporation of the hydroxyapatite-collagen composite material into a polymeric matrix of collagen and chitosan (Fig. 2.1) [98,99]. The general procedure comprised an intended quantity for the fabrication of four cylindrical constructs. 50 mg of chitosan were dissolved in 7 ml of a 0.25 M aqueous acetic acid solution. Subsequently, 3 g of the collagen dispersion were added. After two hours of stirring at (50 ± 5) °C, 100 mg of the dry, powdered hydroxyapatite-collagen composite were added to the mixture followed by vigorous shaking. Four aluminium tubes of 36.2 mm height and 9.3 mm inner diameter were used as moulds. From one side, the tubes were closed with a plastic cap. The suspension was poured into the moulds and the open sides were also sealed with plastic caps. The samples were rapidly frozen in liquid nitrogen and stored in a freezer at - 80 °C. After the removal of the plastic caps, the frozen suspension was lyophilized. Optionally two modifications of the moulding process were applied:

1. To obtain hollow cylinder scaffolds, the plastic caps on both ends of the aluminium tubes were used to fix a central iron stick of 1.5 mm diameter. The sticks were removed with the plastic caps before the lyophilisation.

2. A supported scaffold version resulted from the incorporation of a polyglycolic acid mesh in the lateral surface area. For this reason, the aluminium tubes were lined by two layers of the coarse-meshed Safil® before the suspension was poured into the mould.

Related to a method described by Ueda, the resulting sponges were placed in a test-tube, evacuated to (9 ± 3) mbar and subjected to (145 ± 5) °C for 6 hours [100]. The obtained scaffolds were stored for at least 3 days in isopropanol and dried under reduced pressure prior to following experiments.

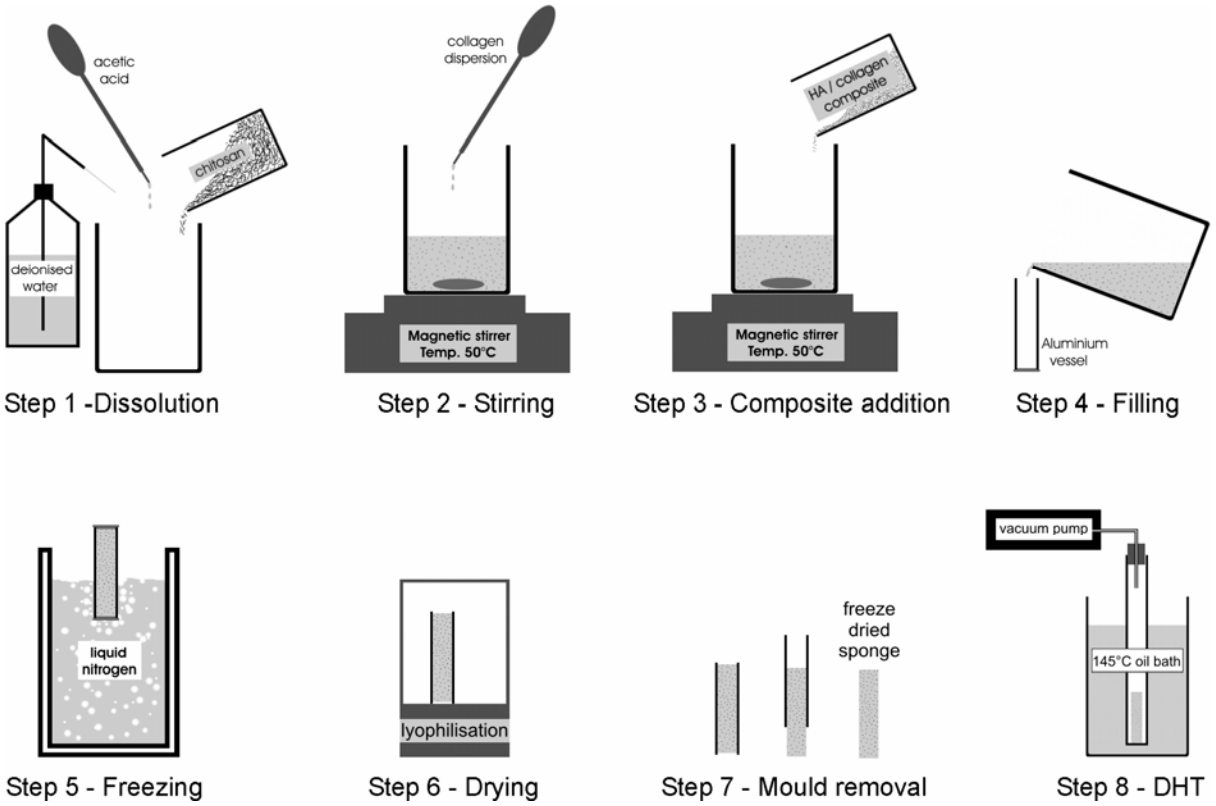

Fig. 2.1 Schematic drawing of the different steps of the fabrication procedure of the cylindrical hydroxyapatite-collagen-chitosan scaffolds

3.2.2 Hydroxyapatite-collagen-chitosan scaffolds with enzymatical crosslinked collagen

Recombinant transglutaminase (TG) was kindly provided by Prof. Pietzsch (Group of Downstream Processing, Martin Luther University Halle-Wittenberg). Production, activation and activity determination of the enzyme was carried out before by the supplier according to Marx et al. [101-103].

The standard procedure for the fabrication of the cylindrical hydroxyapatite-collagen-chitosan scaffolds (described above) was modified towards conditions ameliorating the enzyme activity for the collagen crosslinking. 50 mg of chitosan were dissolved in 2 ml of 0.1 M aqueous acetic acid solution. Subsequently, 3 g of the collagen dispersion were added and the mixture was warmed-up to (50 ± 5) °C. During stirring, 5 ml of a solution containing a) 5.66 Units or b) 12.82 Units transglutaminase in TRIS-buffer pH 8.0 were added. After two hours of stirring at (50 ± 5) °C, 100 mg of the dry hydroxyapatite-collagen composite were added to the mixture followed by

vigorous shaking. The further steps were identical to the standard procedure described in 3.2.1.

3.3 Results and Discussion

3.3.1 Fabrication of cylindrical hydroxyapatite-collagen-chitosan scaffolds

The general procedure proved to be a reliable fabrication technology providing scaffolds in a reproducible way. This conclusion applies for the first modification, i.e., the hollow cylinder geometry, too. The reproducibility of scaffolds with the PGA mesh support was just given in combination with the first modification. Several trials to produce mesh supported full cylinder scaffolds rarely succeeded due to a collapse of the hydroxyapatite-collagen-chitosan matrix in the central part of the cylinder. The constructs fabricated in a reproducible manner are shown in figure 2.2.

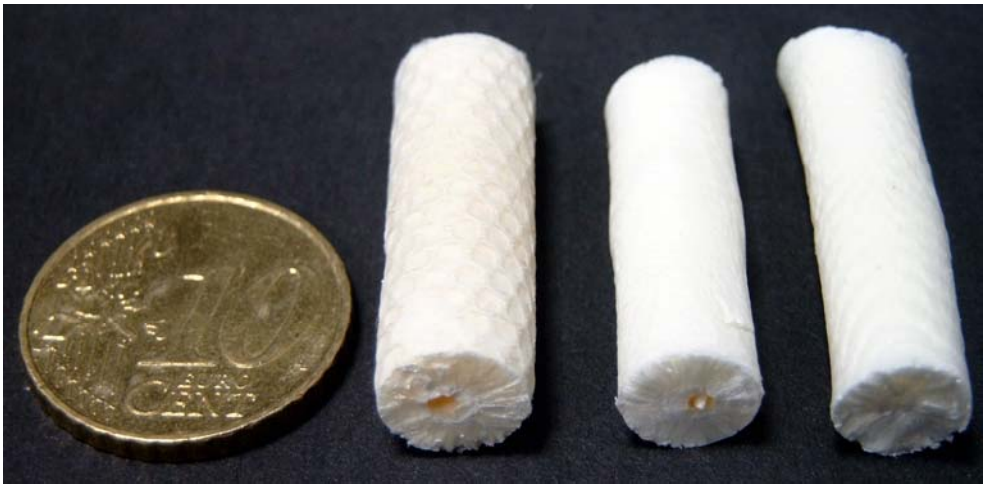

Fig. 2.2 Photograph of the cylindrical hydroxyapatite-collagen-chitosan scaffolds next to a 10 ct coin for size comparison, PGA mesh surrounded construct (left), non mesh-supported hollow cylinder scaffold (middle) and a full cylinder construct (right)

During lyophilisation different degrees of volume contraction occurred for the constructs with the mesh support compared to those without. The outer diameter of the non-supported scaffolds was 7.4 ± 0.5 mm. For the mesh surrounded constructs the volume contraction was less distinct, those scaffolds had an outer diameter of 8.4 ± 0.5 mm (Fig. 2.3). The calculated pore volume fraction was approximately 99 %. Considering the volume contraction, the hollow cylindrical constructs without PGA mesh possessed a porosity of around 62 % and the scaffolds with the PGA mesh of around 80 % in the dry state.

The hollow cylinder geometry might have several advantages. For example it shortens the pathway of restricted diffusion into the matrix. This provides a more sufficient nutrient and oxygen supply of cells inside the scaffold. The central hole could also provide space for vascularisation and it could be filled with a degradable gel for controlled release of growth factors or cell seeding purposes.

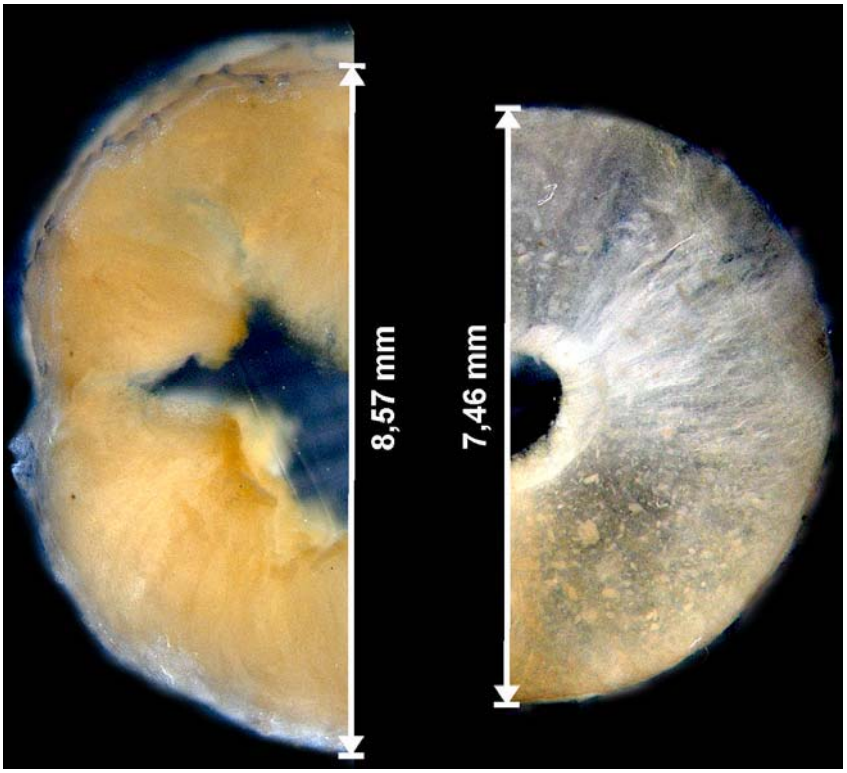

Fig. 2.3 Impinging light microscopic images of cross-sections of the hollow cylindrical hydroxyapatite-collagen-chitosan scaffolds embedded in epoxy resin, PGA mesh surrounded construct (left), non mesh-supported scaffold (right)

Compared to most of the manufacturing strategies of synthetic scaffold materials, where remaining residues of toxic organic solvents are a serious problem, the materials hydroxyapatite, collagen and chitosan feature the important advantage to be processible in an aqueous environment [29]. The a priori avoidance circumvents difficult removal and analysis of residues, saves costs and is non-polluting.

It is reported that the rate of freezing is an important parameter to yield lyophilized sponges with varying pore sizes [42]. Due to the fabrication procedure no optimization was possible in this field, because the quick freezing was necessary to avoid the precipitation of the hydroxyapatite-collagen composite material. A delay of the solidification of the suspension would result in an inhomogeneous hydroxyapatite distribution in the scaffolds as shown in chapter 6.

For that reason, Hu et al. developed a method to entrap precipitating hydroxyapatite during the gelation of a chitosan solution. After drying, a dense, rod-shaped nanocomposite with uniformly distributed hydroxyapatite resulted, which possessed appropriate mechanical properties. Regarding its applicability, the authors supposed that the composite could be used for fixation purposes of bone fractures [38]. The use as a scaffold is not contemplated, probably because of the lack of pores in the construct. Many other scientists focus more on mixtures of collagen and hydroxyapatite to obtain materials with very close composition to natural bone. Itoh et al. for example described the implantation of a construct composed of hydroxyapatite nanocrystals aligned along collagen molecules, which is additionally used as a carrier for an osteogenic growth factor. The quite dense block shows strong weight bearing properties and is supposed to induce new bone formation on its surface [73]. Nevertheless, the proof of complete biodegradation remains to be done. Therefore it is interesting that no real growth of bone tissue inside the matrix is reported. This could be due to the lack of a system of open pores throughout the entire construct, what is generally agreed to be the preferred design for a bone tissue engineering scaffold [1].

High porous systems composed of hydroxyapatite and collagen are described by Gelinsky et al. and by Pek et al. [104,105]. Those scaffolds provide sufficient mechanical and degradation stability due the applied chemical cross-linking procedure. Remaining residues of the crosslinkers are a serious problem, which gives reason to avoid their application completely [31]. Most of the reported hydroxyapatite-collagen composite scaffolds fabricated without the use of chemical crosslinkers still have insufficient mechanical properties and degradation behaviour, which can be improved by further processing [29,32]. Hu et al. for example successfully incorporated the hydroxyapatite-collagen composite into poly (L-lactic acid) scaffolds [75]. Following this example, the resulting composite was used as one source material for the subsequent scaffold fabrication.

The mesh surrounding was mainly done to achieve a mechanical support. Furthermore it represents the feasibility to incorporate solid structures of other materials to fabricate more tailored and complex systems. From the manufacturing point of view a slow or low water solubility and stability up to 150 °C are preconditions of the incorporated material to endure all the fabrication procedures.

As already mentioned Poly(α-hydroxy acids) are well suited for this purpose. The drawbacks of their application can be diminished. E. g., the hydrophilicity of PGA surfaces is increased through the presence of chitosan and the acidic metabolites can be partially neutralized by its weak alkaline degradation products [6,106]. A strong pH drop can also be attenuated by the buffering effect of hydroxyapatite, which is working at non-physiological pH-values, around pH 4 [1,23,39]. The extent of the acidic degradation was shown to be much more relevant inside bulky, nonporous systems [107,108]. Hence, a homogeneous distribution of the hydroxyapatite-collagen composite material would not circumvent a pH gradient inside a compact PGA scaffold. A more acidic construct core will not improve cell colonization and tissue regeneration, considering that one major problem is limited penetration and maintenance of living cells inside scaffolds [23]. Therefore, the core of the present system is composed of hydroxyapatite, collagen and chitosan. To not completely abandon the appropriate properties of the Poly(α-hydroxy acids) the feasibility of the incorporation of a stabilizing PGA mesh on the lateral surface of the cylindrical scaffold was accomplished. The number of surrounding layers as well as the choice of the material offer some variation possibilities. Consequently, the mechanical and degradation properties of the stabilizing shell could be tailored for the progression of bone regeneration. Furthermore, a surrounding PGA mesh may not exhibit the certain extent of the acidic degradation as it is reported for the bulky constructs [107,108].

The high temperature and low pressure conditioning at the end of the scaffold fabrication turned out to be indispensable for sufficient scaffold stability. Without this procedure called dehydrothermal treatment (DHT), the hydroxyapatite-collagen-chitosan matrix had very poor load bearing properties and decomposed within one hour in an aqueous environment. DHT is an established cross-linking method for collagen scaffolds known to enhance the mechanical properties [22,27]. Compared to the widespread use of chemical crosslinkers, it has the big advantage that no toxic residues remain in the material [31]. Additionally, it can serve as sterilization method. As reported by Geiger et al. and approved in preliminary experiments, the traditional sterilization methods of autoclaving or the use of dry heat are not feasible for this purpose due to substantial damages of the constructs. Irradiation techniques are also unsuitable because they lead to an increase in collagen degradation and deteriorate mechanical properties [22]. Furthermore, it is more practicable for a process cycle

when cross-linking and sterilization are completed in one step. The conditions of the DHT are supposed to cause the formation of new amide bonds in protein-based materials [22]. For this reason it seems evident that DHT makes collagen more resistant to enzymatic degradation as described in the literature [22,27,31]. But also contrary assumptions are reported [109]. Regarding blends of collagen and chitosan, Taravel & Domard described improved mechanical properties of the the polyanion/polycation complex through dehydrothermal treatment of the lyophilized sample [87]. This fact as well as a pure cross-linking of collagen could give rise to the notably higher mechanical performance of the hydroxyapatite-collagen-chitosan scaffolds. Beyond that, it is probable that the significant longer stability in an aqueous environment after DHT is caused by the removal of acetic acid residues, which are known to promote the chitosan solubility.

The applied conditions were adopted from Ueda et al. and are known to work well for the crosslinking of pure collagen sponges [100]. For future optimization, alternative values for the temperature, processing time and pressure should be tested. Friess reported that moisture residues can cause breakdown of helical structures and proteolysis during DHT [31]. For further experiments it is recommended to start the vacuum treatment of the scaffolds prior heating to reduce the water content and therewith possible alterations of the collagen.

3.3.2 Hydroxyapatite-collagen-chitosan scaffolds with enzymatical crosslinked collagen

Transglutaminases are a group of enzymes responsible for various post-translational alterations of different proteins [97,110]. The intra- or intermolecular linkages resulting from the enzymatic reaction are covalent ε-(γ-glutamyl)lysine bonds [111]. For the human body, transglutaminase is a not a foreign entity. It has several physiologic implications like increasing the stability of proteins and facilitating cell adhesion [110].

For the storage of the enzyme it is a common practice to freeze a buffered solution containing high amounts of glycerol as a cryoprotectant. In preliminary experiments the presence of glycerol turned out to be detrimental for a successful scaffold fabrication. With more than 2 % (w/w) of glycerol in the formulation no eligible product was obtained, whereas between 2 % and 0.5 % (w/w) resulted in shrunken scaffolds. A probable reason is the limited force of attraction between collagen

molecules in solutions containing glycerol or glucose [112]. This could prevent the formation of a mechanically stable lyophilisate. Consequently, in the fabrication procedure described in the experimental part, no glycerol is contained. It was removed before by size exclusion chromatography. The resulting scaffold is shown in figure 2.4.

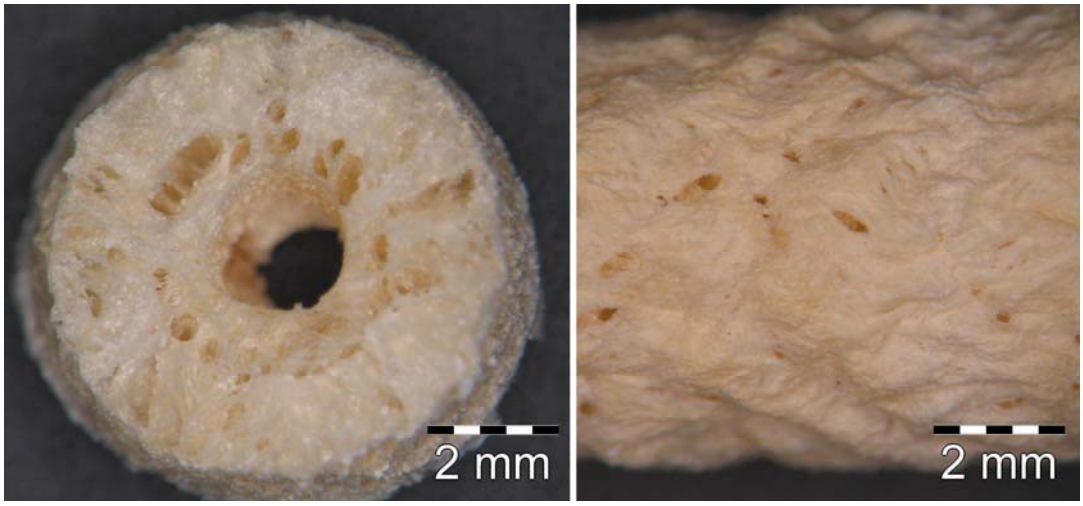

Fig. 2.4 Impinging light microscopic images of the hydroxyapatite-collagen-chitosan scaffolds crosslinked with transglutaminase, cross section (left), lateral view (right)

The enzymatic crosslinking was used additional to the DHT and resulted in a substantial stability enhancement of the entire scaffold. From the first impression, it could be seen as an alternative for the incorporated PGA mesh. The combination of both reinforcement principles was not evaluated.

In contrast to the standard formulation (see 3.3.1), for the scaffold fabrication with transglutaminase an 8.75 times lower content of acetic acid was contained. A slightly acidic milieu turned out to be essential for the chitosan solubility, whereas a neutral pH-value would be optimal for the enzyme activity. Hence, the compromise was required to accomplish both. Additional to the crosslinking, the differing pH-value of the formulation could have contributed to the higher stability of those scaffolds. In the standard procedure, the pH-value was between pH 3 to 4, whereas in the enzyme containing formulation the pH-value was between pH 5 to 6, due to the lower content of acetic acid. As reported in chapter 1, the interaction between collagen and chitosan seems to be stronger at pH 5. In further experiments, the extents of these two impacts (crosslinking and pH effect) on the overall stability should be evaluated.

3.4 Conclusion and Outlook

Cylindrical scaffolds composed of collagen, chitosan and hydroxyapatite were successfully produced by a suspension-lyophilisation technique. Various modification trials resulted in reproducible fabrication strategies for full and hollow cylinder scaffolds, hollow cylinder scaffolds surrounded by a PGA mesh and enzymatical crosslinked hollow cylinder scaffolds. All the constructs were further processed by DHT and incubated in isopropanol before further experiments.

Chapter 4 – Alternative approaches towards scaffold fabrication

4.1 Introduction

For a screening on the safety of the materials, another sample geometry than the cylindrical shape was desired. A sheet like design is sufficient and convenient for samples to be loaded into the cavities of well plates and to be cultured with a choice of cells. In the following chapter, the coating of PGA meshes by a variety of formulations is described. Even if such matrices do not intrinsically provide a capacious volume to assemble high amounts of artificial tissue, there are several clinical applications of sheet like constructs as shown by Okano and co-workers [113,114].

The forward-looking technology of rapid prototyping (a.k.a. solid freeform fabrication) is aimed at a highly customized scaffold fabrication regarding the exact geometrical requirements. Whereas the term rapid prototyping subsumes a broad range of engineering techniques, the common ground is the principle to start from the bottom and build up layers to manufacture 3D objects. Each newly formed layer adheres to the previous [26]. Just a couple of the available solid freeform fabrication methods are suitable for the fabrication of implantable constructs, e.g. three dimensional printing, fused deposition modelling, laser sintering, three dimensional plotting, stereolithography and inkjet printing [26,115].

The desired and partly already fulfilled impact for the clinical practice is the feasibility to create highly-customizable scaffold geometries in a reproducible fashion. Derived from diagnostic imaging facilities, e.g., computer tomography or MRI, the information of a defect site is applied to generate a tailored scaffold model by computer-aided design software. Using these data, the physical constructs can be manufactured utilizing specific materials and the mentioned robotic fabrication systems [26,116].

Some authors even suggest that it might be possible to close the gap between nanostructure and higher order architecture by rapid prototyping technologies [9,32]. This could be done by including cells and controlled drug delivery systems directly into the manufacturing processes [116].

Beyond all the optimism: It should be kept in mind that each of these technologies relies on a very limited choice of materials because the mechanisms behind are based on special chemical or physical properties of the processed entity [115]. By far not all of them can be used to generate matrices from collagen, chitosan and/or

hydroxyapatite and even less technologies are able to work directly with mixtures of those [117].

In the present study preliminary experiments were carried out to find a processable composition for the scaffold fabrication with the 3D plotting equipment GeSiM Nano-Plotter™. For the machining, the components have to be in a pourable state, e.g. solutions, dispersions or melted mass. Like in other 3D plotting techniques, the desired shape is achieved by solidification of the material after being extruded, as a result of the contact with the mounting medium.

In comparison to other rapid prototyping methods a quite high variety of materials can be handled by 3D plotting. Even viscous liquids, as solutions of chitosan or dispersions of collagen are processable. The costly and time consuming evaluations of the plotting conditions, which are specific for every material, are reported as a drawback of the method [115]. But it can also be seen as the big challenge and possibility the method offers for parameter variations and formulation expertise to meet the demands of exactly tailored constructs.

4.2 Materials and Methods

4.2.1 Coating of polyglycolic acid meshes

Five different formulations were used for the coating. The detailed compositions are listed in table 2.1. For the pure collagen coating, the dispersion of 1 % collagen in 0.5 % aqueous hydrogen peroxide was used directly. The formulations containing collagen and chitosan were prepared related to the methods of Guo and Zhang [98,99]. The collagen dispersion was dropped into a solution of chitosan in 1 % (V/V) aqueous acetic acid solution. After two hours of stirring at 50±2 °C, appropriate amounts of the hydroxyapatite-collagen composite material were added and the entire preparation was shaken. The resulting aqueous dispersion was dropped on a Teflon® foil placed on an aluminium plate. Two superposed layers of the fine-meshed polyglycolic acid mesh (50 × 50 mm) were immersed and soaked with the resulting liquid film, subsequently covered by a second Teflon® foil and weighted by an additional aluminium plate. The whole assembly was put into a freezer of -80 °C for at least 30 min. Subsequently, the frozen samples were lyophilized between the Teflon® foils. After detaching the foils, the coated meshes were cut into stripes of 15 mm width and 50 mm length.

Table 2.1 Composition of the different samples of the coated PGA meshes

	Uncoated PGA mesh	Pure collagen	Collagen-chitosan	Standard composition	Composition with low HA conc.	Composition with high HA conc.
Number of layers of the PGA mesh	1	2	2	2	2	2
Amount of collagen dispersion [g]	-	5.0	2.5	1.5	2.21	1.13
Amount of chitosan [mg]	-	-	25	25	30	23
Amount of water [ml]	-	-	2.5	3.5	2.8	3.9
Amount of acetic acid [µl]	-	-	50	50	50	50
Amount of HA/ collagen composite material [mg]	-	-	-	50	39	56

Referring to the method described by Ueda et al., a combination of low pressure and high temperature was used for hardening the coated meshes [100]. The coated mesh stripes were filled into a test-tube which was closed by a valve and evacuated to a pressure of 9±3 mbar. Subsequently, the vessel was lowered into an oil bath of 145±5 °C for 6 hours.

The obtained coated samples as well as the pure mesh, taken as a blank sample, were stored for 1h in 70 % (V/V) aqueous ethanol and dried under reduced pressure prior to following experiments.

4.2.2 Preliminary experiments for scaffold fabrication with the GeSiM Nano-Plotter™

Pre-tests for the finding of an applicable formulation

The approaches of Ang et al. and of Landers et al. were used as starting points to develop formulations for the scaffold fabrication by 3D-plotting [115,117]. The experimental details of important steps in the finding of an applicable formulation are listed in table 2.2. To report briefly, different blends of chitosan or chitosan and collagen with water and acetic acid or an aqueous sodium alginate solution were prepared. The mixtures were injected through a 1 ml syringe with a 21-gauge canula into various solutions of either β-glycerol phosphate or sodium hydroxide or calcium chloride in water or ethanol.

Table 2.2 Different formulations used for the pre-tests for the 3D-plotting

Plotting medium	conc.	Mounting medium	conc.	Conclusion
Chitosan in 1 % HAc	3 % (w/v)	aqueous GP solution	6 % (w/v)	An unstable extrudate was obtained, due to the dilution through the injection.
Chitosan in 1 % HAc	6 % (w/v)	aqueous GP solution	12 % (w/v)	The Chitosan solution was too viscous for being pressed through the canula.
Chitosan in 1 % HAc	4 % (w/v)	aqueous GP solution heated to 60 °C	12 % (w/v)	The Chitosan solution was very viscous and hard to press through the canula. After 10 min the developed gel-like fibers were transferred into an aqueous 0.2 M NaOH solution. The result were solid fibres.
Chitosan in 1 % HAc	3 % (w/v)	solution of $CaCl_2$ in water	1.5 % (w/v)	A clear solution was obtained without any visible solidified material.
Sodium alginate in water	5 % (w/v)	solution of $CaCl_2$ in water	0.3 % (w/v)	Single fibres arose but did not attach onto each other. The fibres remained stable after three times washing with water and storage in water over night.
Sodium alginate in water	5 % (w/v)	96 % (v/v) EtOH	-	Single fibres arose but did not attach onto each other. The fibres remained not stable after washing with water.
Chitosan in 1 % HAc	3 % (w/v)	solution of NaOH in 96 % (v/v) EtOH	2 % (w/v)	Single fibres arose but did not attach onto each other. The fibres remained stable after three times washing with water and storage in water over night.
Chitosan in 2 % HAc	2.4 % (w/v)	solution of NaOH in 96 % (v/v) EtOH	1 % (w/v)	Single fibres arose. The next layer with orthogonally aligned fibres, did not attach to the beneath one. The solidification was too fast.
Chitosan in 2 % HAc	2.4 % (w/v)	solution of NaOH in 96 % (v/v) EtOH	0.85 % (w/v)	Single fibres arose. The fibres were too bulky because the solidification was too slow. The next parallel fibre did not stay seperate from the neighbouring one.
Chitosan in 2 % HAc	2.4 % (w/v)	solution of NaOH in 96 % (v/v) EtOH	0.90 % (w/v)	Single fibres were slightly too bulky because the solidification was too slow. Some of the parallel fibres did not stay separate from the neighbouring ones.
Chitosan in 2 % HAc	**2.4 % (w/v)**	**solution of NaOH in 96 % (v/v) EtOH**	**0.95 % (w/v)**	Single and around 1 mm thick fibres arose. The parallel fibres stayed separate. The next layer with orthogonally aligned fibres, did attach to the beneath one.
Chitosan in 2 % HAc with 0.6 % (m/v) col	2.4 % (w/v)	solution of NaOH in 96 % (v/v) EtOH	0.85 % (w/v)	Single fibres were slightly too bulky because the solidification was too slow. Some of the parallel fibres did not stay seperate from the neighbouring ones.
Chitosan in 2 % HAc with 0.6 % (m/v) col	**2.4 % (w/v)**	**solution of NaOH in 96 % (v/v) EtOH**	**0.90 % (w/v)**	Single and around 1 mm thick fibres arose. The parallel fibres stay separat. The next layer with orthogonally aligned fibres, did attach to the beneath one.
Chitosan in 2 % HAc with 0.6 % (m/v) col	2.4 % (w/v)	solution of NaOH in 96 % (v/v) EtOH	0.95 % (w/v)	Single fibres arose. The next layer with orthogonally aligned fibres, did not attach to the beneath one. The solidification was too fast.

Experiments with the GeSiM Nano-Plotter™

Optimized in the pre-tests, the formulation containing chitosan and collagen was used for the experiments with the plotting equipment. 120 mg of chitosan were dissolved in 2 ml of 0.83 M aqueous acetic acid solution. 3 g of the collagen dispersion were added. The mixture was stirred at room temperature for one hour and subsequently filled into a cartridge with a capacity of 10 cm^3. By the GeSiM Nano-Plotter™, the suspension was plotted through a 10 mm long capillary with an inner diameter of 0.26 mm into a solution of 0.9 % (w/v) sodium hydroxide in 96 % (v/v) ethanol (Fig. 2.5). Some plotting parameters like chart speed, cartridge pressure and the distance between capillary tip and plotting medium surface have been varied to achieve a trouble-free operation. Ultimately, an 80 mm/s chart speed and 3 bar cartridge pressure were used to print single lines of the polymer dispersion. After 20 parallel lines, the next layer was printed orthogonally at the top of the previous. Scaffolds with a quadratic base area of 400 mm^2 and a height of 5 mm made of up to 30 layers of single lines were produced by this technique. The constructs were maintained in the alkaline-ethanolic solution for around 10 min to achieve a complete solidification. Finally, the constructs were washed for at least three times with deionised water, quick frozen in liquid nitrogen and stored at –80 °C upon lyophilisation.

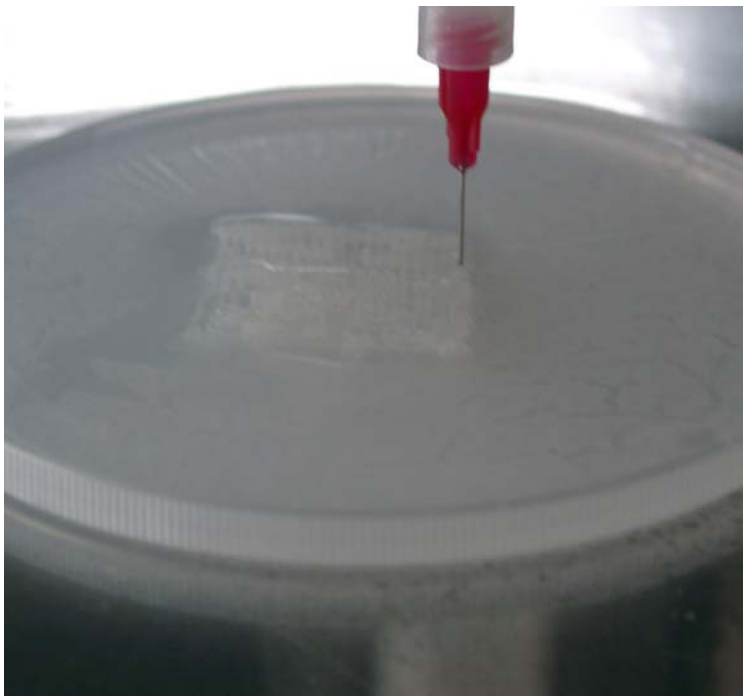

Fig. 2.5 Photograph of the plotting of the chitosan containing collagen dispersion into the ethanolic sodium hydroxide solution by the GeSiM Nano-Plotter™

4.3 Results and Discussion

4.3.1 Coating of polyglycolic acid meshes

With all the different formulations, the coating of the PGA meshes succeeded in a reproducible fashion. In preliminary experiments it turned out to be important to weight the whole assembly during the freezing procedure to achieve a homogeneous sample surface. Without the load, alterations of the distance between the Teflon® foils occur during the solidification of the suspension during freezing. The additional aluminium plate forced the two Teflon® foils to keep the distance given by the two layers of the PGA mesh in between. Consequently, the suspension froze without vertical expansion and generated a uniform and smooth surface on both sides of the mesh (Fig. 2.6).

Compared to the fabrication of the cylindrical scaffolds, the freezing process was slower. Thus, there is a probability of an inhomogeneous distribution of the hydroxyapatite-collagen composite material due to its sedimentation during the freezing. This problem would just occur in composite containing samples and would lead to coated meshes with varying properties of the two surfaces.

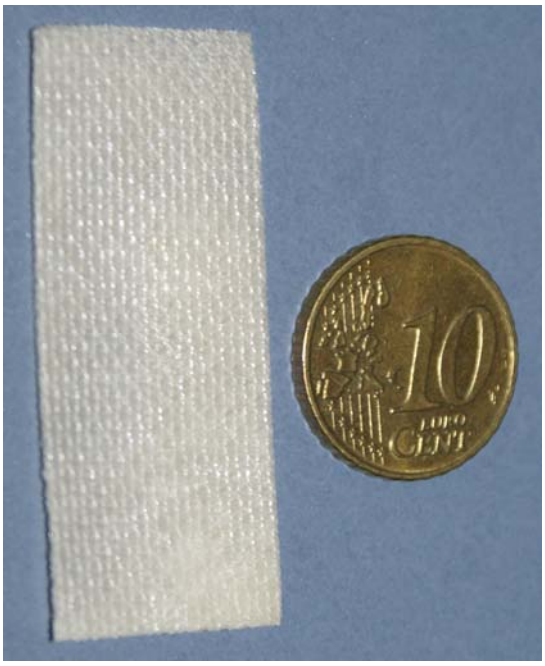

Fig. 2.6 Photograph of a coated PGA mesh construct next to a 10 ct coin for size comparison. The construct is composed of two layers of PGA mesh coated with the standard composition as given in table 2.1.

4.3.2 Preliminary experiments for scaffold fabrication with the GeSiM Nano-Plotter™

Pre-tests for the finding of an applicable formulation

Due to the manual handling of the syringe in the pre-tests, the varying pressure caused dropping and tearing of the ejected strand of the plotting medium. Hence, it turned out to be more successful for obtaining single solid fibres when the tip of the canula was below the surface of the mounting medium during the ejection of the mixtures.

No functioning composition was found for plotting a sodium alginate solution into a calcium chloride containing mounting medium. Due to the very fast reaction between alginate and the calcium ions, the second layer with orthogonally aligned fibres did not attach to the first one. As shown by Landers et al. it would be possible to slow down the reaction by the addition of EDTA to enable the binding of the single fibres to form a stable construct [115]. No attempts were done to facilitate and optimize a formulation with sodium alginate, but rather the focus was centred on compositions containing chitosan and collagen.

The pre-tests resulted in formulations for the plotting of a chitosan solution or an aqueous chitosan collagen mixture into solutions of sodium hydroxide in ethanol (Fig. 2.7). The results of important steps in the finding of an applicable formulation are listed in table 2.2.

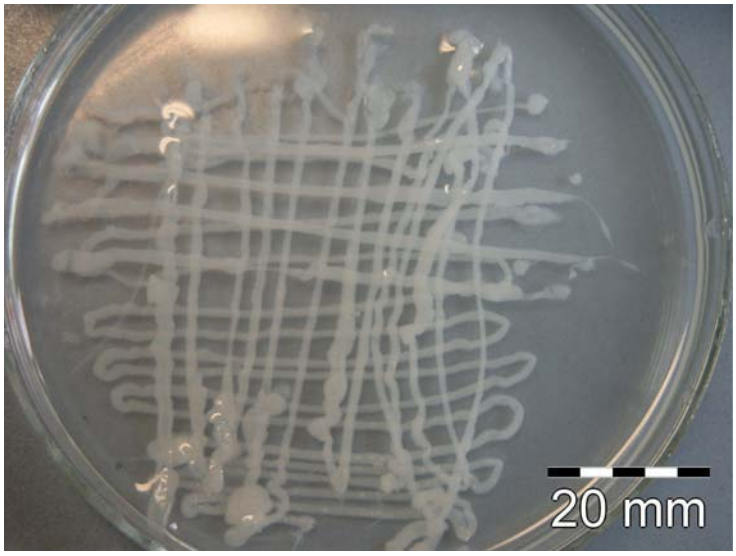

Fig. 2.7 Photograph of the result of the pre-tests for the 3D-plotting, the polymer composition solidified in fibres due to the contact with the ethanolic sodium hydroxide solution

Experiments with the GeSiM Nano-Plotter™

In contrast to the pre-tests no precise plotting was achieved when the tip of the capillary was below the surface of the mounting medium. The contact of the plotting medium with the ethanolic sodium hydroxide solution before its ejection resulted in jamming of solidified polymer on the capillary, which caused frequent strand tearing. Therefore a distance of at least 2 mm between capillary tip and plotting medium surface was maintained during the whole plotting process.

The removal of the mounting medium and the subsequent washing with deionised water was successful as well as the freezing in liquid nitrogen. Even after the storage at -80 °C the structure of the construct retained undamaged. But the lyophilisation caused alterations of the matrix intactness, visible as cracks (Fig. 2.8). No further optimization attempts have been done due to the limited availability of the Nano-Plotter™ equipment. Perspectives for improvements in further experiments would be the application of a flexibilizer, e.g., glycerol or the insertion of a stabilizing, implantable mesh between some layers, e.g., PGA mesh or a modification of the lyophilisation towards more gentle drying conditions.

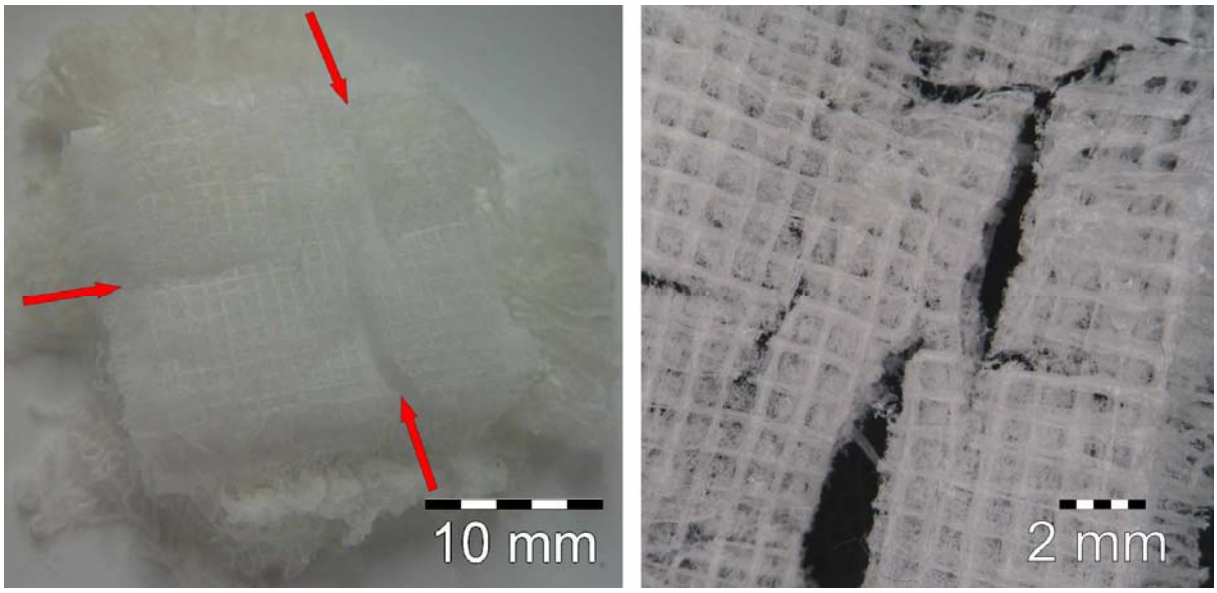

Fig. 2.8 Images of the lyophilised construct fabricated with the GeSiM Nano-Plotter™, photograph with arrows indicating the cracks (left), impinging light microscopic image (right)

State of the art and perspective for further developments

Profound work in this field has been carried out by Czernuszka and co-workers [26-28]. The strategy is based on a mould produced by an inkjet printer. Aqueous dispersions of collagen or biomimetic hydroxyapatite-collagen composite materials were casted into the mould, frozen and altogether immersed in ethanol, which was removed by critical point drying. In doing so, the mould as well as the ice crystals were dissolved in ethanol to leave a porous structure. Hence, the mould dictates the shape and size of the branched shafts drawn through the resulting constructs. In contrast, the structures of the internal pores were a result of the freezing procedure and therefore not controllable by the rapid prototyping itself but rather by the cooling conditions. Water crystallization as feasibility to control the pore structure could possess some disadvantages as reported for the conventional scaffold fabrication techniques, like the incapability of control over the exact pore size and geometry, over the spatial distribution of pores as well as over the existence and structure of internal channels within the scaffold [26]. Beyond that, the direct inclusion of cells during the manufacturing process seems infeasible with the reported conditions.

The 3D plotting technology as applied in this study and also reported by Ang et al. and Landers et al. offers more control possibilities over the internal scaffold geometries [115,117]. Branched shafts drawn through the constructs could be obtained by skipping one or more lines in the regular pattern, while the geometry and the spatial distribution of pores are adjustable by the array and spacing of the printed lines. Additionally, the GeSiM Nano-Plotter™ can work with several print heads simultaneously, which provides the opportunity to tune properties of the entire construct as for example anisotropic properties or reinforcements of regions which will be more exposed to mechanical stress. Growth factor containing formulations or patterns of other functional proteins could be plotted inside constructs to achieve a guided cell growth like a spatial directed vascularisation [118]. Furthermore a specific positioning of cells into the scaffold during its manufacturing could be feasible, which was already reported for comparable plotting systems [119]. In a continuation of the present study growth factors as well as cells would have to be protected from the mounting medium. This could be achieved by various encapsulation technologies as shown for growth factors by Isobe et al. and for cells by Murua et al. [120,121].

The result and the highlighted perspective show the possibilities this forward-looking technology offers to fabricate constructs so close to the natural prototype.

4.4 Conclusion and Outlook

PGA meshes were successfully coated by a variety of formulations in a reproducible fashion. After the lyophilisation of the frozen constructs they, were cut into stripes and further processed by DHT.

Additionally, with several formulation trials and preliminary experiments, the first steps were made to pave the way for a scaffold fabrication strategy by the forward-looking technology of 3D plotting. The achieved results did not represent a final stage, but provide a proof of principle and leave space for future improvements.

PART III – SCAFFOLD CHARACTERIZATION

Chapter 5 – Characterization of the size of the mineral constituent inside the scaffolds

5.1 Introduction

The hydroxyapatite grain size on the nanometer level was shown to be important for a successful biodegradation [9,35,36,40]. It is reported that osteoclasts produce more tartrate-resistant acid phosphatase and show a greater formation of resorption pits on nano-sized hydroxyapatite than on conventional hydroxyapatite [7]. Additionally, the already mentioned important osteoblast to fibroblast ratio can also be positively influenced by the use of nano-scaled materials [7,21]. Furthermore, a high content of nano-hydroxyapatite is preferable as it supports protein adsorption on surfaces and thus mediates osteoblast adhesion [7,8,27]. In consequence hydroxy-apatite particles with a grain size in the nanometer range are widely accepted to support the healing of bone lesions [29]. Hence, dispersions of pure nanocrystalline hydroxyapatite are already a part of the medicinal practice, whereat controversial opinions exist. Globular structures occurring at the implantation site are suggested as aggregates of the hydroxyapatite particles, which causes a reasonable doubt about their complete biodegradability [37]. Also the migration of the hydroxyapatite nanocrystallites into surrounding tissues has been reported [8]. A polymeric embedding could be able to separate and cover the single particles until they would be resorbed during stepwise matrix degradation [32]. Thus, the question arises if the nano-sized hydroxyapatite crystals remain after further processing. A probable aggregation or particle growth by Ostwald ripening could adversely affect the biological outcome [29]. Due to the anchoring of the particles inside the opaque matrix, no light scattering techniques for particle size measurements were applicable without a sample alteration. In contrast to the few reports about detailed size determination of mineral particles inside scaffolds, several publications can be found about such investigations on natural tissues [9,91,122-124]. Due to the alikeness of the samples the analytical principles should apply for both. Until now, no definite answer was given about an exact size of the hydroxyapatite in natural bone, what seems logical considering the diversity of biological systems [9]. But owing to intense

research, the range of sizes at the nanoscale is well defined. Most reports describe plate like mineralites with a length of 25 to 50 nm, a width of 15 to 50 nm and a thickness of 2 to 20 nm [5,13,29,36]. Only one report was found about significant bigger hydroxyapatite crystals with dimensions of 500 nm × 500 nm × 5nm [77]. The applied methods for the evaluation of the particle size includes transmission electron microscopy (TEM), atomic force microscopy (AFM), small angle x-ray scattering (SAXS) and x-ray diffraction (XRD). The assets and drawbacks of the different methods for this purpose are reviewed by Cui et al. [9].

As reported in chapter 2, the XRD results already indicate a small grain size and low crystallinity of the hydroxyapatite in the composite material. After the description of its application in the scaffold fabrication in the previous section, this chapter is focused on the investigation of the particle size of the hydroxyapatite inside the collagen-chitosan construct using the mentioned analytical techniques. For these experiments, full cylinder scaffolds without PGA mesh surrounding were used. To evaluate alterations due to the processing, samples of the pure hydroxyapatite-collagen composite material without chitosan were additionally examined. Cylindrical collagen-chitosan scaffolds without hydroxyapatite were fabricated as blank samples to facilitate its identification in the SAXS and AFM data. Additional experiments were performed to evaluate if the distribution of hydroxyapatite throughout the collagen-chitosan scaffold can be analysed by benchtop-MRI.

5.2 Materials and Methods

5.2.1 Fabrication of blank samples

The general procedure described in chapter 3 was modified to obtain scaffolds with a collagen to chitosan ration of 1:1 without the addition of the hydroxyapatite-collagen composite material. 50 mg of chitosan were dissolved in 5 ml of 0.25 M aqueous acetic acid solution. Subsequently, 5 g of the collagen dispersion were added. After two hours of stirring and vigorous shaking, the suspension was poured into the moulds. The further steps were identical to the standard procedure described in 3.2.1.

5.2.2 Small angle x-ray scattering (SAXS)

The powdered hydroxyapatite-collagen composite material and 10 mm high pieces of the hollow cylinder shaped collagen-chitosan sponge and the

hydroxyapatite-collagen containing collagen-chitosan scaffold were compressed. A press for infrared spectroscopy samples (Specac) was used to obtain plate shaped compressed samples with a thickness of about 500 µm for the hydroxyapatite-collagen composite material and around 200 µm for the different scaffold samples. The applied pressure was 60 kN.

The SAXS setup consisted of a rotating copper anode (Rigaku), an X-ray optics device (Osmic: Confocal Max-Flux) and a Bruker Hi-Star 2-D detector. The X-ray optics focused the beam and served as a monochromator for Cu-K_α radiation. Typical exposure times were 3 minutes.

A rough estimate of the size scale of the structure under study can be made by a Guinier analysis of the data for small q giving the radius of gyration (R_g). Here q is the scattering vector with $q=4\pi/\lambda \sin\theta$, where θ denotes the scattering angle and λ the wavelength of the radiation. For the analysis, the logarithm of the intensity (I) is usually plotted versus the squared scattering-vector. The resulting diagram is called Guinier plot. Derived from equation 3.1, the slope of the linear part of I(q) in the plot is equal to $R_g^2/3$ [124]. The approximation is suitable for small q values. The condition for the validity is $q \cdot R_g < 1$.

$$I(q) = I_0 \cdot e^{-q^2 R_g^2 / 3} \qquad 3.1$$

5.2.3 Transmission electron microscopy (TEM)

The powdered dry hydroxyapatite-collagen composite material was immersed in epoxy resin according to Spurr and polymerized at 70 °C for 24 hours [125]. Ultrathin sections (80 nm) were made with an Ultracut R ultramicrotome (Leica, Wetzlar, Germany) and observed with an EM 900 transmission electron microscope (Carl Zeiss SMT, Oberkochen, Germany) using 80 kV acceleration voltage. Micrographs were taken with a Variospeed SSCCD (Tröndle, Moorenweis, Germany).

5.2.4 Environmental scanning electron microscopy (ESEM)

Additional to the scaffolds, a modified sample preparation was used for the ESEM study. The same suspension containing chitosan, collagen and the hydroxyapatite-collagen composite was filled on a Teflon® coated dish and quick frozen at -80 °C. After subsequent lyophilisation, the sample was investigated with

ESEM (Philips ESEM XL 30 FEG, Philips Electron Optics) in gas mode by detecting secondary electron or backscatter electron images.
The ESEM investigation was also carried out with scaffolds containing the enzymatical crosslinked collagen. The constructs fabricated using 12.82 Units transglutaminase served as samples for this survey.

5.2.5 Atomic force microscopy (AFM)

All AFM equipment was purchased from TopoMetrix Corporation (Santa Clara, US). The hydroxyapatite-collagen composite material was used in the powdered form. Samples from the pure collagen-chitosan sponge and the hydroxyapatite-collagen containing collagen-chitosan sponge were taken as approx. 500 µm thick cross sections obtained by cutting with a razor blade. The samples were affixed on the surface of adhesive foil placed on metal sample holders. All AFM scans were made with the TMX 2010 Discoverer instrument under ambient laboratory conditions. AFM was operated in the non-contact mode at a resonant frequency of 282 kHz. A silicon cantilever was used with a probe tip radius of approx. 10 nm. The accuracy of the method was monitored by the repeated measurement of a standard grid.

5.2.6 MR Imaging of the distribution of the hydroxyapatite

The measurement equipment and the general settings were described in chapter 1. Averages of 16 single scans were used resulting in a complete measuring time of about 10 min. For some samples, the scaffold fabrication was modified to obtain scaffolds with an inhomogeneous hydroxyapatite distribution. Those were used to evaluate if BT-MRI is capable for its visualization. Therefore, the aluminium tube containing the suspension was placed for 3 min on the lateral surface before freezing. The composite material is precipitating if a delay occurs between filling the aluminium tubes and the fast freezing, what was intentionally done for those samples to achieve an inhomogeneous distribution of hydroxyapatite. All the other scaffold production steps were carried out like described above.

5.3 Results and Discussion

5.3.1 Small angle x-ray scattering (SAXS)

The decay of the intensity proportional to q^{-4} in the SAXS pattern obtained from the compressed collagen-chitosan sponge without hydroxyapatite is typical for

the scattering of X-rays at the interface between two phases, as for example the boundary between air and the polymer matrix [Fig. 3.1]. It is concluded that in this sample the scattering is caused by the porous structure of the sponge. The size of the pores cannot be determined from these data, as is it too large and therefore outside of the sensitive range of the instrument.

The data obtained from samples containing hydroxyapatite deviate from simple q^{-4}-behavior [Fig. 3.1]. As shown in table 3.1, the electron density of hydroxyapatite is much higher than the one of the other components, it is reasonable to conclude that the scattering signal is dominated by the hydroxyapatite particles.

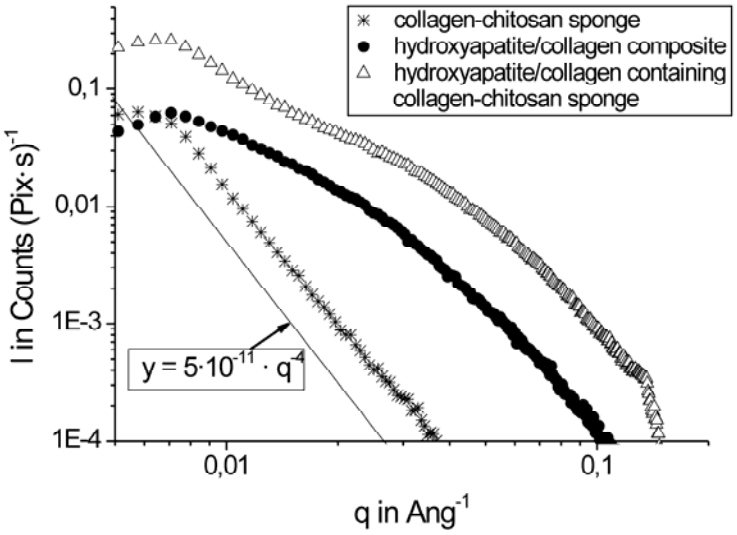

Fig. 3.1 SAXS patterns of compressed samples of a pure collagen-chitosan sponge, the hydroxyapatite-collagen composite material and the hydroxyapatite-collagen containing collagen-chitosan sponge. For comparison of the slope a straight line with the slope of q^{-4} is included. The low intensity values for $q < 0.008$ Ang^{-1} are caused by the beam stop. Hence, the proximate maxima of the scattering intensity are of no relevance.

Tab. 3.1 Electron density of the scaffold components and the parameters used for its calculation

Parameter	Hydroxyapatite	Chitosan [a]	Collagen
Density [g/cm^3]	3.08 [126]	1.29 [127]	1.40 [128]
Molecular weight [g/mol]	502.3	85000 [43]	280300 [b]
Electron density [e$^-$/cm^3]	$9.23 \cdot 10^{23}$	$3.6 \cdot 10^{23}$	$2.29 \cdot 10^{23}$

[a] Deacetylation degree of Chitoclear FG95 TM1369 is 95 % [43]

[b] Full amino acid sequence of equine collagen is not available; therefore the calculations were performed using the sequences of two α1 chains and one α2 chain of bovine collagen type I

By the Guinier approximation an estimation of the hydroxyapatite crystal size in the composite material was feasible as reported by Kinney [Fig. 3.2] [124]. The corresponding result for R_g of the hydroxyapatite in the compressed composite material is around 16 to 18 nm. For the obtained data the product of q and R_g is about 1.1 to 1.7, i.e. the particle size is close to the resolution limit of the instrument. Therefore, the result is taken as a rough estimation for the particle size of the incorporated hydroxyapatite.

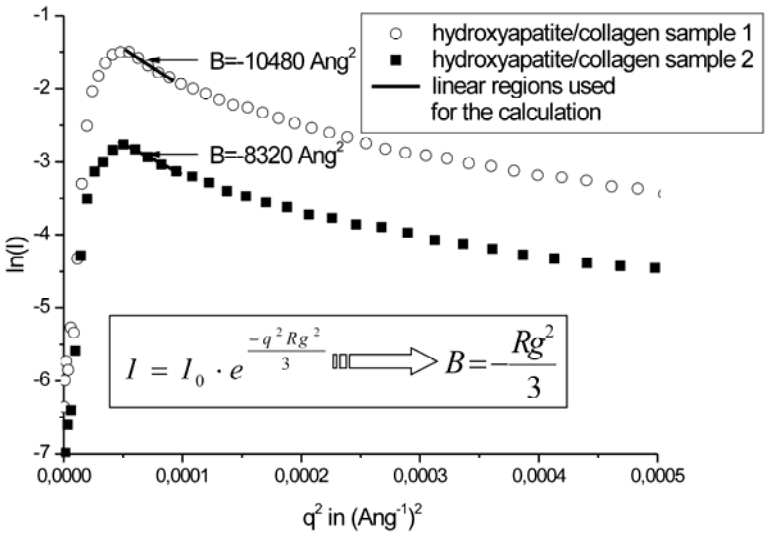

Fig. 3.2 Guinier-plot of the SAXS patterns of two different regions of the compressed hydroxyapatite/collagen composite material. The linear segments with the slope notifications show the region used for the calculation, which is shown as an inset.

The inflection point in the curve of the compacted hydroxyapatite-collagen containing collagen-chitosan sponge could be indicative for a smaller scale structure than in the pure hydroxyapatite-collagen composite [Fig. 3.1]. As it is unlikely that the hydroxyapatite particles become smaller by the sample preparation procedure, it is not straightforward to relate this structure to the hydroxyapatite particles directly. The more strongly increasing scattering intensity at small q might be due to an increased tendency for aggregation of the hydroxyapatite particles, certainly the microstructure of the composite is somewhat modified. The shape of the scattering curve is not very specific and while the data give evidence that the materials are nanostructured, a determination of the exact size of the hydroxyapatite particles seems not feasible.

5.3.2 Transmission electron microscopy (TEM)

As already emphasized in the discussion of the SAXS results, hydroxyapatite has a higher electron density compared to collagen. In TEM images, this difference gives rise to the obtained contrast. Hence, the dark needle shaped units visible in figure 3.3 are suggested to be hydroxyapatite particles. Due to the solely two dimensional impression, a blade shape would also be possible. As evaluable from the present data, the longest dimension of most of the particles seems to be less than 50 nm. The particle shape, the contrast ratio as well as the overall impression visible in the obtained image shows a remarkable analogy to the TEM image of mineralized collagen published by Cui et al., reprinted in figure 3.4 [9].

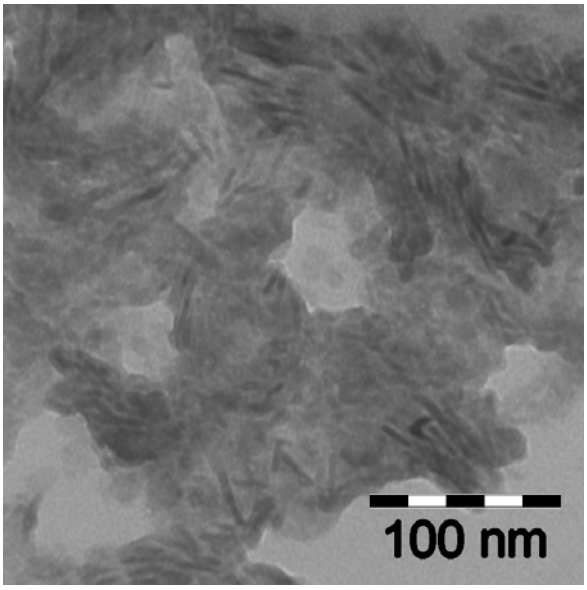

Fig. 3.3 TEM image of the hydroxyapatite/collagen composite material embedded in epoxy resin

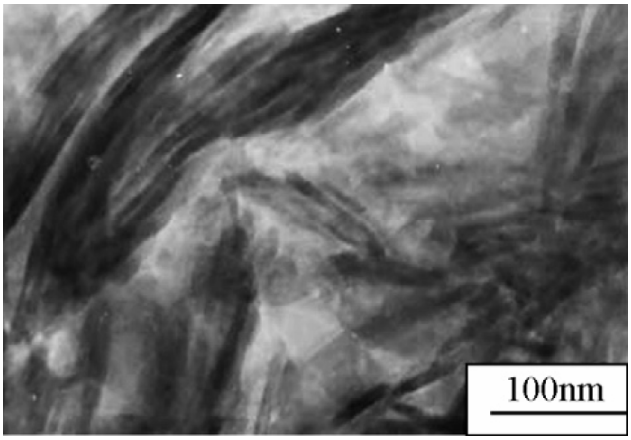

Fig. 3.4 TEM image of mineralized collagen fibrils published by Cui et al. [9], Figure reproduced courtesy of Elsevier

5.3.3 Environmental scanning electron microscopy (ESEM)

The ESEM image shows the highly porous structure of the scaffold with polymeric ligaments circularly directed into the central part (Fig. 3.5 a). With the secondary electron detector, no considerable contrast can be seen within the matrix material. By means of the back scattering electron detector (BSE) a material composition related contrast was available additional to the sample surface topography (Fig. 3.5 b). Due to its composition of elements with a relative high atomic number, hydroxyapatite would appear bright in the ESEM images. In comparison, the polymer matrix of collagen and chitosan (which just contains C, O, N, H) looks dark. Several micrometer large hydroxyapatite or hydroxyapatite-collagen particles are visible on the material surface. At higher magnification, these seem to be conglomerates. The polymeric matrix also looks like assembled by more bright and darker regions (Fig. 3.5 c). Particularly at the high magnification image, the structured nature of the continuous material is obvious with very small grains embedded in the collagen-chitosan matrix (Fig. 3.5 d). The bright appearance of the grains suggests it to be smoothly distributed hydroxyapatite particles. The vertical dark lines are artefacts due to the electron beam interaction with the sample material.

No detailed investigation of the size of the mineral constituent inside the scaffolds was performed for the scaffolds containing the enzymatical crosslinked collagen. However, some information about this topic was obtained from the ESEM investigation. Compared to the laminar structures visible in the images of the non-transglutaminase crosslinked scaffolds, these samples possess a more fibrous microstructure as evident in figure 3.6. The second obvious difference refers to the hydroxyapatite or hydroxyapatite-collagen particles. Although it was applied in the same concentration, in the enzymatical crosslinked scaffold more of the particles are visible. They also appear like conglomerates but the single pieces seem to be larger. No indication of a polymeric embedding like in the non-transglutaminase treated samples was found. Two reasons are supposed for these findings. First, the enzymatical treated collagen may provide fewer sites for the electrostatic interactions with chitosan due to the crosslinking. Hence, the collagen of the composite material is more affected, what could lead to its enhanced agglomeration. Second, the pH-value of the dispersion for the scaffold fabrication is different between the standard formulation and the formulation with transglutaminase as described in subitem 3.3.2. The pH-value of around 5, used as a compromise to enable the

enzyme reaction was additionally shown to support the electrostatic interaction between collagen and chitosan as reported in chapter 1. Thus, the different pH-values of the formulations could also be responsible for an enhanced agglomeration of the composite.

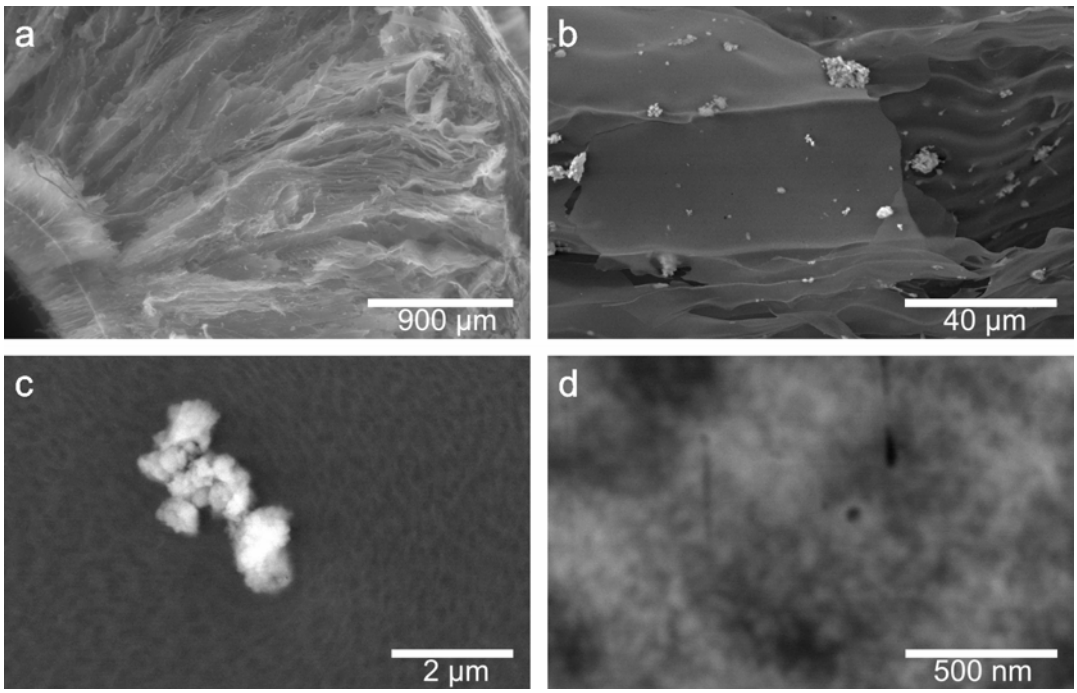

Fig. 3.5 ESEM images of the hydroxyapatite-collagen containing collagen-chitosan matrices. Overview of a scaffold cross section detected by the secondary electron detector (a), area representative for the surface of the polymeric matrix inside the scaffold detected with the BSE detector (b), image section focused on one of the hydroxyapatite agglomerates on the surface of the polymeric matrix inside the scaffold detected with the BSE detector (c), high magnification image of the sample lyophilized on the Teflon® coated dish taken with the BSE detector (d)

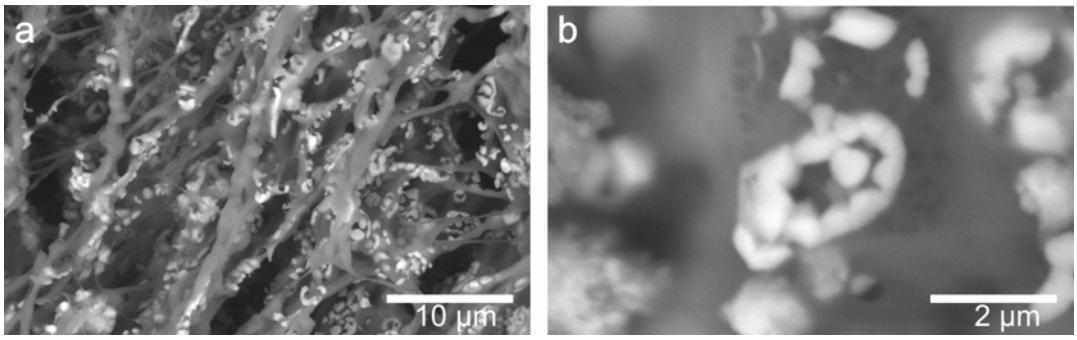

Fig. 3.6 ESEM images of an enzymatical crosslinked hydroxyapatite-collagen-chitosan scaffold taken with the BSE detector. Area representative for the surface of the polymeric matrix inside the scaffold (a), image section focused on one of the hydroxyapatite agglomerates on the surface of the polymeric matrix inside the scaffold (b)

5.3.4 Atomic force microscopy (AFM)

The AFM image of the hydroxyapatite-collagen composite shows a surface roughness of the material with round shaped granules of 100 - 200 nm in diameter, sticking out of the surface for 3 to 13 nm (Fig. 3.7 b). Thus, the obtained surface representation is suggestive for the constitution of the composite material as an aggregate of closely packed particles.

No granular structures can be seen in the AFM image of the collagen-chitosan sponge without hydroxyapatite (Fig. 3.7 a). It shows a more planar but rough surface with parallel aligned and towards one direction elongated elevations of 20 -120 nm thickness and 2 - 8 nm height.

Both structural characteristics, granular as well as elongated elevations, were found for the hydroxyapatite-collagen containing collagen-chitosan sponge. Through this obvious alteration compared to the composite, it seems as if the particles were more separated due to the polymeric embedding (Fig. 3.7 c). The granular elevations are 50 - 300 nm in diameter, sticking out of the surface for 3 - 30 nm. The elongated elevations are 10 - 50 nm thick and 0.5 - 4 nm high protruded to the surface. For the granules, a higher size variation was observed and the shape derivates more from the spherical contour in the hydroxyapatite-collagen containing collagen-chitosan sponge than in the composite.

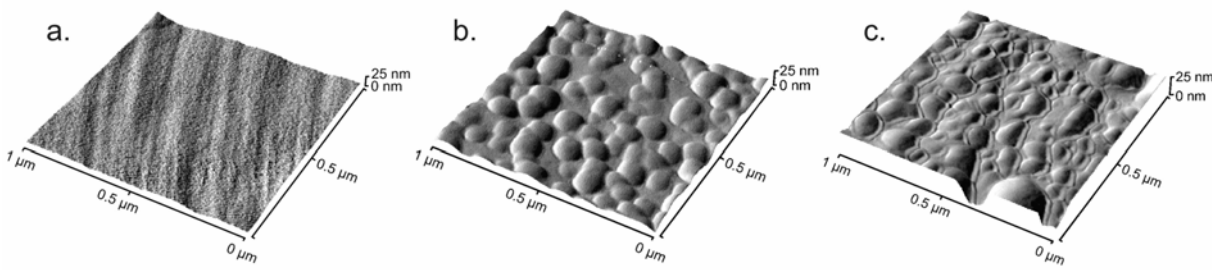

Fig. 3.7 AFM images of surfaces of the polymeric matrix inside of a pure collagen-chitosan sponge (a), the surface of the hydroxyapatite-collagen composite material (b) and the surfaces of the matrix inside a hydroxyapatite-collagen containing collagen-chitosan scaffold (c)

5.3.5 MR Imaging of the distribution of the hydroxyapatite

The intended inhomogeneity of the hydroxyapatite-collagen composite distribution inside the scaffold resulting from the modified production was visualized by MRI. The 3 min delay before freezing caused a higher composite concentration in one site of the hollow cylinder scaffold, visible as a more bright area in the MR image

(Fig. 3.8). In other words, the higher hydroxyapatite concentration resulted in increased signal intensity in T1-weighted MR images. In clinical MRI applications calcium deposits usually have no effect on signal intensity or even reduce it. Henkelman and coworkers investigated the influence of hydroxyapatite on the contrast relations in MR images and showed that this effect is depending on the concentration and the surface area of the calcium salt particles [129]. It is hypothesized that the signal enhancement in T1-weighted MR images is due to the interaction of water protons with the surface of the calcium salt particles [49,130]. Appropriate to the bound state on the crystal surface, the water protons relax more quickly than those distant from the particle, resulting in a faster T1-relaxation process leading to enhanced signal intensity in the images [50]. Hence, a higher concentration of hydroxyapatite would cause a more intensive signal, but there are two limitations. With the rising hydroxyapatite concentration, the proton density is decreasing and the T2 relaxivity is enhanced [51]. Both effects are contrary to the signal enhancement in T1-weighted MR images. A domination of the T1 decreasing effect is caused by a high surface area of the mineral phase, resulting in high signal intensity [129]. Thus, a small particle size of the incorporated hydroxyapatite could be responsible for the bright appearance of the locations with higher hydroxyapatite concentration in the obtained images.

Consequently, it is revealed that BT-MRI can be used for gathering information about inhomogeneities in the hydroxyapatite distribution inside scaffolds and may also provide hints about its surface area. While the concentration ranges for these analytics still have to be evaluated, in the context of the present study the result give additional evidence on the small particle size of mineral phase inside the scaffolds.

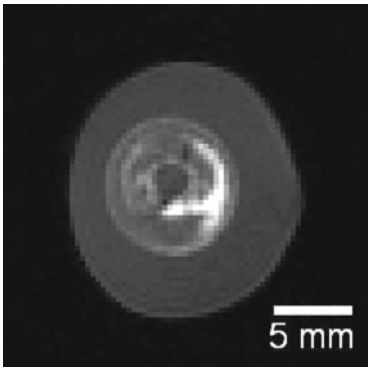

Fig. 3.8 MR Image of the scaffold with inhomogeneous distribution of the hydroxyapatite-collagen composite material, bright areas represent regions of higher hydroxyapatite concentration

5.4 Conclusion and Outlook

By SAXS, TEM and AFM it was shown that the size of the hydroxyapatite particles in the composite material is in the lower nanometer range [131]. This conclusion is supported by the XRD data as described in chapter 2. In future investigations, XRD data could be additionally used for a detailed calculation of the hydroxyapatite particle size by Scherrer´s formula, as reported by Pek et al. [105].

The results of SAXS, ESEM and AFM suggest that the dimension of the mineral particles within the collagen-chitosan matrix is at the nanoscale. Additional to the XRD, future investigations should also examine the scaffold samples by TEM to attain more reliable information about the shape of the embedded mineral entities. The higher variability of the hydroxyapatite particle size inside the scaffold observed by AFM could be an explanation for the accelerated decay of the SAXS curve of this sample at small scattering angles. Also, the microsized hydroxyapatite agglomerates on the surface of the polymeric matrix found by ESEM are probable reasons for the different X-ray scattering behaviour. It has to be investigated in further experiments, if these hydroxyapatite clusters have any adverse effect on the biodegradability of the material, as well as possibilities for an obviation of their presence. Hence, those results give rise for specific attentiveness on single details of the fabrication procedure and they indicate the high optimization potential by variation of several parameters. For example, the pH-value dependent polyelectrolyte interaction between collagen and chitosan in the presence of hydroxyapatite has to be evaluated as it is a probable reason for such aggregations. For a systematic evaluation, infrared spectroscopic investigations might be used. Such studies could build on a high amount of available published data. The interactions between collagen and hydroxyapatite have been investigated by this method, as well as the interactions between hydroxyapatite and chitosan and between collagen and chitosan [7,8,45,46,71,72,88,89]. Alternatively, sophisticated dispersion technologies or concentration variations may prevent the appearance of hydroxyapatite agglomerates on the polymer surface in the scaffolds.

Despite the ESEM investigation was carried out close to the resolution limit, similar conclusions can be drawn from the results, regarding the polymeric embedding. Except the agglomerates on the surface of the polymeric matrix, nano-hydroxyapatite particles seem to be homogenously distributed in the polymeric matrix. On this order of magnitude, the fabricated scaffold possesses some structural similarity with

natural bone. In vitro and also in vivo, this could circumvent the mainly found two step resorption by disintegration and dissolution of synthetic hydroxyapatite crystals, achieving the objective of homogeneous scaffold resorption by osteoclasts [35]. In this regard, experiments proofing the complete biodegradability as well as the biocompatibility of the fabricated constructs have to follow.

Additionally, it was shown that benchtop-MRI is appropriate for the evaluation of the hydroxyapatite distribution in scaffolds. A determination of the required concentration with regard on the particle size or rather the surface area of the hydroxyapatite is recommended for further method development. In the present study the benchtop-MRI results provided supplementary evidence for the small particle size of the incorporated hydroxyapatite.

The ESEM investigations have shown significant differences in the micro- and submicrostructure between the scaffolds containing the enzymatical crosslinked collagen compared to the scaffolds obtained from the standard formulation. In further investigations SAXS, TEM and AFM should also be applied to gain more comprehensive information about the hydroxyapatite particle size inside the enzymatical crosslinked scaffolds.

Chapter 6 – Characterization of physical scaffold properties

6.1 Introduction

A construct intended to be used as an implant to support bone healing has to meet several other requirements beyond the compatibility and biodegradability issues. The stability and the porosity are of particular importance. Logically, both properties stand contrary towards each other. The higher the void volume, the less solid content remains to build a stable matrix [2,132]. Accordingly, the reported fabrication strategies were intended as different compromises to ensure both.

Regarding the properties, high rigidity and stiffness are not always required, but in locations bearing mechanical load direct after implantation they are essential [133]. In contrast, an extraordinary high stability could be even disadvantageous. Too stiff constructs cause restrictions in the formation and remodelling of bone tissue, referred to as stress shielding [9,12,32]. Causative, it is suggested that mechanical stress in the extracellular matrix is spread to the cytoskeleton of the present cells and thereby it is converted into biochemical signals stimulating further bone formation [18,134]. By Wolff´s law, the consequence of this complex interplay in natural bone leading to the highly organized structure is expressed as follows: “the bony architecture aligns with the direction of principal stresses” [18]. Accordingly, to support bone healing an implant needs elastic properties to confer some mechanical stimuli onto the incorporated cells [134].

To enable the attachment and migration of cells inside as well as their survival within the matrix a system of interconnected pores throughout the scaffold is indispensable. Furthermore, it is the precondition for a sufficient diffusion and therefore necessary for the nutrient and oxygen supply of the cells and metabolite removal. Additionally, it provides space for developing vasculature [28,30,47,135]. The desired pore size is supposed to be 5-10 times of the cells diameter, or rather around 100-300 µm [63,115].

Concerning both the pore characteristics as well as the mechanical properties, no definite values are published describing the optimal scaffold for bone tissue engineering, as properly expressed by Dietmar Hutmacher as follows: "It is by no means clear what defines an ideal scaffold/cell or scaffold/neotissue construct, even for a specific tissue type" [2]. Thus it appears that for diverse applications in the field of bone tissue engineering, different requirements exist, opening a certain range for

the mechanical and porosity properties of the constructs to be contingently suitable. Several different constructs will therefore be required to evaluate which scaffold type is the best for the treatment of a special bone defect. If single properties should be related to the success of a therapy, they need to be well defined. Consequently, for a scientific evaluation of this issue, an accurate characterization of those scaffold properties is decisive.

To achieve this objective, several analytical techniques were used for the profound evaluation of the fabricated constructs. The mechanical properties were examined by compression testing and tensile testing. As typical methods for a survey on the porous character of scaffolds, mercury intrusion porosimetry and environmental scanning electron microscopy were used. Furthermore, the progressive method of contrast enhanced MRI was applied to gain a direct insight into mass transport velocities between the scaffolds and an aqueous surrounding.

Additional to the hollow cylindrical and DHT crosslinked hydroxyapatite-collagen-chitosan scaffolds, several other scaffold samples have been investigated by the mentioned methods. The mechanical testing as well as the porosimetric and microscopic evaluations were also carried out with the transglutaminase crosslinked scaffolds. PLGA scaffolds were examined using the contrast enhanced MRI analytics to check the applicability of the method for another sample type and to compare the results with the ones obtained for the scaffolds fabricated in this work.

6.2 Materials and Methods

6.2.1 Mechanical testing

Four variations of the non-mesh supported hollow cylindrical hydroxyapatite-collagen-chitosan scaffolds were investigated (table 3.2). The first was the blank construct without any crosslinking. The second was a scaffold strengthened by dehydrothermal treatment. The fabrication of the first two sample types is described at subitem 3.2.1. The third and the fourth were constructs with enzymatical crosslinked collagen, differing in the amount of transglutaminase used, as reported at subitem 3.2.2. All samples were cut transversal to obtain equal specimen heights of around 4 mm (tables 3.2 and 3.3), maintaining the hollow cylindrical geometry.

Tab. 3.2 Dimensions and quantity of the hollow cylindrical samples used for the compression testing of the hydroxyapatite-collagen-chitosan scaffolds

	Non-cross-linked scaffolds	**Crosslinked scaffolds** (DHT)	**Crosslinked scaffolds** (low TG & DHT)	**Crosslinked scaffolds** (high TG & DHT)
Number of samples	6	5	5	5
Height [mm]	4.37 ± 0.36	4.10 ± 0.20	4.08 ± 0.24	4.04 ± 0.15
Inner diameter [mm]	2.50 ± 0.00	2.50 ± 0.00	2.58 ± 0.13	2.60 ± 0.07
Outer diameter [mm]	7.63 ± 0.15	7.92 ± 0.04	6.90 ± 0.14	6.84 ± 0.15

Tab. 3.3 Dimensions and quantity of the hollow cylindrical samples used for the tensile testing of the hydroxyapatite-collagen-chitosan scaffolds

	Non-cross-linked scaffolds	**Crosslinked scaffolds** (DHT)	**Crosslinked scaffolds** (low TG & DHT)	**Crosslinked scaffolds** (high TG & DHT)
Number of samples	7	5	6	7
Height [mm]	4.11 ± 0.23	4.28 ± 0.08	4.23 ± 0.26	4.24 ± 0.22
Inner diameter [mm]	2.50 ± 0.00	2.50 ± 0.00	2.63 ± 0.05	2.53 ± 0.05
Outer diameter [mm]	7.64 ± 0.17	7.96 ± 0.11	6.85 ± 0.20	6.81 ± 0.49

Two different testing methods were applied, tensile testing and compression testing. The measuring equipment consisted of a load cell (ME-Meßsysteme GmbH, Hennigsdorf), two stepper motors for the adjustment of the indenter, one for the main traverse path and one for the fine tuning. The latter, was adjusted to a step size of 0.05 µm. Both were actuated by software developed by the IWM (Fraunhofer Institute for Mechanics of Materials Halle). The traverse path was determined by the step size of the fine tuning motor and the inductive range sensor 250 DC-SE-206 (Schaevitz™). The data acquisition was performed with a sampling rate of maximal 9600 Hz by the measuring amplifier Spider 8-30 (HBM, Darmstadt). For the tensile testing, the samples were fixed with Elastoplast® (Hansaplast Nr 1861, Hamburg) or Araldite® 2021 (Huntsman Advanced Materials, Texas US) glue at the specimen holder. The strain (ε_d) was determined using the following equation:

$$\varepsilon_d = \frac{\Delta h}{h_0} \cdot 100 \qquad 3.2$$

where Δh is the compression of the sample and h_0 is the initial height of the sample.

Details of the compression testing

The parameters were chosen as described in the test standard DIN 53 421, which is used for the evaluation of the stability and deformation properties of hard foams under uniaxial compressive stress [136]. The sample geometry, listed in table 3.2, was differing from the description of the test standard. Before the measurements

were started, a force of 7.9 mN was applied to fix the samples with the intender. A constant traverse speed of 1.45 mm/min was used for all experiments and maintained until a compression strain of 85 % was attained.

For the evaluation of the compression test, stress-strain curves were recorded. The compressive strength (σ_{dB}) and the modulus of elasticity under compression (E_d) also called bulk modulus were, determined using the following equations:

$$\sigma_{dB} = \frac{F_{\max}}{A_0} \qquad 3.3$$

$$E_d = \frac{\Delta F \cdot h_0}{\Delta h \cdot A_0} \qquad 3.4$$

where F_{max} is the force at maximum load and A_0 is the initial cross section surface area. The bulk modulus (E_d) is related to the slope of the linear region of the stress-strain curve.

Details of the tensile testing

The parameters were chosen as described in the test standard DIN EN ISO 1798:2008, which is used for the determination of tensile strength and elongation at break [137]. The sample geometry, listed in table 3.3, was differing from the description of the test standard. A constant tension speed of 2.2 mm/min was used until the samples were ruptured.

For the evaluation of the tensile test stress-strain curves were recorded and the tensile strength (R_m) was determined using the following equation:

$$R_m = \frac{F_{\max}}{A_0} \qquad 3.5$$

where F_{max} is the force at maximum load and A_0 is the initial cross section surface area. Young´s modulus of elasticity (E) was determined by Hooke´s law, using the elastic proportion of the stress-strain curve. The slope of the straight range usually at low values of stress and strain is defined as Young´s modulus [138].

6.2.2 Mercury intrusion porosimetry

The non-mesh supported hollow cylindrical hydroxyapatite-collagen-chitosan scaffolds were chosen as samples for the porosimetry investigation. It was intended to achieve a comparison between the pore sizes of the transglutaminase crosslinked and the non-transglutaminase crosslinked constructs. The measurements were

performed with a Quantachrome Poremaster (Quantachrome Instruments, Florida, US). The data evaluation was done by the Quantachrome Poremaster for Windows® Data Report software, version 1.07. The calculation of the pore size is based on Washburn´s equation. For the applied mercury a surface tension of 0.48 N/m and a material contact angle 140 ° were assumed. This is close to the values proposed by Elder et al. for comparable experiments [42].

6.2.3 Environmental scanning electron microscopy (ESEM)

By ESEM, the internal structure was compared between scaffolds containing the enzymatical crosslinked collagen and those with untreated collagen. Dry samples of the different hollow cylindrical hydroxyapatite-collagen-chitosan scaffolds were investigated with ESEM (Philips ESEM XL 30 FEG, Philips Electron Optics) in gas mode by detecting secondary electron images.

6.2.4 Mass transport measurements by MRI

Additional to the investigation of the hydroxyapatite-collagen-chitosan scaffolds, the mass transport measurements by MRI were performed with PLGA scaffolds. The full cylindrical constructs were kindly provided by Professor Dr. M. Schulz-Siegmund and Dr. M. Hacker (Department of pharmaceutical technology of the University of Leipzig). They were composed of the block copolymer poly(D,L-lactide-co-glycolide) (Resomer® RG 756 S, Boehringer Ingelheim Pharma GmbH & Co. KG, Germany) with a molar ratio of D,L-lactide to glycolide of around 75:25. For the fabrication, the technology described by Hacker et al. was applied [135].

Imaging of velocity differences in the mass transport

The measurement equipment and the general settings were described in chapter 1.

Mesh supported hollow cylindrical hydroxyapatite-collagen-chitosan scaffolds served as samples for the first experiments. To evaluate if BT-MRI is suitable for the imaging of velocity differences in the mass transport between scaffold and surrounding medium, some scaffolds were perforated using a 21 gauge canula (Fig. 3.9). Those samples were used as comparison specimens.

Averages of 16 single scans were used resulting in a complete measuring time of about 10 min. Mass transport between scaffolds and surrounding medium was observed by means of dynamic contrast agent-enhanced MRI using the conserved

phosphate buffer (see chapter 2) containing 1 mM gadolinium(III)-diethylamine-pentaacetic acid (Gd-DTPA). Images were recorded before and at several time periods after replacing the incubation buffer with Gd-DTPA buffer. By means of the IDL type RI Image Display software version 1.0.2. (Oxford Instruments) the obtained image data were used to generate intensity profiles for the quantification of velocity differences of the contrast agent penetration. An average of twelve parallel profiles, all acquired in the indicated central region, was created for each image (Fig. 3.10).

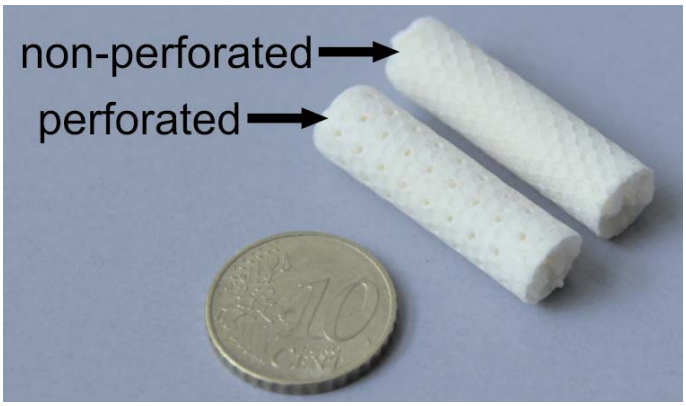

Fig. 3.9 Photograph of a perforated and a non-perforated scaffold next to a 10 ct coin for size comparison

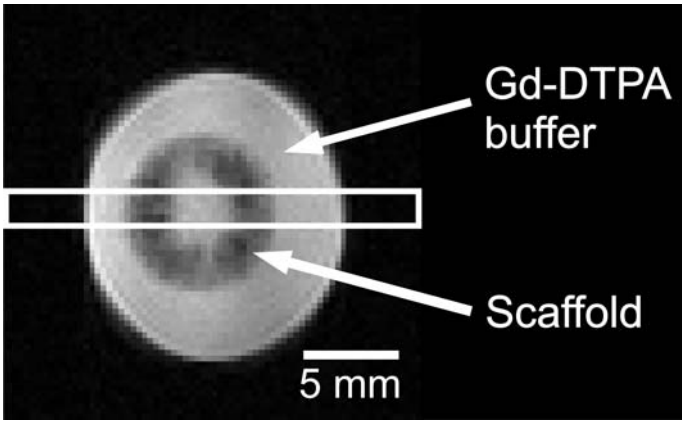

Fig. 3.10 MR image representative for one stage of the contrast agent penetration into the scaffold, the area inside the white frame was used to generate the intensity profiles

Optimization of the method

In order to advance the introduced dynamic contrast agent-enhanced benchtop-MRI analytic, several developments and investigations were made to improve the method. (1) To facilitate the investigation of different scaffold types, a second fixture was developed for a more easy and reliable location of the sample inside the imaging vessel (Fig. 3.11).

(2) To set a fixed maximum intensity in the images, a capillary filled with a reference solution was additionally positioned next to the sample within the new fixture (Fig. 3.11). A solution of 0.83 g/l gadolinium(III)-diethylaminepentaacetic acid (Gd-DTPA) in conserved phosphate buffer was used for this purpose.

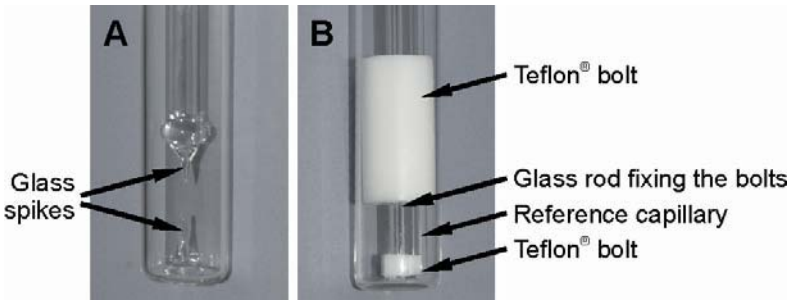

Fig. 3.11 Imaging vessels for fixation and incubation of the scaffolds during the MRI experiments, (A) equipment for scaffold fixation between two glass spikes and (B) equipment for the adjustment of a scaffold next to the reference capillary with two Teflon® bolts

(3) Dynamic contrast agent-enhanced MRI experiments were additionally carried out with the PLGA scaffolds of a pore size range of 100 – 200 µm. The results were used to check the applicability of the method for this scaffold type and to compare the velocities of the mass transport with results obtained for the hydroxyapatite-collagen-chitosan scaffolds.

(4) To achieve a decelerated contrast agent penetration the application of a high molecular weight contrast agent named Gd-DTPA-HES was tested. It is composed of several Gd-DTPA complexes bonded on chains of hydroxyethyl starch (HES). Synthesis and characterization of this polymeric contrast agent are described in detail by Besheer [139]. Gd-DTPA-HES with a molar substitution of DTPA of 18 mol% and a molar mass of the uncoupled HES of 70,000 g/mol was applied. For the experiments a solution of 1.57 g/l of Gd-DTPA-HES in conserved phosphate buffer (see chapter 1) was used.

Imaging of mass transport and gas release in PLGA scaffolds

Dynamic contrast agent-enhanced MRI was carried out with the PLGA scaffolds of a pore size range of 100 – 200 µm and of 200 – 500 µm using the already mentioned Gd-DTPA-HES solution. The experimental conditions were applied as described above and in the general settings of the benchtop-MRI in chapter 2. For long time storage over weeks, the samples were maintained in the imaging-vessels and placed

in an incubator at (37 ± 1) °C. Additional to the slices perpendicular to the main magnetic field, one parallel slice was recorded for the imaging of the gas release.

6.3 Results and Discussion

6.3.1 Mechanical testing

Remarkable differences in the mechanical properties were found between the scaffolds with the transglutaminase crosslinked collagen and those containing untreated collagen. The results obtained for the non-enzymatical treated samples strongly deviate from the typical behaviour of a solid spongy construct exposed to mechanical stress. As the outcome is much more representative, the evaluation of the scaffolds containing the enzymatical crosslinked collagen is described first.

In the stress-strain curve of the compression testing an almost linear increase of the strain is visible for stress values below 0.04 N/mm^2 for the scaffolds crosslinked with 5.66 Units transglutaminase (figure 3.12, low TG). This segment of the curve indicates the elastic portion. It is referred to the compression of the porous structure. The slope was used for the calculation of the bulk modulus [140]. The results are given in table 3.4. For further increasing strain, the curve shows an inflexion point, the yield point. It indicates the end of the elastic deformation. More pressure resulted in structural damage termed plastic deformation.

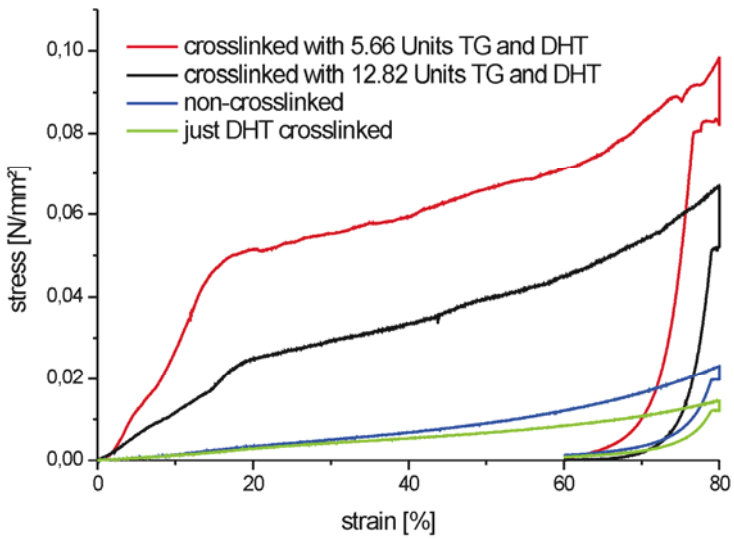

Fig. 3.12 Compression testing stress-strain curves of the four different types of hydroxyapatite-collagen-chitosan scaffolds, shown curves are results of a representative single measurement

Tab. 3.4 Results of the evaluation of the mechanical testing

	Non-cross-linked scaffolds	**Crosslinked scaffolds** (DHT)	**Crosslinked scaffolds** (low TG & DHT)	**Crosslinked scaffolds** (high TG & DHT)
Compressive strength σ [N/mm^2]	0.032 ± 0.019	0.017 ± 0.002	0.145 ± 0.078	0.079 ± 0.010
Bulk modulus E_d [N/mm^2]	0.013 ± 0.006	0.009 ± 0.003	0.197 ± 0.102	0.140 ± 0.092
Tensile strength R_m [N/mm^2]	0.010 ± 0.002	0.012 ± 0.001	0.033 ± 0.013	0.022 ± 0.013
Young´s modulus E [N/mm^2]	0.098 ± 0.034	0.107 ± 0.049	0.409 ± 0.206	0.600 ± 0.490

For the tensile testing at low strain values, an almost linear increase of the stress is also visible in the stress-strain curve (figure 3.13). This portion of the curve is referred to the elastic length expansion of the specimen. The slope was used for the calculation of Young´s modulus [140,141]. The results are given in table 3.4. For further increasing strain, the curve shows a stress maximum. It indicates the rupture of the sample. Beyond the maximum, usually no more stress can be applied by further increasing strain. An additional local maximum as found in figure 3.14 (orange curve) is indicative for a non-uniform rupture. It points to a poor reproducibility of the measurement due to different ways of failure. The described results are typical for solid constructs with a porous internal structure. The elastic portion of the stress-strain curve found under compression as well as under tension is due to the extent of construct distortion provided by reversible deformation of the single pores. The calculated values of the tensile and the compressive strengths and both moduli as well as the shapes of the stress-strain curves suggest that the scaffolds crosslinked with 5.66 Units transglutaminase (low TG) possess stronger mechanical properties than the constructs crosslinked with 12.82 Units of the enzyme (high TG). Future investigations should focus on a proof and explanation of this assumption and the optimization of the applied enzyme concentration.

The stress-strain curves obtained from the non-crosslinked and the just dehydrothermally treated samples are quite similar for the compression testing as well as for the tensile testing (Fig. 3.12 and 3.13). The shape of the curves reveals that the mechanical properties of both non-enzymatical treated scaffold types strongly deviate from the typical mechanical behaviour of porous solid constructs. They possess no yield point, no stress maximum and hence no elastic portion. These outcomes complicate the calculations of bulk modulus and Young´s modulus. Consequently, the segments of the stress-strain curves below 0.1 % strain were used

for the calculation of both moduli. In contrast to the enzymatical treated scaffolds, no definite peak indicating the point of rupture was found in the stress-strain curves of the tensile testing. The slower increase and the much lower maximum of the curves points more on a steady fraying out instead of a sudden rupture of the scaffold (Fig. 3.13).

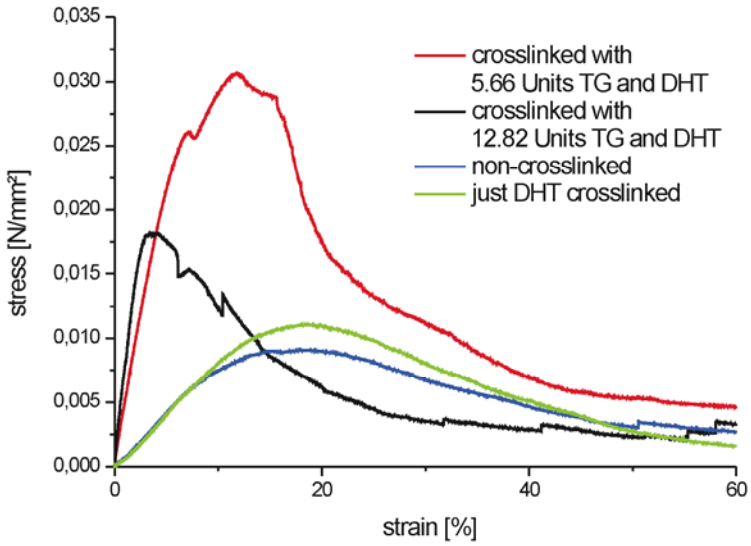

Fig. 3.13 Tensile testing stress-strain curves of the four different types of hydroxyapatite-collagen-chitosan scaffolds, shown curves represent mean curve progressions averaged from all performed measurements

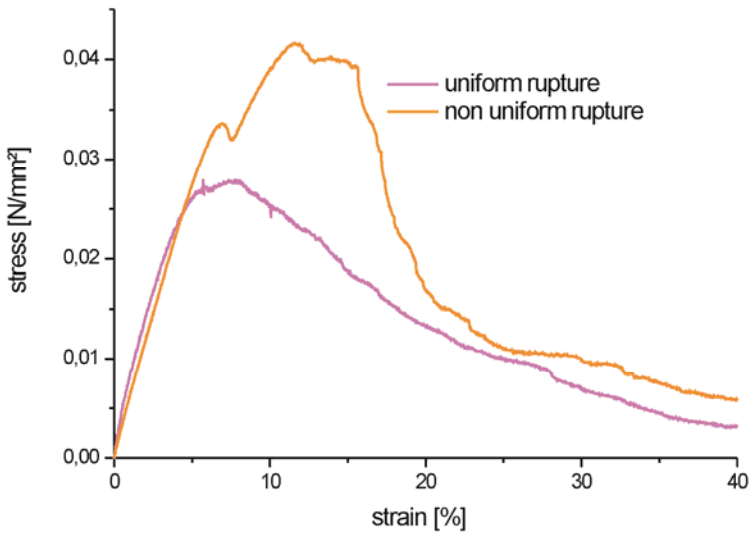

Fig. 3.14 Tensile testing stress-strain curves of two single measurements of the hydroxyapatite-collagen-chitosan scaffolds crosslinked with 5.66 Units transglutaminase, the curve shape points on different progression of the rupture processes

The overall obtained results are appropriate for a comparison of the mechanical properties of the different analyzed constructs. It was shown that the enzymatical treated scaffolds are much more resilient against compression and tension than the non-treated ones. Compared to natural human bone, all investigated samples exhibit poor mechanical stability. Even the mechanical weaker bone type, the trabecular bone, possesses around forty to two thousand fold higher values of tensile strength and bulk modulus than the enzymatical crosslinked hydroxyapatite-collagen-chitosan scaffolds [138,140]. The strategy to support bone regeneration by a scaffold mimicking the cartilaginous template during endochondral bone formation was already mentioned in the introduction (see chapter 1). Regarding this strategy, it appears more relevant to compare the experimental data with published mechanical properties of cartilage than with those of bone. For articular cartilage a bulk modulus of around 1 N/mm^2 is reported. This is still five to then times higher than the values measured for the enzymatical cross linked hydroxyapatite-collagen-chitosan scaffolds [142,143]. Concerning this matter, Chen and Boccaccini mentioned that “it might not be necessary to have a starting scaffold with a mechanical strength equal to that of bone because cells and extracellular matrix secreted by cells in vitro or in vivo can increase the scaffold strength” [39]. For Young´s modulus of tissue engineered cartilage constructs this issue was experimentally proven by Kasaharan et al. [144]. Compared to soft cartilage, the hydroxyapatite-collagen-chitosan scaffolds show up to five times enhanced Young´s moduli. Even the non-enzymatical treated samples are in the same range as the natural tissue for this measure [143].

For freeze dried collagen sponges of comparable solid matter content, Young´s modulus is reported to be around 5 kPa [145]. This is around twenty times less than the values obtained for the non-enzymatical treated hydroxyapatite-collagen-chitosan scaffolds. Hence, it seems as if the presence of the hydroxyapatite-collagen composite material and/or the chitosan within the formulation yield improvements in the mechanical stability of freeze dried collagen sponges. Comparing the measured bulk modulus with data reported for the commercially available collagen scaffolds from Becton Dickinson this assumption is relativised [146]. Because the values of the non-enzymatical treated scaffolds are lower. Whereas, the bulk moduli of the trans-glutaminase cross linked scaffolds are around four times higher [146]. In contrast, porous composite scaffolds with more than 50 % (wt) of Poly(α-hydroxy acids) in the solids content mainly have much higher mechanical stability than the hydroxylapatite-

collagen-chitosan scaffolds and are also stronger than natural cartilage [39]. The glutaraldehyde crosslinked β-tricalcium phosphate-alginate-gelatin hybrid scaffold reported by Eslaminejad et al. appears to be more comparable with the constructs fabricated in the present study. The described scaffold is intended to be used in bone tissue engineering and its compressive strength is in the same range as the value of the enzymatical treated scaffolds. But the bulk modulus is around ten fold higher, even than the value for the enzymatical treated scaffolds [147].

A definite comparison with published data about scaffold systems from other research groups appears complicated. It should be done with care because no established standards, specified for the biomechanical testing of bone or bone tissue engineering scaffolds, have been available in the literature. Therefore, lots of the published data are inaccurate as mentioned by Keller and Liebschner [138]. In this scope, they point on specific reasons for the poor situation and give proposals for advancement. To avoid the variation in sample geometry a specimen height of at least 10 mm and a diameter of 6 to 8 mm is proposed for cylindrical samples [138]. Unfortunately, just the sample diameter was in this range (tables 3.2 and 3.3). An underestimation of Young´s modulus and of the compressive strength could result from a non-parallel alignment between top and bottom surface [138]. This was possibly a systematic error in the performed examination because an exact cutting of the scaffolds by hand using a razor blade was quite difficult. It was not possible to fully prevent such misalignments.

In most parts of the natural skeleton, the mechanical characteristics of a bone specimen vary when the stress is applied from different directions [140,141]. According to the fabrication procedure and particularly due to the hollow cylindrical geometry, it is reasonable to suggest such anisotropy also for the scaffold specimens. Hence, the tests should be performed in several different directions for a more extensive characterization. Commonly, four different methods of mechanical stress tests were applied in the field of bone tissue engineering. Those investigate tension, compression, bending and torsion [140]. In future experiments all four should be performed for a comprehensive analysis of the mechanical properties of a scaffold. The complexity of an analytical determination is even boosted by the diversity of the mechanical stresses under natural physical strain. In contrast, defined experimental conditions are required to ensure sufficient reproducibility. Hence, just single components or simple combinations of the multiple force effects can be

evaluated. Additionally, the result interpretation of mechanical stress tests of constructs for bone tissue engineering is complicated due to little knowledge about an exact objective, as already mentioned in the introduction of this chapter. Beside this limitation, the absence of water or body fluids in the investigated samples makes it impossible to refer the results to stress occurring in vivo [148]. Due to the fluid component, emerging mechanical energy is partially dissipated. This property is called viscoelasticity. It leads to non-linear mechanical behaviour and is typical for biological tissues [138,141]. A comprehensive survey article about theoretical models describing the interaction of the solid and fluid phases in bone was published by Cowin [149]. The preferred model is based on Biot's theory [150,151]. It considers bone as fluid-saturated, porous, and elastic solid [149]. Upon loading, the extracellular fluid is squeezed through the bone matrix. The boundary friction between solid and fluid phase resulted in an attenuation of the impact force, whereas the elasticity of the solid phase additionally accounts for the reversibility of the deformation [10,149]. Because of the absence of elastic portions in the stress-strain curves of the non-enzymatical treated samples, it is suggested that even very slight stresses lead to permanent scaffold deformations or rather structural damages. Consequently, non-enzymatical treated, non-mesh enforced constructs seem to be not suitable for bone tissue engineering in load bearing applications. Especially, in the common approaches of mechanical stimulation during scaffold cultivation such constructs could fail due to the poor elasticity [148]. Hence, future experiments should rather focus on the enzymatical treated samples. But for a concluding remark, the elasticity has to be characterized during incubation in aqueous medium. Additionally, mechanical properties should be analyzed on the micro- and nanoscale by atomic force microscopy. It was shown by Rehfeld et al., that key markers of early osteogenic lineages were expressed by mesenchymal stem cells when the elasticity of the microenvironment corresponds to the elasticity of the pre-mineralized bone matrix [134].

Regarding the scaffold fabrication, improvements of the mechanical stability could be achieved by increasing the solid fraction in the formulation. Therefore, a collagen dispersion of higher concentration would be required, to keep the proportions between the components. Alternatively, the 1 % collagen dispersion could be lyophilized and reconstituted with less dispersant.

It has to be kept in mind that all the presented data about the mechanical properties of the scaffolds were obtained with non-mesh supported scaffolds. It is quite certain, that the PGA surrounding has a substantial stabilizing impact on the mechanical features of the constructs. Prospective, several layers of the mesh surrounding or variations of the mesh material could be used to tune the scaffold properties towards tailored characteristics.

6.3.2 Mercury intrusion porosimetry

No successful measurement was achieved with the non-transglutaminase crosslinked scaffolds due to the compression of the samples. It is supposed that the weak mechanical stability and small pore sizes prevented the required mercury intrusion. The entire sample was irreversibly compacted by the raising mercury pressure during the experiment.

The pore sizes of the crosslinked scaffolds fabricated using two different amounts of transglutaminase were found to be quite similar. A number weighted average pore size of about 60 µm was determined for all measured samples. The detailed results are presented in table 3.5. One example plot of a calculated pore size distribution is shown in figure 3.15. The cumulative frequency plot reveals that in all samples 50 % of the pores are larger than 65 µm and more than 15 % are larger than 100 µm. Therefore, it can be assumed that the application of transglutaminase in the scaffold fabrication leads to a significant change of the internal scaffold structure towards more stable and larger pores. However, the size of most of the pores is still below the necessary minimal value of 100 µm, reported for bone tissue engineering applications [63,115,132]. Most of the publications about the characterization of scaffolds evaluate pore size data by the traditional methods of porosimetry and microscopy [19,42]. For comparability reasons, these methods have also been applied in the present study.

In the literature different opinions were reported regarding a specific optimal pore size [2,27,39,63,132]. For a successful outcome, the interconnectivity of the pores is mentioned to be the more critical factor, being a precondition for the migration of cells and adequate mass transfer throughout the scaffold [2,132,152]. Hence, the permeability of a construct would be an important attribute to prove its interconnectivity.

Mercury intrusion porosimetry is known for its limitations regarding the analytics of irregular pore geometries [2]. In future investigations complementary results could be obtained by measurements of the surface adsorption of nitrogen by the Brunauer-Emmet-Teller method as reported by Gelinsky et al. or by micro-computed tomography as reported by Hutmacher and Ann [2,104].

Tab. 3.5 Results of the pore size evaluation by mercury intrusion porosimetry

	sample	Most frequently occurring pore size	50 % cut-off pore size value	Proportion of pores bigger than 100 µm
Scaffolds crosslinked with 5.66 Units TG	1	60.3 µm	70.0 µm	19 %
	2	60.8 µm	65.8 µm	18 %
Scaffolds crosslinked with 12.82 Units TG	1	58.0 µm	64.7 µm	17 %
	2	64.5 µm	64.9 µm	16 %

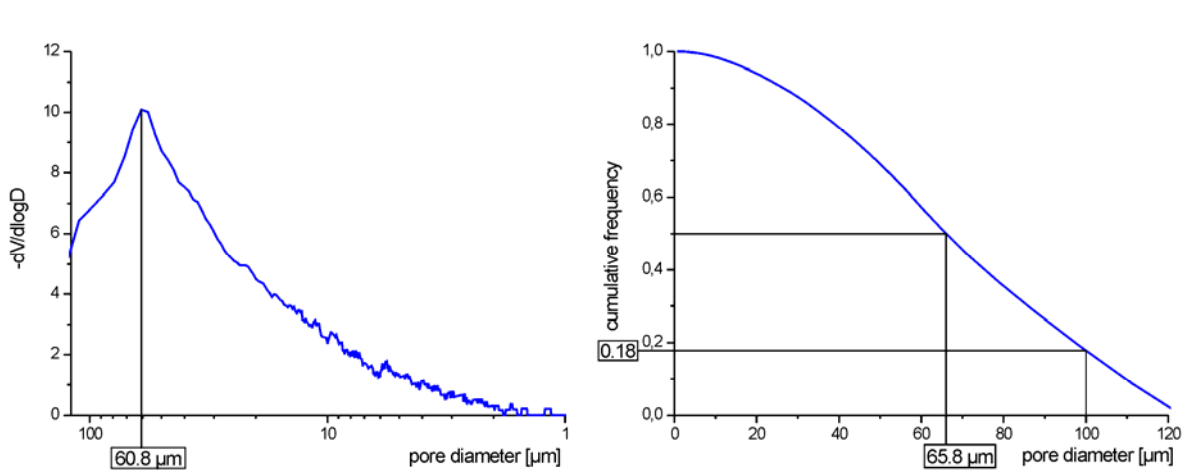

Fig. 3.15 Example plots of the porosimetry data of the second sample of the scaffold crosslinked with 5.66 Units transglutaminase, pore size distribution (left), cumulative frequency plot (right)

6.3.3 Environmental scanning electron microscopy (ESEM)

The ESEM images show the high porous internal structure of the hollow cylindrical hydroxyapatite-collagen-chitosan scaffolds (figure 3.16 top row). It is obvious that the pores are larger in the scaffold containing the enzymatical crosslinked collagen. This conclusion is confirmed by the results of the impinging light microscopy (figure 3.16 bottom row). Possibly, this outcome reflects the more associated state of the collagen caused by the crosslinking. Such findings are reported in the literature as well. Garcia et al. also prepared collagen scaffolds using transglutaminase. He concluded that “Pores of the cross-linked scaffold are larger

than their equivalents in the native scaffold due to the tighter assembly of the collagen fibrils." [153].

An exact value for the mean pore size was not specified. Such estimation is complicated due to the high variability of the size and the shape of the single pores.

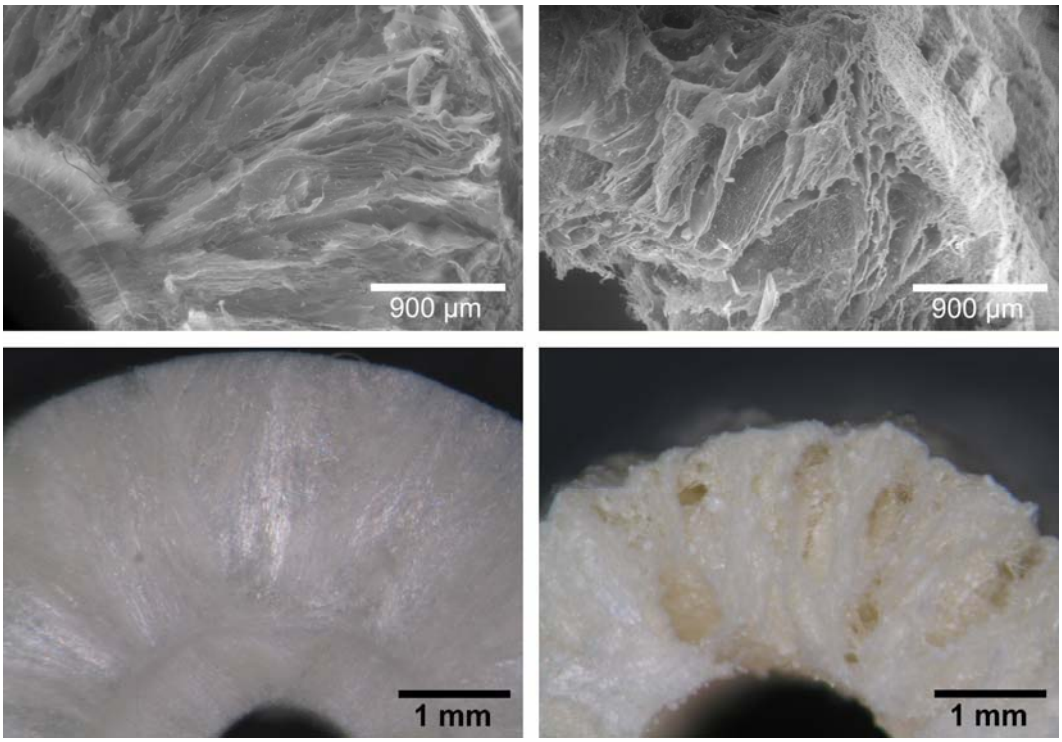

Fig. 3.16 Microscopic images of cross sections of the hydroxyapatite-collagen-chitosan scaffolds, ESEM images (top row), impinging light microscopic images (bottom row), non-crosslinked construct (left), scaffold crosslinked with 5.66 Units transglutaminase (right)

6.3.4 Mass transport measurements by MRI

Imaging of velocity differences in the mass transport

The results of the dynamic contrast agent-enhanced MRI experiments are shown in figure 3.17. It is obvious that the contrast relations in the images are strongly changing through the addition of the contrast agent. Before buffer exchange, the highest signal intensity was generated by the protons of bound water inside the scaffold, visible as more bright area in the MR image. After replacing the buffer by Gd-DTPA buffer, the inverse situation was observed. The water protons of the surrounding medium have generated higher signal intensity due to the presence of the positive contrast agent Gd-DTPA, which reduces the T1 relaxation time of the water protons drastically. The delay of the contrast agent penetration into the scaffold is indicated by its darker appearance. Through the progression of the Gd-DTPA

penetration, the intensity of the scaffold enhances. Hence, the contrast decreases, as observed in the images of the following time periods. An acceleration of the contrast agent penetration for the perforated scaffold compared to the non-perforated one can be assumed from the images (Fig. 3.17). About one hour after the Gd-DTPA buffer addition the almost complete permeation of the perforated scaffold is apparent. In the non-perforated scaffold, more or less contrast agent free regions can still be seen as dark points after one hour.

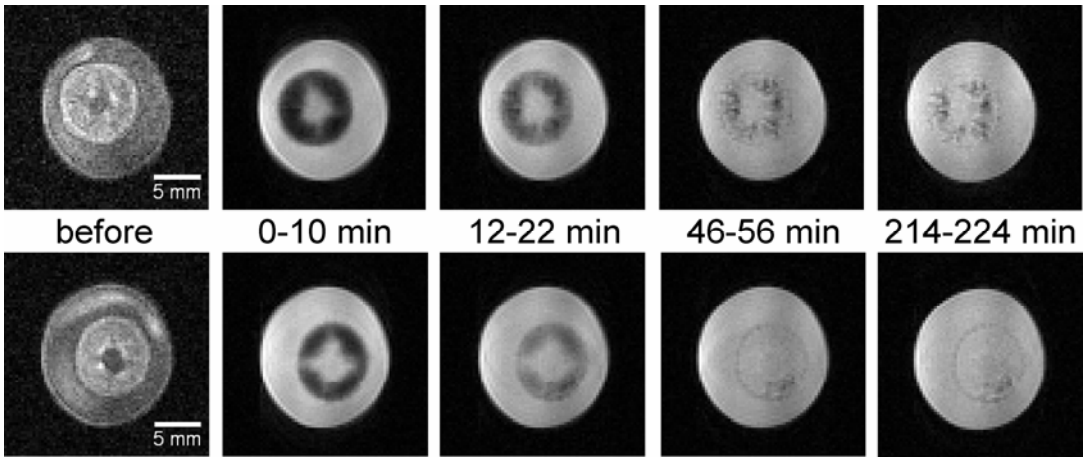

Fig. 3.17 Penetration of Gd-DTPA into scaffolds, MR images averaged before and at different time periods after the contrast agent addition, (top row) not perforated scaffold and (bottom row) perforated scaffold

The profiles also show the compensation between the intensities of the buffer and the scaffold by time, reflecting the contrast decrease in the images (Fig. 3.18). The declining signal intensity of the buffer is due to the concentration decrease of the contrast agent. This is caused by Gd-DTPA free buffer leaving the scaffold during the experiment, whereas the signal enhancement of the scaffold is the result of the proceeding penetration of Gd-DTPA. After one day of incubation with the contrast agent there are still differences in the signal intensity between the scaffold and the surrounding medium. Nevertheless these profiles are representative for the stage of the full penetration into the matrix. The reason for the differences in the signal intensity is the density effect of the scaffold. In other words, the volume taken up by the scaffold material is not accessible for protons and Gd-DTPA, which are responsible for the intensity. The differences between the perforated scaffold and the non-perforated one become more obvious in the profiles. The intensity values for the perforated scaffold at around 1 hour and at 1 day after the contrast agent addition are nearly the same.

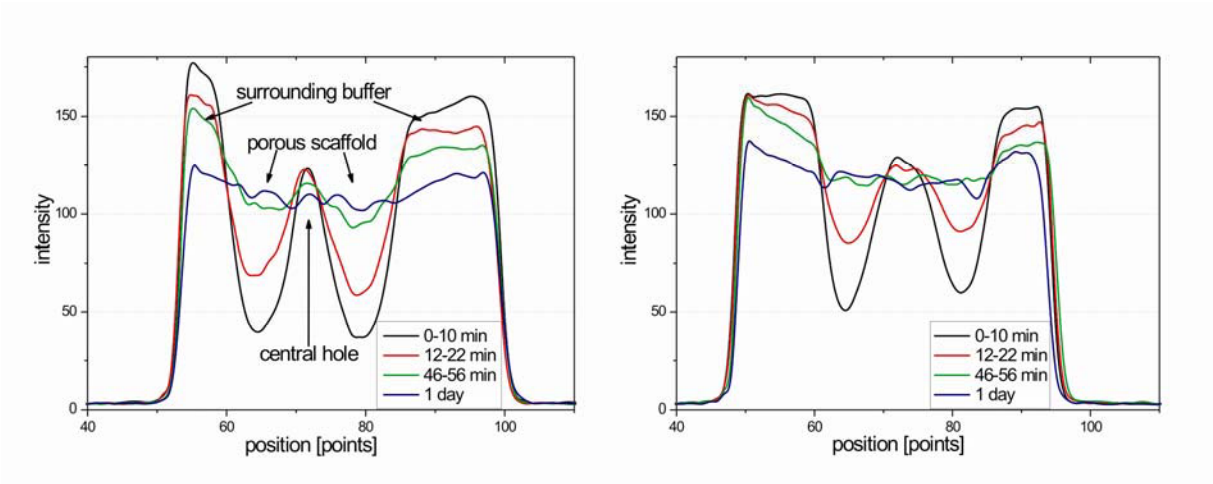

Fig. 3.18 Penetration of Gd-DTPA into scaffolds, intensity profiles averaged from twelve slices through each image of the different time intervals after the contrast agent addition, (left) not perforated scaffold and (right) perforated scaffold

In the profiles of the non-perforated sample, an alteration of the intensities is still visible between these time points, representative for the incomplete penetration after 1 hour. Additionally, the intensity of the perforated scaffold at 12 to 22 min after the contrast agent addition has already reached around half of the rate between the 0 to 10 min and the 1 day values, whereas the intensity of the non-perforated scaffold has just one third of the values between the same time points. Both observations indicate clearly the higher penetration velocity of Gd-DTPA into the perforated scaffold. The results are suggestive of the mass transport between scaffolds and surrounding medium, revealing the duration of the hindered diffusion. It is well established that the pore size in scaffolds should be larger than 100 µm to prevent cells from deficiencies in oxygen and nutrient supply [63,132]. However, the pore size is typically measured microscopically in dry state. During incubation in culture medium or body fluids, many scaffold materials are in a swollen state. Hence, the actual space for diffusion processes may vary between two scaffold samples of the same nominal pore size due to the different composition. Dynamic contrast agent-enhanced MRI experiments can provide more relevant data, because a direct visualization of the velocity of mass transport throughout the matrix is obtained [65]. In this study, such processes inside the scaffold have been followed up by means of Gd-DTPA, achieving the proof of principle that dynamic contrast agent-enhanced experiments are feasible by BT-MRI. The enhancement of penetration by large interconnected pores was clearly demonstrated. Passive diffusion is sufficient for mass transfer from capillaries to cells over a distance up to 200 µm [20]. For more complex constructs, a vascularisation of

the matrices is essential as angiogenesis is a prerequisite for bone formation in general [154]. Large interconnected pores do not only ensure the sufficient oxygen and nutrient supply and metabolite removal by passive diffusion, but also provide space for growing blood vessels. Experiments with contrast agents of higher molecular weight provide more inside in this field. The perfusion through a vascular system can be examined by macromolecular contrast agents, which are barely penetrating the endothelium of the vessels [155]. The migration of signalling proteins like growth factors through a matrix could also be simulated by this method delivering a contrast agent of comparable properties directly into the matrix.

Optimization of the method

(1) The glass equipment facilitated an exact sample positioning for the hollow cylindrical constructs, due to the glass spikes plunging into the central hole of the scaffolds (Fig. 3.19 A). The smaller cylinder height and the planar base and top area complicate this type of fixation for the PLGA scaffolds (Fig. 3.19 B). Even damages could be caused by the penetration of the glass spikes. This drawback was completely avoided by the developed Teflon® fixture (Fig. 3.19 C and D).

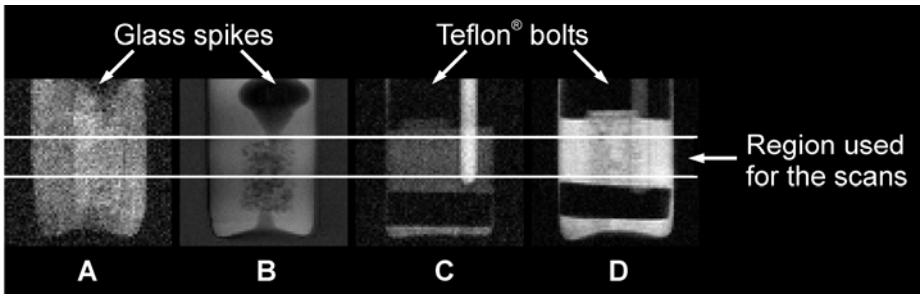

Fig. 3.19 MR images of scaffold slices parallel to the main magnetic field, (A) hydroxyapatite-collagen-chitosan scaffold fixed with glass spikes, (B) PLGA scaffold fixed with glass spikes and PLGA scaffolds next to the reference capillary fixed with Teflon bolts (C) in buffer without contrast agent and (D) in buffer with contrast agent

(2) The maximum intensity in the images changed at different stages of the contrast agent penetration, as visible in the middle row of figure 3.20. Thus, an absolute quantitative evaluation was impossible. The magnitude of this variation is even more apparent in the intensity profiles (Fig. 3.16). In the top row of figure 3.20 the advantage of the reference capillary is obvious. The Gd-DTPA concentration in the capillary is 1.5 times higher than in the surrounding buffer. Hence, it generates the maximum intensity in the images. Intensity alterations of the incubation medium

during the experiment are the logical consequence of the mass transfer, but with the reference this is no longer influencing the maximum intensity. Before the contrast agent addition the maximum intensity is solely dominated by the reference capillary. Thus, the intensity difference between scaffold and surrounding medium is very low. In consequence, the scaffold is not visible (Fig. 3.20). This disadvantage could only be prevented when the reference capillary is removed for the initial imaging.

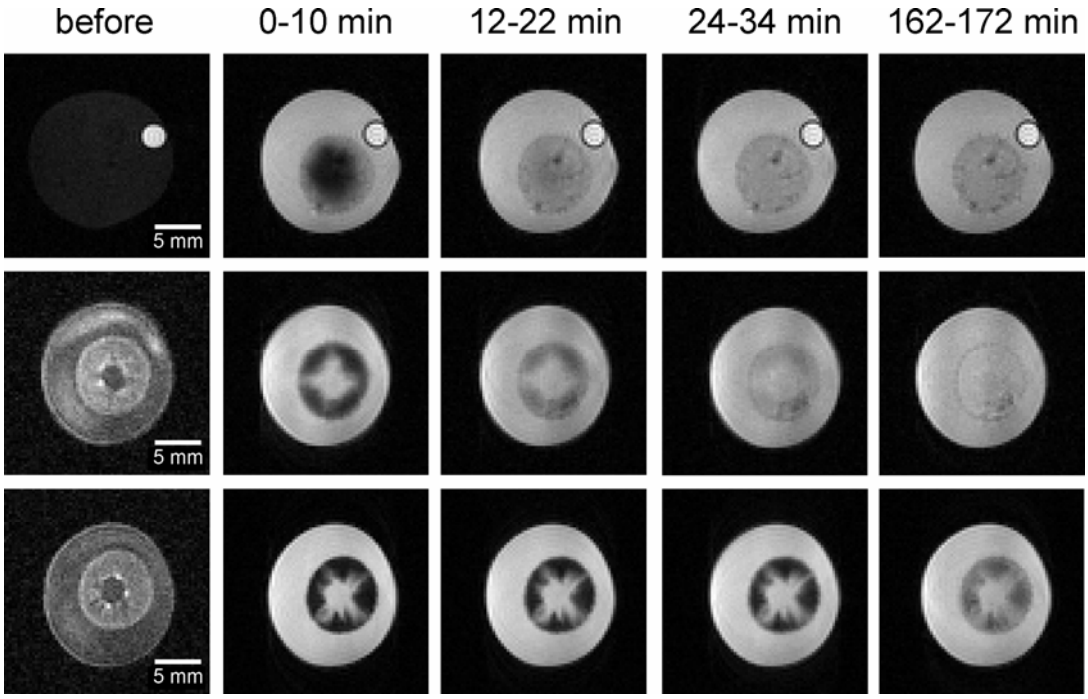

Fig. 3.20 MR images averaged before and at different time periods after the contrast agent addition, (top row) Gd-DTPA penetration into a PLGA scaffold with a pore size range of 100 to 200 µm, (middle row) Gd-DTPA penetration into a perforated hydroxyapatite-collagen-chitosan scaffold and (bottom row) Gd-DTPA-HES penetration into perforated hydroxyapatite-collagen-chitosan scaffold

(3) The first result of the dynamic contrast agent-enhanced MRI experiment with a PLGA scaffold (pore size range of 100 to 200 µm) is shown in the top row of figure 3.20. Gd-DTPA is penetrating very fast through the whole construct. Within around 20 min, the scaffold and the surrounding medium are almost at the diffusion equilibrium. Two conclusions were drawn from this result. First, even with perforations the mass transport within the hollow cylindrical hydroxyapatite-collagen-chitosan scaffolds is slightly more restricted than in PLGA scaffolds with a pore size between 100 to 200 µm (figure 3.20). Second, for comparative investigations of PLGA scaffolds with bigger pore sizes than 200 µm the experimental conditions have

to be modified to either slow down the contrast agent penetration or to scan for shorter time periods.

(4) As reported before, the full penetration of the Gd-DTPA into the perforated hollow cylindrical hydroxyapatite-collagen-chitosan scaffold is assumed to be completed after one hour. By the application of the macromolecular contrast agent a significant deceleration of the contrast agent penetration was achieved. Even after around three hours the diffusion equilibrium was not reached (figure 3.20, bottom row). Additionally, the quality of the obtained images is much better by the application of Gd-DTPA-HES instead of Gd-DTPA. The contrast is clearer and therefore more details of the internal scaffold structure are visible. Probably two reasons account for this outcome. The first is the more intense MRI signal enhancement of Gd-DTPA-HES, due its higher relaxivity [139]. The second is the higher molecular weight of Gd-DTPA-HES compared to Gd-DTPA. The different size of the contrast agent molecules substantially influences their distribution characteristics. Below a certain dimension, the domains inside the scaffold could only be attained by the smaller Gd-DTPA. Consequently, the internal scaffold structures at the visible scale are more clearly reflected using the high molecular weight contrast agent.

Imaging of mass transport and gas release in PLGA scaffolds

A distinct variability was found in the velocity of the mass transport between the surrounding medium and different regions of one PLGA scaffold (Fig. 3.21). Whereas in some locations the contrast agent penetrates from all sites around into the scaffold core, in others it just enters from one site. This leads to remarkable differences in the time spans necessary for reaching the diffusion equilibrium and hence complicates the comparability with other samples. Probable reasons for this outcome could be a polymer film at one site of the scaffold remaining from the fabrication or inhomogeneities of the structure or the size of the internal pores.

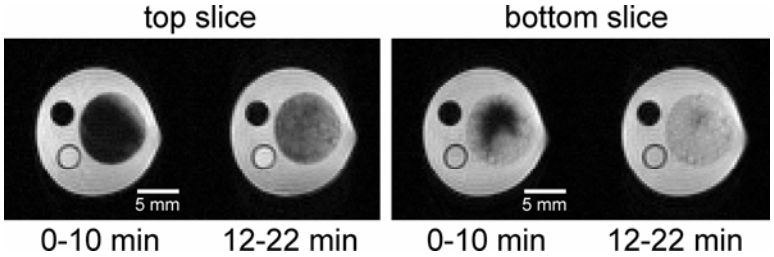

Fig. 3.21 MR images of the Gd-DTPA-HES penetration into a PLGA scaffold, the difference between the two slices is indicative for variations in the mass transport in different regions of the construct

One example somehow demonstrative for the impact of the pore size on the mass transport velocity is shown in figure 3.22. After 12 - 22 min the difference in the contrast agent penetration velocity between the samples with differing pore sizes is already obvious. For further investigations and more detailed conclusions special attention has to be drawn first, on all available slices of one scaffold and second, on the reproducibility with several samples.

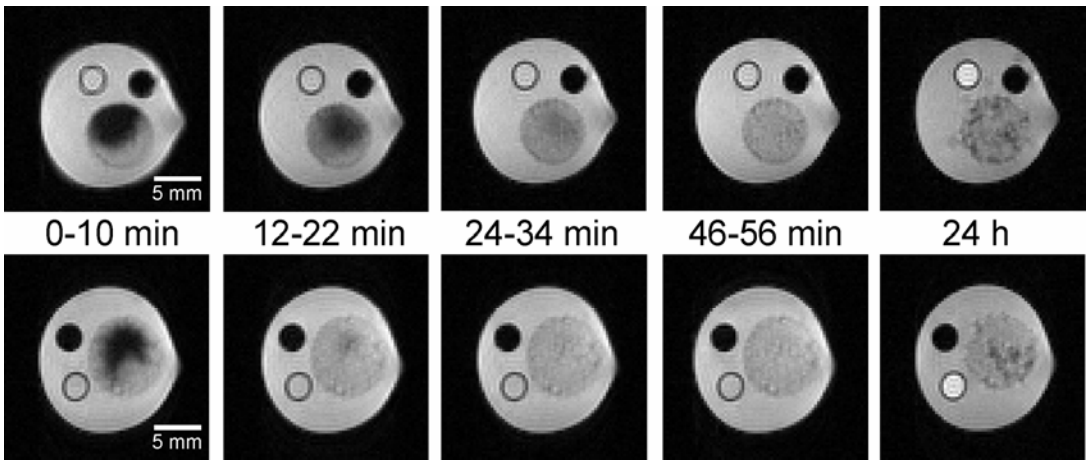

Fig. 3.22 Penetration of Gd-DTPA-HES into PLGA scaffolds, MR images averaged at different time periods after the contrast agent addition, (top row) scaffold with a pore size range of 100 to 200 µm and (bottom row) scaffold with a pore size range of 200 to 500 µm

During the investigation, it was discovered that in images taken after 24 hours of incubation again dark areas appear inside the scaffold (Fig. 3.22). Since this area was brighter in the image of the same sample in time steps before, this finding could not be related as region of delayed contrast agent penetration. After 72 hours of incubation small gas bubbles were visible leaking out of the scaffold surface. For this reason the incubation was continued and the imaging was focused on the emerging gas volume. The feasibility to investigate the formation of gas volumes inside aqueous surroundings by benchtop-MRI was already reported before by Strübing et al. for carbon dioxide in matrix tablets [69]. Due to the complete absence of protons in the gas bubbles this volumes also appear as black areas in the MR images. The reason for the appearance of the gas found in the PLGA scaffolds is not known. Probably very small gas bubbles were incorporated into the polymeric matrix of the scaffold during its fabrication. Upon incubation the PLGA becomes hydrated and hence more flexible, allowing the gas bubbles to merge. By time more and more gas

is released giving rise to one big accumulation of gas inside the scaffold close to the surface of the incubation medium as visible in figure 3.23.

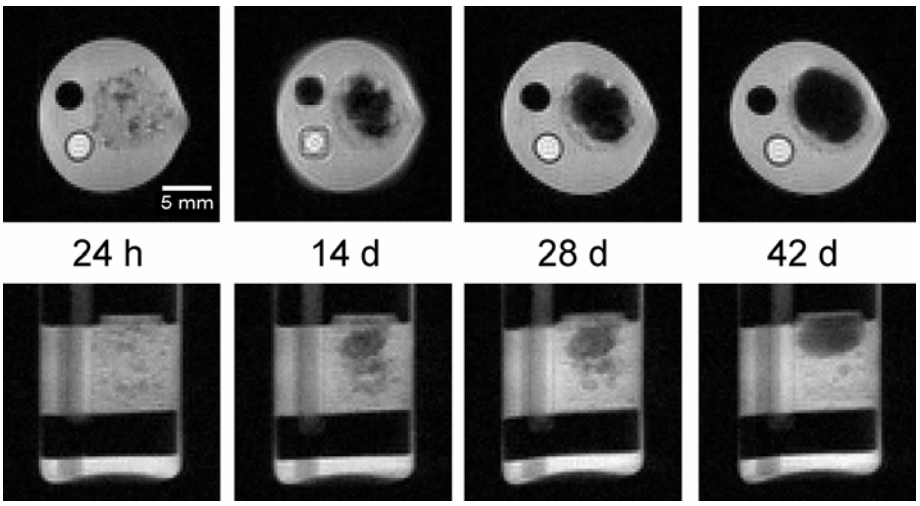

Fig. 3.23 MR images showing the gas accumulation inside a PLGA scaffold with a pore size range of 200 to 500 µm as a result of the incubation in the Gd-DTPA-HES containing buffer over time, (top row) perpendicular and (bottom row) in parallel to the main magnetic field

6.4 Conclusion and Outlook

Considering the results of the mechanical testing, of the porosimetry and of the microscopic evaluation of the internal structure, the following conclusions can be drawn. First, the scaffolds containing enzymatical crosslinked collagen possess an internal structure of open pores and show a mechanical behaviour typical for porous constructs. In contrast, non-enzymatical treated scaffolds seem to have a more lamellar internal structure and no real system of single interconnected pores. This assumption is substantiated by the results of the mechanical tests. For the non-enzymatical treated scaffolds, a lack of elasticity was found, which resulted in permanent structural damages even for low compression or tension. Suggestions were made for improvements in future experiments. It is especially emphasized that the mechanical properties have to be investigated with constructs incubated in an aqueous medium. It was shown by Burger et al. that the fluid flow inside the bone matrix and the resulting impact on the osteocytes is the mechanosensory link between the macroscopic description of bone adaptation by Wolff's law and the cellular activities responsible for the remodelling mechanism [10]. Consequently, a comprehensive evaluation should compare fluctuation of liquid in bone, cartilage and

medium incubated scaffolds [149]. Such investigations could include for example MRI experiments as described by Neu et al. or focus on electrokinetics to analyze strain-generated potentials as suggested by Cowin [149,156]. Subsequently, the results have to be evaluated together with data on porosity, mechanical properties and mass transfer. In this context, dynamic contrast agent-enhanced MRI was applied to investigate velocity differences in the mass transport between scaffold and surrounding medium. The method was successfully established for the new BT-MRI equipment and fundamentals for a quantitative evaluation were accomplished. The more constrained mass transport in the perforated hollow cylindrical hydroxyapatite-collagen-chitosan scaffold compared to the PLGA scaffold with a pore size of 100 - 200 µm indicates that an improvement regarding the size and/or the interconnectivity of the pores is necessary. Additionally, an accumulation of gas bubbles inside the PLGA scaffolds during incubation was imaged.

Due to the more appropriate internal structure and mechanical properties, further investigations should focus on the transglutaminase crosslinked scaffolds. The dynamic contrast agent-enhanced MRI experiments should imperatively be carried out with those constructs. A trial, if the PGA mesh support also works on enzymatical treated constructs is recommended as first objective of future experiments. Variations of the mesh support are supposed as a challenging perspective towards tailored scaffolds in respect to mechanical properties, degradation kinetics and features of the lateral surface of the cylindrical constructs.

PART IV – IN VITRO EXPERIMENTS OF SCAFFOLDS COLONIZED WITH CELLS

Chapter 7 – Cells cultured on cylindrical hydroxyapatite-collagen-chitosan scaffolds

7.1 Introduction

At the final stage of the development of tissue engineering scaffolds, an experimental application in a living creature is indispensable until now. For ethical and financial reasons, it is desirable to reduce the scale of such experiments to the scientific essential minimum [157]. For this purpose, profound preliminary investigations are crucial. In vitro experiments offer a practical opportunity to obtain information towards the safety. Unaltered, tissue specific cells gained from host tissue would provide more relevant results regarding biocompatibility evaluation. In contrast to cells from continuous culture, those cells lose typical characteristics during maintenance outside their natural environment quite fast [158,159]. This accounts for poor availability of sufficient cell amounts and high effort for the experiments, and therefore limits their application. Hence, for a first impression of the suitability of a new scaffold system, the seeding of a continuous cell culture onto the construct appears to be appropriate. Additionally, the commercial availability of those cells ameliorates the experimental reproducibility [157,160].

In the present study, MG63 human osteosarcoma cells (LGC Promochem, London, UK) were used because they are known to be a relevant model on some points of osteoblast behaviour and due to the ease of their cultivation [154]. The need for large sized scaffold systems and the related analytical problems were already mentioned in the general introduction part (1.4). In this regard, two main objectives were pursued by the experiments described in this chapter. The first was the preliminary observation of the cylindrical hydroxyapatite-collagen-chitosan scaffolds as a matrix to support cell growth and survival in a three-dimensional fashion. The second was the establishment of benchtop-MRI as a tool for the assessment of the first. Additionally, confocal laser scanning microscopy (CLSM), Transmission electron microscopy (TEM) and histology were used to verify the results of the MRI evaluation.

Until now, the majority of in vitro-studies are carried out in two-dimensional approaches mainly as experiments on the ground of well plates or culture dishes. A main drawback of these investigations is the absence of possibilities to reflect the intricate interplay inside a living entity. Because of this difference in the complexity between in vitro and in vivo experiments, a gap appears which often complicates the result interpretation. For this reason there is a need for analytical methods to investigate three-dimensional microenvironments as they are closer to the in vivo conditions or as expressed by Rehfeldt et al., "cell biology research seems increasingly headed toward this added dimension" [134]. Additional to the characterization of the developed scaffolds, a further advancement in the field of benchtop-MRI towards the examination of three-dimensional cell cultures could therefore facilitate progress in various fields of nature science.

7.2 Materials and Methods

7.2.1 Culture of MG63 cells

MG63 human osteosarcoma cells (LGC Promochem, London, UK) were cultured at 37 °C and 5 % CO_2 aeration in Dulbecco´s Modified Eagle Medium (DMEM; Biochrom AG, Berlin) containing 10 w/w% fetal bovine serum (Biochrom AG, Berlin), 1 w/w% penicillin/streptomycin (PromoCell GmbH, Heidelberg).

7.2.2 Labeling of MG63 cells with superparamagnetic iron oxide nanoparticles

For the labeling procedure as well as for the examination of the labeling efficiency modified standard protocols were applied [54,67,161]. Carboxydextran coated SPIO´s (Resovist®, Schering) and poly-(L)-lysine (PLL) were added to DMEM yielding concentrations of 84 µg Fe/ml and 2.25 µg PLL/ml and shaken at room temperature for 120 min. MG63 cells growing to 70 % of confluence were incubated with the labeling medium for 20 h. After three washing steps with phosphate buffered saline, the cells were trypsinized with an aqueous solution of 0.25 w/w% trypsin and 0.1 w/w% EDTA for 5 min, counted and used for further experiments.

7.2.3 Colonization of the cylindrical hydroxyapatite-collagen-chitosan scaffolds with MG63 cells

A suspension volume of 1.0 ml, containing 1.5 million labeled or non-labeled cells in DMEM, was gradually dropped on the lateral surface area or into the central

hole of a dry, hollow cylindrical hydroxyapatite-collagen-chitosan scaffold. After soaking up the cell suspension, the scaffold was transferred into a well of a 6 well plate and cultured in DMEM. One day later, the sample was removed into a new well with 8 ml of fresh medium. Medium exchange was performed three times a week.

7.2.4 Staining, light microscopy and histology

The light microscopic examination of specimens stained with Prussian blue and counterstained with nuclear fast red was done for two purposes. First, to evaluate the labeling efficiency of MG63 cells with the SPIO´s and second, to investigate the fate of cells and SPIO´s after being colonized on the scaffolds.

Examination of labeling efficiency

Labeled or non-labeled cells were seeded and cultured on coverslips in 12 well plates. After 16 h, the cells were fixed with 2 % glutaraldehyde for 10 min and subsequently incubated for 30 min in 1 % potassium ferrocyanide in 3 % aqueous hydrochloric acid. Next to washing steps, the slides were immersed in nuclear fast red solution for 10 min and rinsed with water. After dehydration in ascending alcohol series, the slides were cleaned with xylene and covered with Clarion mounting medium.

Histological sections of colonized scaffolds

After 4 weeks of cell cultivation, the samples were fixed in 4 % buffered formalin solution for 2 h, dehydrated in an ascending alcohol series and embedded in paraffin Roti-Plast. Thin sections were prepared by means of a rotary microtome (HM 340E, Mikron Instruments, San Marcos, CA, USA) and transferred onto glass slides. The paraffin was removed by incubation in Roti-Histol, followed by sample rehydration in a descending alcohol series. The sections were stained and subsequently embedded like the samples for the light microscopic examination of labeling efficiency.

7.2.5 Transmission electron microscopy (TEM)

On one hand, TEM was used to evaluate the labeling efficiency of MG63 cells with the SPIO´s and on the other hand, the fate of the labeled cells after being colonized on the scaffolds was investigated.

For the first purpose, labeled or non-labeled cells were centrifuged and after removal of the culture medium the cells were fixed with 3 % glutaraldehyde in 0.1 M sodium

cacodylate buffer (SCB; pH 7.2) for two hours at room temperature. After fixation, the cells were rinsed in SCB, immobilized with 4 % Agar in SCB and postfixed with 1 % osmiumtetroxide in SCB for one hour at room temperature. Subsequently, the samples were rinsed with water, dehydrated in a graded ethanol series (70 % ethanol contained 1 % uranyl acetate (Chemapol, Czech Republic)), infiltrated with epoxy resin according to Spurr and polymerized at 70 °C for 24 hours [125].

Ultrathin sections (80 nm) were made with an Ultracut R ultramicrotome (Leica, Wetzlar, Germany). Sections were post-stained with uranyl acetate and lead citrate in an EM-Stain apparatus (Leica) and subsequently observed with an EM 900 transmission electron microscope (Carl Zeiss SMT, Oberkochen, Germany). Micrographs were taken with a slow scan camera (Variospeed SSCCD camera SM-1k-120, Tröndle, Moorenweis, Germany).

For the evaluation of the fate of the labeled cells after being colonized for four weeks on the scaffolds, the constructs were removed from the culture medium.

Subsequently, they were fixed with 3 % glutaraldehyde in 0.1 M sodium cacodylate buffer (SCB; pH 7.2) for two hours at room temperature and postfixed with 1 % osmiumtetroxide in SCB for one hour at room temperature. The further steps were identical to the preparation of the samples for the evaluation of the labeling efficiency.

7.2.6 Confocal laser scanning microscopy (CLSM)

MG63 cells were cultured for five weeks on the scaffolds, investigated weekly by BT-MRI and finally examined by CLSM. Scaffolds were cut into slices to obtain information about the distribution of viable cells across the scaffold. Cross sections of the samples were transferred into a well with 5 µg/ml fluorescein diacetate dissolved in DMEM. After 5 min of incubation, the scaffold was analyzed with CLSM (DM IREZ TC5 SP2/AOBF, Leica, Wetzlar, Germany). The wavelength for excitation was set to 485 nm and for detection to 520 nm.

7.2.7 Magnetic resonance imaging (MRI)

Localization of Known Amounts of Labeled Cells on the Scaffold Surface

MG63 cells were labeled with iron oxide as described in the materials and methods section (see 7.2.2). A suspension containing 2.5 million labeled cells in 1 ml of DMEM was used to seed 100,000; 50,000 and 25,000 cells on three different, distinct positions located in line on the lateral surface area of the scaffold. The construct was

cultivated in a six well plate for twelve hours, subsequently transferred into the imaging vessel and positioned in the BT-MRI device. Two slices of 2 mm thickness parallel to the main magnetic field were selected. The other imaging parameters were set as described in the general introduction part (see 1.6).

Periodic monitoring of the scaffold colonization over time

For investigation of scaffold colonization by MG63 cells, the samples were taken out of the well and transferred with 4 ml of incubation media into a test tube with sample holder. A capillary containing the silicon oil Dimeticon 350 (Caesar & Loretz GmbH, Hilden, Germany) was positioned next to the scaffold, as an internal standard for setting the maximum intensity in the MR images. Averages of 128 single scans were used resulting in a complete measuring time of about 90 min. After the imaging procedure, the samples were transferred back into the well plates for further cultivation.

7.3 Results and Discussion

BT-MRI could be used to visualize the distribution of labeled cells within scaffolds. Prosperous precultivation of scaffolds with cells is a precondition in many tissue engineering approaches for the development of artificial substitutes for human tissues [14]. Noninvasive analytical tools are required to gain insight into the cell distribution in these matrices. For the assessment of the cell position after the seeding by BT-MRI, the magnetic cell labeling was shown to be obligatory. Non-labeled cells cannot be visualized by BT-MRI in aqueous culture media. The interaction of water protons in the cytoplasm with macromolecular cellular components does not sufficiently decrease the T1 relaxation time to obtain a visible contrast. Hence, an established protocol was modified and employed for cellular labeling by PLL as a transfecting agent and a clinical approved contrast agent [54,67].

7.3.1 Labeling of MG63 cells with superparamagnetic iron oxide nanoparticles and evaluation of the labeling efficiency

For most related studies, dextran coated SPIOs have been used. The applicability of these particles in combination with the common transfecting agents is well approved and interferences altering cell viability, function and differentiation can

be precluded to a high extent [161]. Only a few reports are available about cell labeling with the carboxydextran coated SPIOs used in this study [68,162-164].
In light microscopy, the Prussian blue stained iron depositions appear blue coloured. Due to the nuclear fast red counterstaining cellular structures are red, while the cell nuclei are stained more intensively (Fig. 4.1). The absence of the blue coloured inclusions in the non-labeled cells indicates that the observed iron deposits in the labeled cells originate from the incubation with SPIO and PLL.

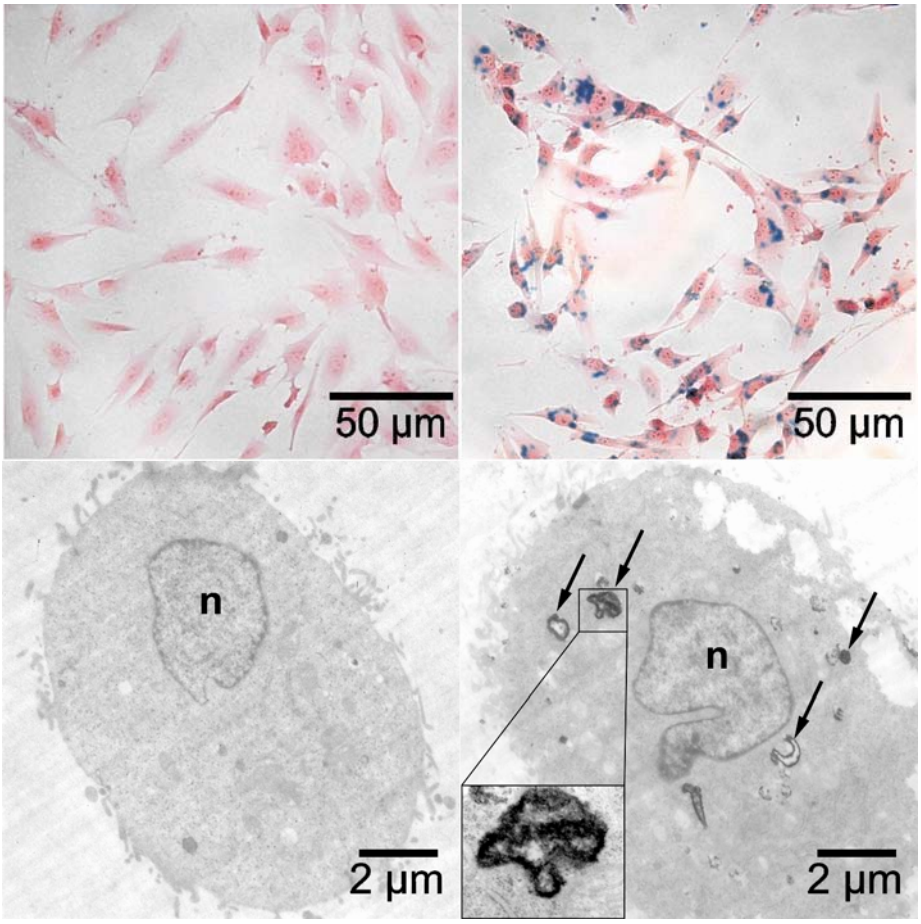

Fig. 4.1 Light microscopic images of MG63 cells stained with Prussian blue and counterstained with nuclear fast red (top), TEM images of MG63 cells (bottom), non-labeled control (left), SPIO labeled cells (right), blue colour or arrows indicates the iron depositions

The outspread cell shape in the images is related to the preparation technique using cells cultivated on the coverslips. In the electron microscopic images, a rounder cell shape was observed, caused by trypsinization before glutaraldehyde fixation. Dark units, indicating a more electron dense material, can be seen inside compartments of the labeled cells in the TEM image (Fig. 4.1). Regarding the dark appearance and the absence in non-labeled cells, these spots are supposed to originate from iron

oxide. Those particles are mainly attached to membranes of the compartments. Both microscopic techniques visualize that the SPIO´s were successfully internalized into the MG63 cells by the applied labeling procedure.

In the literature, the iron concentration used for cell labeling with carboxydextran coated SPIOs varied between 0.9 and 933 µg/ml. Other experimental details, e.g. incubation time, application of transfecting agent and cell population, do also differ strongly [68,162-164]. Compared with the established protocol for cell labeling with dextran coated SPIOs, in this study a three to fourfold higher concentration of iron oxides and a 3 to 6 times higher concentration of PLL were used [54,56,67]. For further experiments, interferences altering cell viability, function and differentiation have to be examined. Both methods applied for the investigation of the labeling efficiency show that substantial amounts of the SPIOs were taken up by MG63 cells. In the TEM images, an endosomal accumulation of the SPIOs was visible, as already reported in the literature for other cell populations [54,161,165].

7.3.2 Evaluation of the colonization of the cylindrical hydroxyapatite-collagen-chitosan scaffolds with MG63 cells

A comparison of MR images of cells seeded on the lateral surface area of the hollow cylinder scaffolds show that only the magnetite labeled cells can be visualized (Fig. 4.2). The SPIO´s act as so-called negative contrast agents. Labeled cells appear dark, while there is no contrast between the scaffold and non-labeled cells.

It must be noted that a homogenous cell distribution within the scaffold was not achieved. Even the seeding inside the central hole resulted in an accumulation of the cells on the inner surface area of the hollow cylinder (Fig. 4.3).

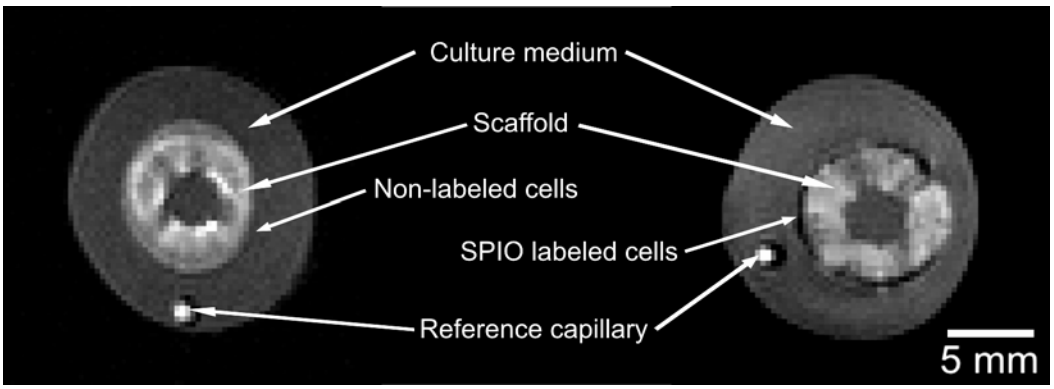

Fig. 4.2 MR Images of scaffolds colonized with MG63 cells on the lateral surface area, non-labeled cells (left), SPIO labeled cells (right)

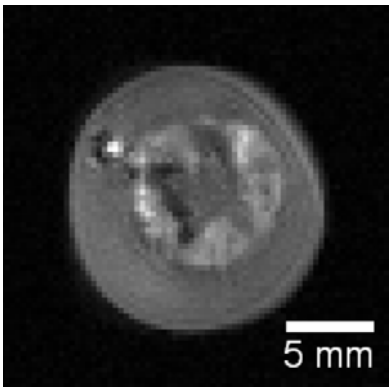

Fig. 4.3 MR Image of a scaffold with SPIO labeled MG63 cells seeded into the central hole

For cell seeding on scaffolds, the used “dropping on” technique is a common method. Usually, a pre-wetting of the scaffolds is necessary [96,166]. Because of the good wettability of the hydroxyapatite-collagen-chitosan scaffolds, this step was redundant, as the cell suspension is soaked up by the dry matrix. By adjusting the volume of the cell suspension, a complete uptake by the scaffold is achieved. This procedure may increase the amount of adherent cells because an outflow of redundant cell suspension is avoided. The theoretically possible maximum cell density of around 1000 cells/mm^3 for 100 % cell adhesion is below the typical range in tissue engineering approaches [67,96,166,167]. For a cell distribution limited to the lateral surface, a density of around 2000 cells/mm^2 was calculated. For a smooth surface, this would be already in the range of confluency.

It was possible to monitor the result of the seeding procedure, revealing that the cells attach close to or on the surface and did not penetrate deeply into the scaffold.

Hence, the localization of known amounts of labeled cells on the scaffold surface was executed successfully. Due to the negative contrast enhancement by the SPIOs, the positions of the labeled cells on the scaffold were clearly visible. The higher volume of the suspension used to seed the higher amount of cells resulted in a larger detected area of attached and labeled cells. It is obvious that cell numbers as low as 25,000 cells located in the scaffold are sufficient for detection (Fig. 4.4).

The equipment developed for the sample fixation during the MR imaging turned out to be very convenient for the scaffold transfer from the 6 well plates into the MRI device. It allowed even the repeated analysis and scaffold transfer once a week, maintaining sterile conditions around the sample. For the scaffolds colonized on the lateral surface area, no growth or migration of cells into the matrices was observed

by MRI even after 4 weeks of culturing (Fig. 4.5). This finding was supported by results derived from histology, CLSM and TEM.

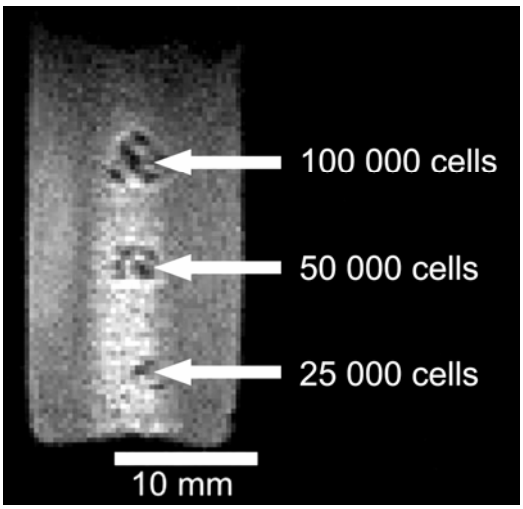

Fig. 4.4 MR Image of the scaffold surface with three clusters of different concentrations of SPIO labeled cells

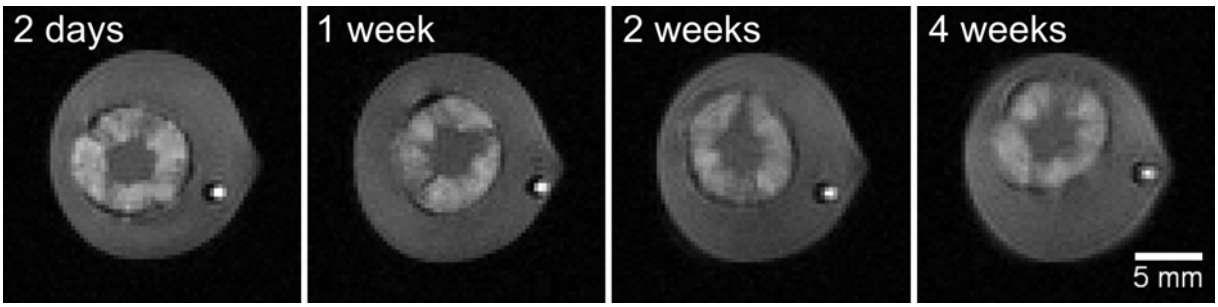

Fig. 4.5 MR Images of the same scaffold colonized with SPIO/PLL labeled MG63 cells on the lateral surface area after different time periods of culturing

The light microscopic image of the scaffold cross section shows that the predominant amount of cells and of iron depositions is located on the scaffold surface (Fig. 4.6). Inside the scaffold, in a distance of 400 to 500 µm from the surface, almost no cell or iron depositions can be seen. A similar outcome resulted from the TEM evaluation. Cells containing iron depositions are visible on the scaffold surface. Furthermore, it seems as if the cells inside the matrix, close below the surface, contain less or no iron depositions (Fig. 4.7). Up to now, it is unknown if any slight cellular migration took place inside the constructs. If there was no active movement of cells into the scaffold, propagation could bring daughter cells more deep into the constructs. In this case, the decreasing intracellular iron concentration could be due to several repetitions of cell division. Another reason for this finding could be a release of the

SPIOs from labeled cells. An indication for such events was found in preliminary experiments. The details are shown in the appendix (Fig. 5.1). The decrease of intracellular iron label is a main constraint of cell tracking by MRI [58,67]. Future investigations should thoroughly analyze this issue.

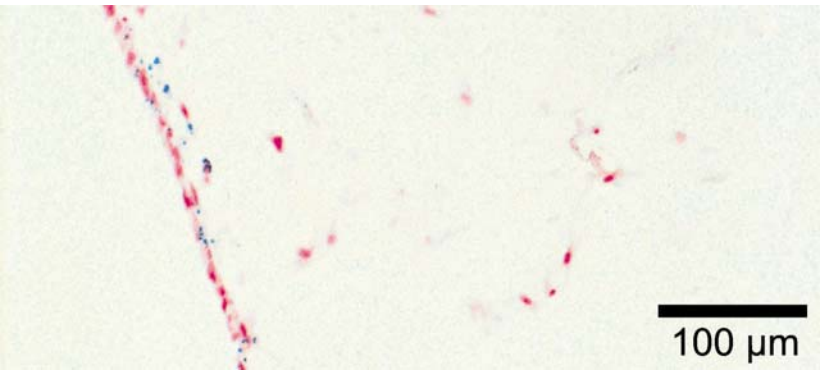

Fig. 4.6 Light microscopic image of the border area of a scaffold cross section with SPIO labeled MG63 cells colonized on the lateral surface area, stained with Prussian blue and counterstained with nuclear fast red, red colour indicates cell nuclei and blue colour indicates iron depositions

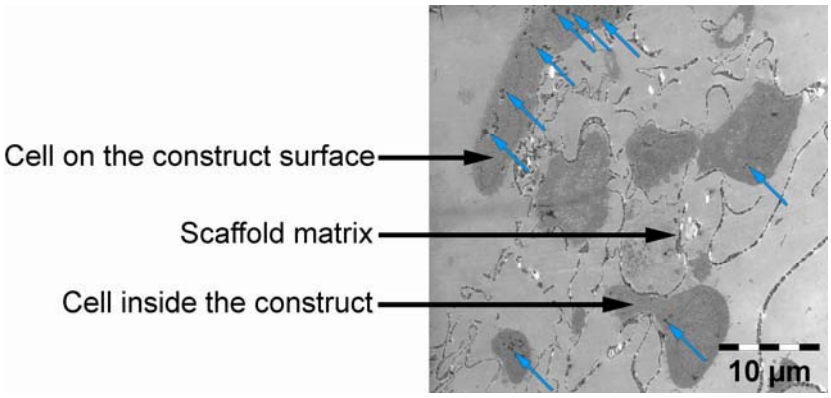

Fig. 4.7 TEM image of the border area of a scaffold cross section with SPIO labeled MG63 cells colonized on the lateral surface area, blue arrows indicate the iron depositions

Regarding the cell growth mainly on the construct surface, analogue results were found by CLSM. Only viable cells are able to hydrolyse fluorescein diacetate and accumulate the resulting fluorescein intracellularly [168,169]. The widespread fluorescence observed on the scaffold surface suggests a confluent cell growth. In the inner region of the scaffold uncovered by the intersection, a contrary result was obtained. Only little fluorescence was found indicative for a restricted cell penetration into the three-dimensional matrix (Fig. 4.8).

A probable reason for this is the small the pore size, which may keep the cells on the surface during seeding and also delimited the mass transfer during further cultivation [28]. Maybe this effect was enhanced by static culture conditions and cells on the surface shielding the scaffold.

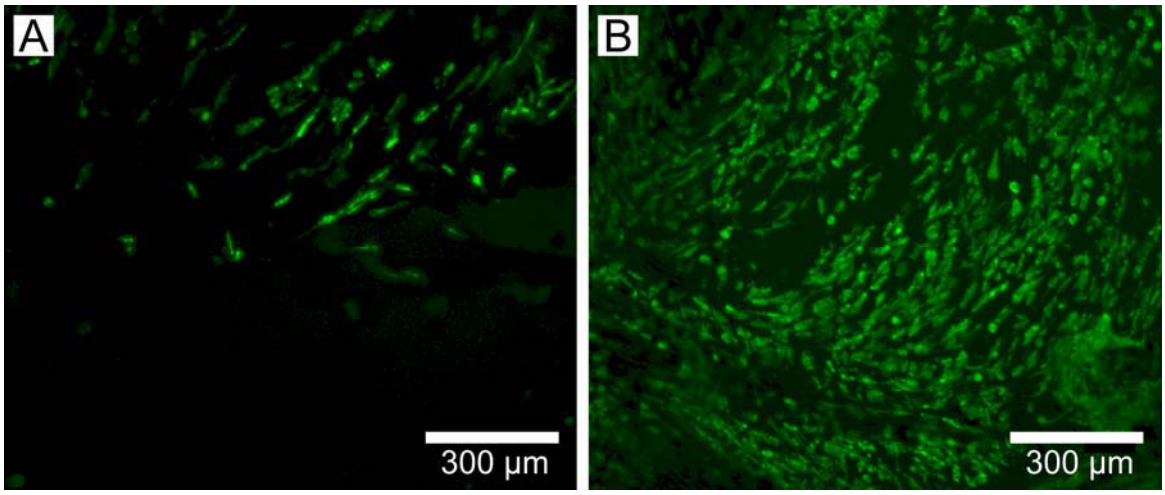

Fig. 4.8 CLSM image of cells stained with FDA growing on the scaffold, in the inner region of a cross section (A) and on the surface (B)

7.4 Conclusion and Outlook

An established protocol for cell labeling with dextran coated SPIOs was modified towards the use of carboxydextran coated SPIOs. The success of labeling the MG63 cells was demonstrated by two microscopic methods. Future experiments should investigate if the procedure has any effect on cell viability or function, especially, if the method is intended to be used for more sensitive cell types like the precursors of bone cells [54,161].

In the next step, the labeled cells were seeded on the cylindrical hydroxyapatite-collagen-chitosan scaffolds. The outcome was successfully imaged using the BT-MR equipment. Even after 4 weeks of culturing, no considerable ingrowth of MG63 cells throughout the matrix was observed by MRI. The same observation was made by histology, CLSM and TEM.

Therefore, further development should be directed towards the attraction of cells to colonize the entire construct. Several strategies will have to be attempted to meet this goal. Variations for an enhancement of the mass transfer are recommended to achieve sufficient oxygen and nutrient supply of the cells located more inside.

The application of scaffolds with larger interconnected pores might be beneficial, as for example the enzymatical crosslinked hydroxyapatite-collagen-chitosan scaffolds (see 3.2.2). In this direction, some progress was already seen in preliminary experiments accomplished with a perforated scaffold as described in chapter 6 (Fig. 3.9). Large sized channels throughout the constructs seem to enhance the growth of cells inside the scaffold (Fig 5.2 in the appendix). Additionally, the mass transfer could be accelerated by agitation or perfusion of the liquid surrounding of the colonized constructs during the cultivation in bioreactors [65].

Furthermore, it should be evaluated if an active cell migration can be stimulated by the incorporation of cell attracting substances. Beyond the promotion of vascularisation and ossification, such chemotactic properties are known for the growth factors BMP-2 and VEGF [170]. A starting point for experiments in this direction could be the insertion of a growth factor containing gel into the central part of the hollow cylindrical hydroxyapatite-collagen-chitosan scaffolds. The growth factor release from this gel should be sustained to generate a concentration gradient throughout the entire scaffold.

Chapter 8 – Cells cultured on the coated polyglycolic acid meshes

8.1 Introduction

Although cell viability on the scaffold surface was shown in the previous chapter, the contribution of the single components thereto and for the overall applicability, is still unknown. In this regard, variations between the concentration of collagen, chitosan, and the hydroxyapatite-collagen composite should provide useful information. The outcome could give impulses for an optimization of the scaffold fabrication formulation. For such a screening on composition variations, the sheet like scaffold design was chosen. Three circumstances account for this decision. First, the coated PGA meshes permit to stamp out disc shaped samples for cultivation in cavities of 24-well microtiter plates. Second, it is not a big effort to fabricate a considerable higher amount of samples. Third, because of the smaller sample size a substantial lower cell quantity is sufficient for the construct colonization. All three conditions facilitate an easy handling and experiments which tend toward a high throughput screening-like suitability test of scaffold compositions.

The successful proof of cell viability on the surface of the cylindrical hydroxyapatite-collagen-chitosan scaffolds in the previous chapter was performed with an osteosarcoma cell line [171]. As already mentioned, this is a practicable approach to obtain a first impression on the suitability, but further experiments towards a safety evaluation should come closer to the tissue engineering aim. Concerning this matter Patrick J. Doherty mentioned that, “yet, continuous cultures are often derived from tumors and may not express the characteristics of the original tissue”. He further advised that “primary cell lines can provide cultures that are close to the biological nature of the tissue of origin” [160]. For that reason, primary human chondrocytes and osteoblasts were used for the continuation of the cell compatibility assessment. This screening was evaluated with the water soluble tetrazolium 1 (WST-1) assay [172]. The outcome is a measure for the cell viability and therefore comprises information about the cell compatibility. However, regarding the tissue engineering goal even this result has to be taken with care. It is well known, that the extracellular environment has a crucial influence on the fate of the colonized cells [173]. Indeed, the viability of primary cells is an important indication, but allows no expectations about the maintenance of the cellular tissue specificity. For this reason, the most

promising samples of the cell viability screening were additionally investigated by histology.

8.2 Materials and Methods

8.2.1 Cell compatibility evaluation with primary chondrocytes and osteoblasts

Sufficient amounts of primary human chondrocytes and osteoblasts were provided by an already established method reported by Schoen et al. [174]. In brief, the cells were isolated by digestion of cartilage or sprouted from bone usually discarded after surgical intervention and propagated up to three passages in monolayer. For all operations with those cells, DMEM medium (Gibco, Invitrogen GmbH, Karlsruhe, Germany) plus supplements (fetal calf serum, penicillin, streptomycin, magnesium chloride and ascorbic acid) was used.

By a hollow punch, disc shaped samples with a diameter of 8 mm were stamped out of the coated mesh-stripes and out of the pure PGA mesh, which was always used as a blank sample. The exact compositions of the investigated samples were shown in table 2.1 (page 42).

In a first experimental approach three different sample types of the coated PGA meshes were investigated, the first coated with pure collagen, the second coated with collagen and chitosan and the third coated with the standard composition of collagen, chitosan and hydroxyapatite.

In the second experimental approach samples containing collagen, chitosan and hydroxyapatite in variable proportions were used.

The third experimental approach was used to evaluate the reproducibility of the results obtained with the PGA mesh coated with the standard composition.

After the already reported ethanol incubation and drying of the specimens, 50,000 cells per disc were seeded onto the material surface. After four days in vitro incubation, the specimens were transferred into a new well and the vitality of the cells in the former well and on the surface of the scaffold was estimated with the help of the WST-1 assay (Roche Diagnostics GmbH, Germany) [172]. 200 µl of the diluted reagent (1:10) were added to the culture medium. After two hours of incubation under cell culture conditions, the absorbance of the supernatant was measured at a wavelength of 450 nm and 620 nm as reference. The obtained optical density values were related to the values obtained for the unmodified PGA meshes, which were set as 100 % viability.

8.2.2 Histological staining

Samples of the PGA mesh coated with the standard composition (see 4.2.1 table 2.1) were colonized with cells under the same conditions as for the biocompatibility evaluation. Medium exchange was carried out every other day.
After two weeks in culture, the samples were fixed in 4 % buffered formalin solution over night and embedded in Technovit 9100 (Haslab GmbH, Switzerland) according to the manufacturers instructions. Thin sections (5 µm) were prepared by means of a microtome (Jung Biocut, Germany) and transferred onto glass slides. The sections were stained either by haematoxylin/eosin staining or by alcian staining [175,176]. The slides were covered with Entellan mounting medium (Merck KGaA, Germany).

8.3 Results and Discussion

8.3.1 Cell compatibility evaluation with primary chondrocytes and osteoblasts

The highest number of viable chondrocytes was obtained for the PGA mesh coated with collagen, chitosan and hydroxyapatite, compared to the pure PGA mesh and the PGA meshes coated with collagen or with the mixture of collagen and chitosan (Fig. 4.9A). The variation of the three components did not result in any significant difference in the viability of the cells for the particular materials (Fig. 4.9B). Hence, PGA meshes coated with the standard composition of collagen, chitosan and hydroxyapatite seem to be well suited for the cultivation of primary human chondrocytes.

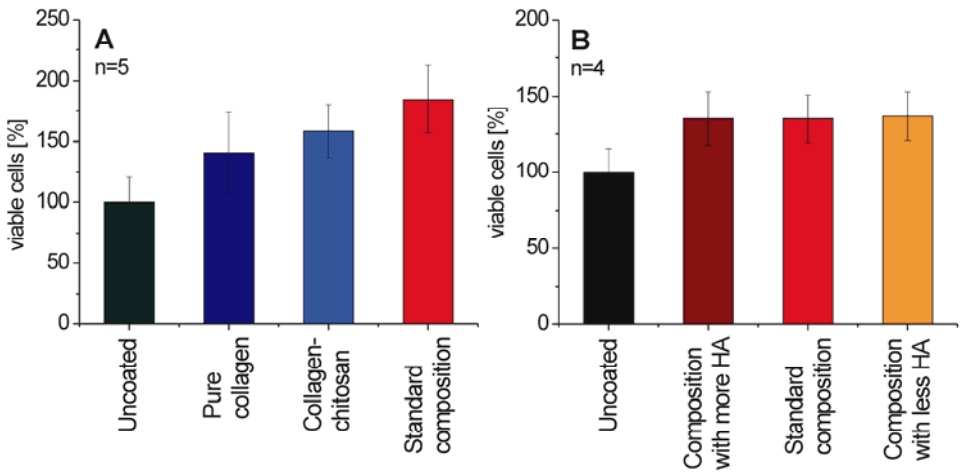

Fig. 4.9 Viability of primary human chondrocytes on PGA meshes analyzed by WST-1 assay, first experimental approach with different coated PGA meshes (A) and second experimental approach with samples containing collagen, chitosan and hydroxyapatite in variable proportions (B); Each specimen was measured in quadruplets in one experiment. (n… indicates the specimen number of one modification)

The biocompatibility evaluations with primary osteoblasts yield contrary results. Seeding osteoblasts on the modified PGA-surfaces coated with the mixture of collagen and chitosan showed the highest number of viable cells (Fig. 4.10A). From this result, in the second experiment the composition of collagen and chitosan should be changed in order to get a further improvement. Both variations performed better than the standard composition (Fig. 4.10B). The results did not permit to determine one of the coating formulations to be preferred for the cultivation of primary human osteoblasts. Compared to the results obtained with the chondrocytes, no clear tendency was found. Contrary to the expectations, it seems as if the samples with nano-sized hydroxyapatite are more favourable for the colonization with chondrocytes than with osteoblasts.

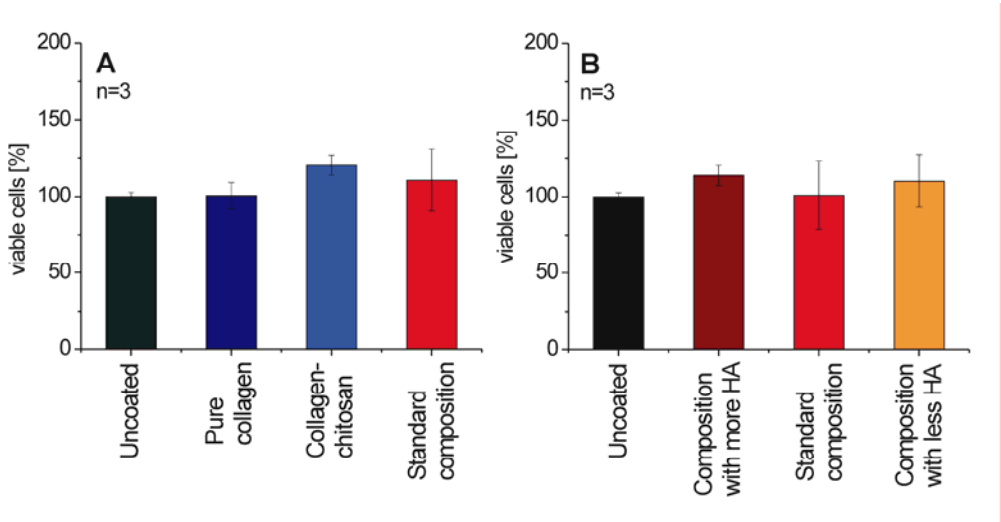

Fig. 4.10 Viability of primary human osteoblasts on PGA meshes analyzed by WST-1 assay, first experimental approach with different coated PGA meshes (A) and second experimental approach with samples containing collagen, chitosan and hydroxyapatite in variable proportions (B); Each specimen was measured in quadruplets in one experiment. (n… indicates the specimen number of one modification)

With both cell types, a quite good reproducibility of the material fabrication as well as of the cell viability tests was shown by the repeated evaluation of the mesh coated with the standard composition (Fig. 4.11).

Usually, cell viability is measured by the MTT assay [177]. The applied WST-1 assay is as well based on the reduction of a tetrazolium compound into a formazan dye, which is subsequently quantified. The advantage of the WST-1 assay is the high water solubility of the reaction product. Thus the colorimetric measurement can be done directly [172]. The cultivation and direct measurement in the 24-well microtiter

plates turned out to be very practicable. In future experiments, various formulations could be coated on PGA meshes before trials of more complex scaffold fabrication. For example, the effect of additional components like alginate, hyaluronic acid, heparin, chondroitin sulphate and others on the cell compatibility can be assessed. For sure, this approach is not directly comparable with the automated high throughput screening introduced by Clemens van Blitterswijk, termed “Materiomics” [178,179]. But it is a simple approach enabling a fast cell compatibility screening of a multitude of different compositions intended for scaffold fabrication. Even under general laboratory conditions a quite high number of samples can be tested with not too big effort.

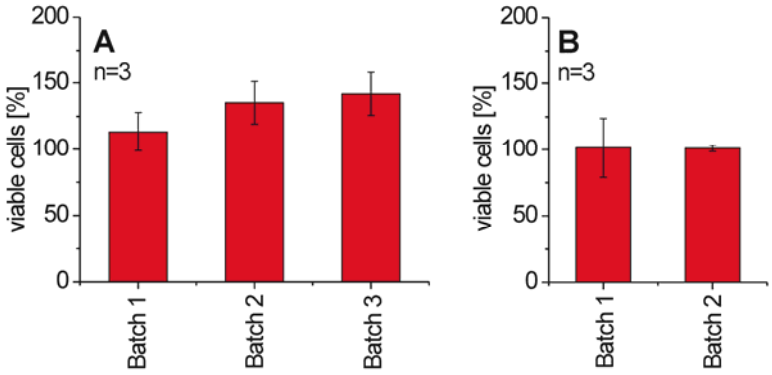

Fig. 4.11 Results of the repeated evaluation of PGA meshes coated with the standard composition, viability of chondrocytes (A) and osteoblasts (B) analyzed by WST-1 assay; Each specimen was measured in quadruplets in one experiment.
(n… indicates the specimen number of one modification)

To ensure the maintenance of their chondrogenic and osteogenic characteristics, the cells were cultured not more than up to three passages in monolayer prior the experiments. Due to phenotypic changes after several passages, the feasibility to keep primary cells in culture is restricted [159]. Once obtained, the cells have to be used for experiments rather expeditious. The practicability of the described procedure ameliorates a spontaneous and advantageous utilization of those cells.
Due to the results reported in chapter 7 and in this subitem, it can be assumed that no cytotoxicity emanates from the collagen, chitosan, hydroxyapatite and PGA mesh containing constructs described in this work. Nevertheless, the term biocompatibility is deliberately not used to express the outcome. Indeed, the found absence of cytotoxicity is one particular indication for it, but for a biocompatibility evaluation much more comprehensive analytics have to be accomplished [160]. In vivo studies

followed by clinical trials have to be performed to finally call the scaffold composition biocompatible. Before those experiments, several other investigations on safety tasks could be made in vitro. For example, haemocompatibility, mutagenicity, and some tracts of immunogenicity are accessible by in vitro studies [157]. Conceivably, some tests would be notably facilitated by the use of the coated PGA meshes instead of complex scaffold constructs.

Especially regarding the immunogenicity, Seo et al. pointed out that ”all biomaterials derived from non-autologous sources will cause some degree of foreign body response after implantation in vivo” [180]. Consequently, for the evaluation of the coating composition, the pure PGA mesh should always be used additionally as a blank sample.

From the obtained WST-1 assay data, no conclusion can be drawn about differences of the cell viability between construct surface and interior. Due to the cell seeding on the surface and the small layer thickness of the coated PGA meshes, no too big impact of the third dimension can be assumed. This obstacle could be seen as a challenge for future investigations. As mentioned by Garcia et al. “Cell viability assays for three-dimensional matrices have not been fully standardised to date” [153]. Stepwise extension of the third dimension by additional mesh layers would be possible during the fabrication as well as during the cell colonization.

8.3.2 Histological staining

The light microscopic evaluations of the specimens of both staining methods reveal the development of cartilage like structures in the samples cultured with primary chondrocytes (Fig. 4.12). Single cells closely associated and surrounded by ECM are clearly visible in the images. In contrast, images of the coated PGA meshes colonized with osteoblasts rarely show cellular associations. Mainly single cells attached to the remaining structures of the constructs are visible (Fig. 4.13). Hence, the results indicate that the PGA meshes coated with the standard composition of collagen, chitosan and hydroxyapatite support the formation of a cartilaginous tissue whereas a bony tissue does not emerge under the applied conditions. The static culture conditions could be one reason for this outcome, because much more perfusion is required for the maintenance of bone tissue, compared to cartilage [19].

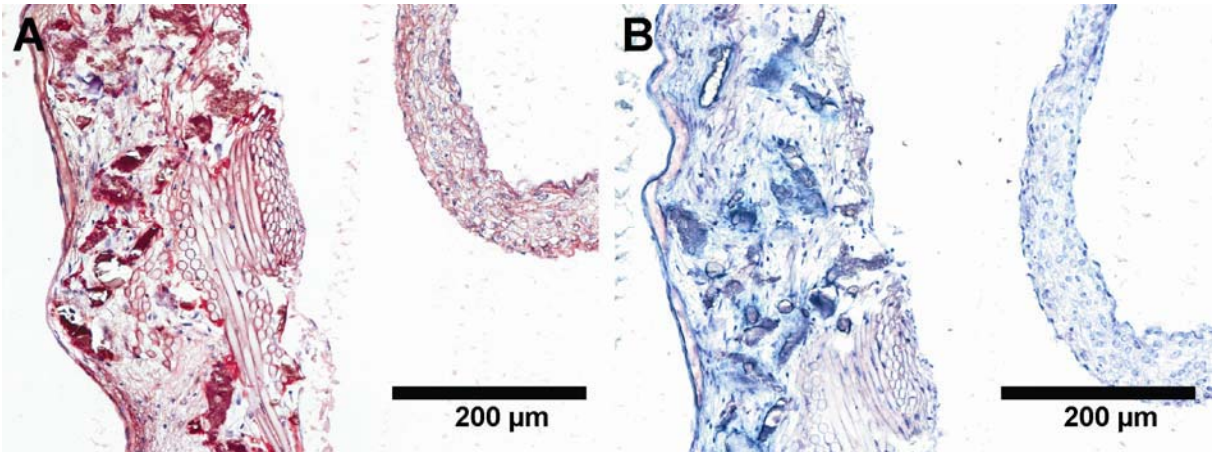

Fig. 4.12 Light microscopic image of the cross section area of a coated PGA mesh colonized with primary human chondrocytes, stained with haematoxylin/eosin (A) and with alcian blue (B)

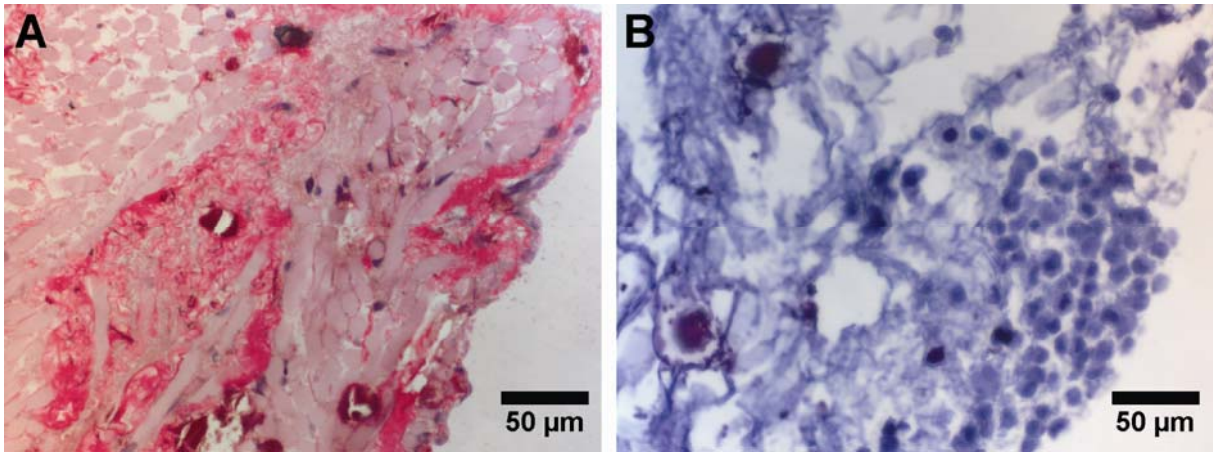

Fig. 4.13 Light microscopic image of the cross section area of a coated PGA mesh colonized with primary human osteoblasts, stained with haematoxylin/eosin (A) and with alcian blue (B)

For the perspective of tissue engineering constructs mimicking the cartilaginous template during endochondral bone formation, this outcome is not necessarily a disqualification. For the regeneration of cartilage defects different scaffold systems are already on the market. Among them even constructs containing PGA or collagen can be found [181]. During natural endochondral bone formation the switch (conversion) between cartilage development and bone formation is induced by hypertrophy of the chondrocytes [16,19,182]. The results of the histological investigation did not clearly give evidence for the presence or the absence of hypertrophic chondrocytes. Future investigations should especially focus on this issue. Several established methods for the characterization and determination of different cartilage types are published and could be applied. Primarily, the ECM or its cellular synthesis are under study. During natural chondrogenesis, mainly type II, IX and XI collagen are secreted [173]. When the chondrocytes become hypertrophic,

they switch to collagen type X in their ECM synthesis [16,173,182,183]. By in situ hybridisation, such alterations could already be detected on the genetic level [182]. Alternatively, specific antibodies against collagen type X can be used for direct immunohistochemical analysis [173,183]. Safranin O can be additionally used for a specific cartilage characterization regarding the content and distribution of GAG [183,184]. Other methods like the measurement of alkaline phosphatase activity or the staining with Movat's Pentachrome technique appear to be more relevant for the investigation of further steps in the tissue formation towards bone [173,185]. In this regard, a matrix calcification and vascularisation should be observed and characterized as well [185]. Both processes represent essential events during the progressing ossification [16,19,154]. For the evaluation, different methods are available. For example, an emerging microvascular structure could be analyzed by immunohistochemistry or by dynamic contrast enhanced MRI [47,155]. The matrix mineralization is usually examined histologically by von Kossa staining [30,49,51,182]. For most of the samples under study this would be not expedient, because they already contain hydroxyapatite. Hence, a positive result would be obtained anyway, even if no further mineralization occurred. The analytic should therefore focus on the expression of specific non-collagenous proteins, which are indicative for a progression of matrix mineralization [5,12,36].

8.4 Conclusion and Outlook

The cell compatibility of the coated PGA meshes was simply and quickly analyzed by the WST-1 assay. Cells were colonized on the PGA mesh coated with the standard composition and subsequently investigated by histology. A clear tendency was found, that meshes coated with collagen, chitosan and hydroxyapatite were well suited for the cultivation with primary human chondrocytes. The results obtained for osteoblasts did not permit such a consistent conclusion. The handling of the coated PGA meshes was found to be very practicable for in vitro experiments in 24-well microtiter plates. In this regard, the discussion part was additionally used for several suggestions towards analytical improvements and further applicable methods. Beside the screening approach, special focus was directed on future prospects to further evaluate if scaffolds mimic the cartilaginous template during endochondral bone formation. Vascularisation and calcification are the main processes which should be found in upcoming experiments. Both are essential

events during endochondral bone formation and can be additionally stimulated using specific growth factors, like VEGF and BMP-2 [120,155]. Spatial directed incorporation of growth factor containing drug release systems into a scaffold could even guide defect targeted tissue development [118].

PART V – SUMMARY

Chapter 9 – Summary

9.1 English version

The objective of the present thesis was the development of a scaffold for bone tissue engineering and its profound characterization. Two tasks of the latter demanded particular attention. One is the particle size of hydroxyapatite and its embedding into a biodegradable polymeric scaffold matrix and the second is the establishment of the new method of benchtop-MRI for the evaluation of such constructs.

The thesis is divided into four parts. The first part is a detailed introduction into the topic, providing basics of natural bone fracture healing and its limitations, as well as fundamentals of the tissue engineering approach to overcome large-scale bone defects. The intended source materials were reviewed towards their suitability in this field. A critical report about the state of the art, focussed on the noninvasive scaffold characterization, signifies the starting point for the practical work. During the beginning of the work, Zeta potential measurements were performed to assess charge properties of collagen and chitosan and interactions between the two polymers. Furthermore, a known strategy was applied for the biomimetic fabrication of a hydroxyapatite-collagen composite material. After its characterization by XRD and TGA, the composite material was used for the scaffold manufacture. Intentionally, no further analysis of the source materials was performed in order to focus on the formulation, optimization and especially the characterization of scaffolds.

The second part is completely dedicated to the different strategies of scaffold fabrication. In this regard, the homogenous embedding of the hydroxyapatite-collagen composite material into a mechanical stable and porous polymeric matrix composed of chitosan and collagen was the main challenge. All applied strategies are based on the lyophilisation of frozen aqueous dispersions. Cylindrical scaffolds were obtained by fast-freezing the formulation inside an aluminium mould in liquid nitrogen. Those constructs were further strengthened by DHT and optional with an additional PGA mesh surrounding or enzymatical collagen crosslinking. Plate shaped

constructs were produced by the coating of PGA meshes and preliminary experiments towards the scaffold fabrication by 3D plotting were performed. The results obtained from the analytical experiments described in the following parts of the thesis, promoted step by step ameliorations of the constructs. The permanent variation of the scaffold fabrication (e.g. full cylinder vs. hollow cylinder, mesh support, crosslinking, perforations) lead to a construct improvement on one hand but complicated the comparability of the results on the other hand.

The third part is focussed on the physicochemical evaluation of the cylindrical shaped hydroxyapatite-collagen-chitosan constructs. By SAXS, ESEM, AFM and TEM, it was revealed that nano-scaled hydroxyapatite particles were successfully embedded inside the polymeric matrix. Additionally, the homogeneity of the hydroxyapatite distribution inside the scaffolds was shown by BT-MRI. In the following, scaffolds containing enzymatical crosslinked collagen were compared with the ones containing non-enzymatical treated collagen regarding their mechanical properties and their internal pore structure. It turned out that the enzymatical crosslinking resulted in scaffolds which can better withstand compressive or tensile stress. They possess an internal structure of open interconnected pores whereas the non-enzymatical crosslinked ones have a more lamellar internal structure. The pore interconnectivity is important for sufficient mass transfer throughout the constructs. A known dynamic contrast agent-enhanced method has been established for the BT-MRI equipment to facilitate more detailed analytics in this challenging field. It was shown that even perforations of the hydroxyapatite-collagen-chitosan scaffolds did not result in a mass transfer comparable to PLGA scaffolds with a pore size of 100 - 200 µm. Additionally, an accumulation of gas bubbles inside the PLGA scaffolds during incubation was imaged.

In the fourth part, in vitro experiments with the cylindrical hydroxyapatite-collagen-chitosan scaffolds and with the coated PGA meshes are reported. In this regard, a BT-MRI method was established to monitor the fate of the cells cultured on scaffolds. It was shown that a cell labeling is essential for the application of this noninvasive analytic. Hence, an osteosarcoma cell line was labeled with SPIOs and the success this approach was demonstrated by two microscopic methods. Labeled and non-labeled cells respectively, were seeded on the cylindrical hydroxyapatite-collagen-chitosan scaffolds. The outcome of the seeding as well as of the further cultivation

was imaged by BT-MRI. In contrast to the surface, no considerable growth of cells was observed inside the scaffolds. This result was confirmed by histology, CLSM and TEM. Several suggestions are made for improvements. The coated PGA meshes were used for investigations of the cell compatibility. In order to obtain information towards an optimal scaffold formulation, several compositions were tested. The outcome of the cell colonization was assessed by histology and a WST-1 assay. It was shown that meshes coated with collagen, chitosan and hydroxyapatite are well suited for the cultivation with primary human chondrocytes. The results obtained for primary human osteoblasts did not permit such a consistent conclusion. Further development of the method is supposed to enable easy and time-saving as well as practicable and cost-saving cell compatibility testing of various scaffold compositions in 24-well microtiter plates.

Overall it was shown, that BT-MRI is a versatile tool for various analytical applications in the field of tissue engineering. Regarding the scaffold development, a final résumé is more difficult. Although several of the obtained results for the developed constructs suggested their suitability for an application in bone tissue engineering, a clear conclusion cannot be drawn. Most of the characterization was done with cylindrical scaffolds containing the non-enzymatical treated collagen. In fact, those constructs contain nano-scaled hydroxyapatite particles dispersed in a quite dense matrix. For bone tissue engineering their pore size might appear too small and their mechanical stability seams to be too low. With regard to the objective of supporting the natural defect repair by endochondral bone formation, these facts can be seen from another perspective. In contrast to bone, cartilage is a substantial less blood perfused tissue, possibly comparable with the dense but fast degradable scaffold core. A remaining porous skeleton, for example a surrounding PGA mesh, could provide an essential support and better perfusion. Less mechanical stability might stimulate the body's self healing capacities, at least in not too strong weight bearing sites. Hence, just the application into different bone defect sites of a living entity will allow a final conclusion. During experiments and result evaluation as well as during the writing, a multitude of ideas and impulses for optimization and improvements emerged. Those are described in the discussion and in the conclusion and outlook parts of the single chapters.

9.2 German version

Das Ziel der vorliegenden Arbeit war die Entwicklung eines Scaffolds für die Züchtung von Knochengewebe und dessen tiefgründige Charakterisierung.
Zwei Schwerpunkte fanden dabei besondere Beachtung. Zum Einen sollte eine Einbettung von nanoskaligen Hydroxylapatitpartikeln in eine Matrix aus bioabbaubaren Polymeren erreicht werden. Zum Anderen war beabsichtigt, die neue Technik des Benchtop-MRI als Methode für die Evaluation solcher Konstrukte zu etablieren.
Die Dissertationsschrift ist in vier Teile gegliedert. Der erste Teil beschäftigt sich mit einer detailierten Hinführung zum Thema. Ein Einblick in natürliche Mechanismen der Heilung von Knochenfrakturen und deren Grenzen wird gegeben. Die als „Tissue Engineering“ bezeichnete Herangehensweise zur Therapie von Knochendefekten großen Ausmaßes wird erklärt. Weiterhin wird ein Überblick über die Eigenschaften der genutzten Ausgangsstoffe bezüglich ihrer Eignung für die Scaffoldherstellung gegeben. Der Ansatzpunkt für die experimentelle Arbeit wird mit einer kritischen Beschreibung des derzeitigen Standes der Wissenschaft verdeutlicht. Besonderes Augenmerk ist dabei auf nicht-invasive analytische Möglichkeiten zur Scaffold Charakterisierung gerichtet. Die praktischen Tätigkeiten wurden mit Zetapotentialmessungen begonnen, um Ladungseigenschaften von Kollagen und Chitosan sowie Wechselwirkungen zwischen den beiden Polymeren einzuschätzen. Weiterhin wurde ein bekannter Ansatz verwendet, mittels einer biomimetischen Methode ein Hydroxylapatit-Kollagen-Komposit zu gewinnen. Nach der Untersuchung dessen mittels Röntgenbeugung und Thermogravimetrie wurde dieses Kompositmaterial für die Scaffoldherstellung genutzt. Auf weitere analytische Prüfungen der Ausgangsstoffe wurde mit Absicht verzichtet, um sich gezielt auf die Formulierung, Optimierung und Charakterisierung der hergestellten Konstrukte zu konzentrieren.

Der zweite Teil ist vollständig den verschiedenen Strategien der Scaffoldherstellung gewidmet. Die größte Herausforderung diesbezüglich war die homogene Einbettung des Hydroxylapatit-Kollagen-Kompositmaterials in eine mechanisch stabile und poröse Matrix aus Chitosan und Kollagen. Alle angewendeten Herstellungsstrategien basieren auf der Lyophilisation gefrorener wässriger Dispersionen. Durch Schockgefrierung der Formulierung in Aluminiumgussformen in flüssigem Stickstoff wurden zylindrische Scaffolds erhalten. Mittels einer Temperaturbehandlung bei Unterdruck

wurden die Konstrukte dann weiter verfestigt. Optional konnte durch enzymatische Kollagenvernetzung oder durch das Einbringen einer Polyglycolsäurenetz-Ummantelung eine weitere Stabilisierung erreicht werden. Plättchenförmige Konstrukte wurden durch die Beschichtung von Polyglycolsäurenetzen gewonnen und Voruntersuchungen für eine Scaffoldherstellung mittels 3D-Plotten durchgeführt. Die Ergebnisse der analytischen Experimente, welche in den folgenden Teilen dieser Arbeit beschrieben sind, brachten die schrittweise Optimierung der Konstrukte voran. Die dementsprechende, permanente Veränderung der Scaffoldherstellungsprozedur führte einerseits zu Konstruktverbesserungen (z.B. Vollzylinder im Vergleich zu Hohlzylinder, Polyglycolsäurenetz-Ummantelung, Kollagenvernetzung, Perforierung) andererseits wird dadurch aber die Vergleichbarkeit der einzelnen Ergebnisse erschwert.

Der dritte Teil der Arbeit konzentriert sich auf die physikochemische Untersuchung der zylindrisch geformten Hydroxylapatit-Kollagen-Chitosan-Konstrukte. Mittels SAXS, ESEM, AFM und TEM konnte deutlich gemacht werden, dass nanoskalige Hydroxylapatitpartikel erfolgreich in die Polymermatrix eingebettet sind. Darüber hinaus wurde durch BT-MRI gezeigt, dass der Hydoxylapatit homogen in den Scaffolds verteilt ist. Im weiteren Verlauf wurden Scaffolds, die enzymatisch quervernetztes Kollagen enthalten, mit denen aus unbehandeltem Kollagen hinsichtlich ihrer mechanischen Eigenschaften und der inneren Porenstruktur verglichen. Es stellte sich heraus, dass aus der enzymatischen Behandlung Scaffolds resultierten, die eine Druck- oder Zugbelastung besser überstehen. Ihre innere Struktur weist offene, untereinander verbundenen Poren auf, wohingegen die Konstrukte aus nicht enzymatisch behandeltem Kollagen eine eher lamellare innere Struktur haben. Eine Interkonnektivität der Poren ist allerdings wichtig um einen ausreichenden Stofftransport durch den Scaffold zu gewährleisten. Für diese herausfordernde analytische Fragestellung wurde eine bekannte Methode zur Verfolgung der Dynamik eines Kontrastmittels für das BT-MRI-Gerät etabliert. Damit wurde gezeigt, dass selbst Perforationen in den Hydroxylapatit-Kollagen-Chitosan-Scaffolds nicht ausreichen, um Stofftransportausmaße zu erreichen, die mit denen von PLGA-Scaffolds mit einer Porengröße von 100 - 200 µm vergleichbar wären. Zusätzlich konnte eine Anreicherung von Gasblasen in den PLGA-Scaffolds während ihrer Inkubation aufgezeigt werden.

Im vierten Teil wird über in vitro Experimente mit den zylindrischen Hydroxylapatit-Kollagen-Chitosan-Scaffolds und mit den beschichteten Polyglycolsäurenetzen berichtet. Dafür wurde eine BT-MRI-Methode entwickelt, um die, auf dem Scaffold angesiedelten, Zellen zu überwachen. Es konnte deutlich gezeigt werden, dass für den Erfolg dieser nicht-invasiven Analytik eine Zellmarkierung erforderlich ist. Deshalb wurde eine Osteosarkom-Zelllinie mit superparamagnetischen Eisenoxid-nanopartikeln markiert und die erfolgreiche Durchführung mit zwei mikroskopischen Methoden nachgewiesen. Daraufhin wurden zylindrische Hydroxylapatit-Kollagen-Chitosan-Scaffolds mit markierten oder nichtmarkierten Zellen beimpft. Das Ergebnis der Besiedlung und auch der weiteren Kultivierung wurden mittels BT-MRI abgebildet. Im Gegensatz zur Oberfläche wurde im Scaffoldinneren kein bedeutendes Zellwachstum gefunden. Dieses Ergebnis konnte mittels Histologie, CLSM und TEM bestätigt werden. Für zukünftige Ansätze sind viele Verbesserungsvorschläge beschrieben. Die beschichteten Polyglycolsäurenetze wurden für Untersuchungen zur Zellkompatibilität verwendet. Um Informationen bezüglich einer optimalen Scaffoldformulierung zu erhalten, wurden verschiedene Zusammensetzungen getestet. Das Ergebnis der Zellbesiedlung wurde mittles Histologie und einem WST-1 Assay erfasst. Es wurde gezeigt, dass mit Hydroxyl-apatit, Kollagen und Chitosan beschichtete Netze für eine Kultivierung von primären, menschlichen Knorpelzellen gut geeignet sind. Das für primäre, humane Osteoblasten erhaltene Ergebnis lässt solch einen klaren Schluss nicht zu. Abschließend wird angenommen, dass eine Weiterentwicklung der Methode eine zeit- und kostensparende Möglichkeit der Zellkompatibilitätstestung schaffen könnte. Verschiedene geplante Scaffoldformulierungen würden so einfach und praktikabel in 24-well Mikrotiterplatten verglichen werden können.

Insgesamt wurde gezeigt, dass BT-MRI ein vielseitiges Hilfsmittel darstellt um verschiedene analytische Aufgaben im Bereich des Tissue Engineering zu erfüllen. Bezüglich der Scaffoldentwicklung ist ein abschließendes Resümee schwieriger. Obwohl einige Ergebnisse die Eignung der Konstrukte für die Züchtung von Knochengewebe nahelegen, ist es nicht möglich, eine klare Aussage diesbezüglich zu treffen. Der überwiegende Teil der Charakterisierung wurde an den zylindrischen Scaffolds mit nichtenzymatisch behandeltem Kollagen durchgeführt. Diese Konstrukte enthalten tatsächlich nanoskalige Hydroxylapatitpartikel aber in einer relativ dichten Matrix. Für die direkte Züchtung von Knochengewebe mag die

Porengröße zu klein erscheinen und die mechanische Stabilität zu gering sein. In Bezug auf das Ziel der Unterstützung einer natürlichen Defektheilung durch endochondrale Knochenbildung können diese Fakten aber aus einer anderen Perspektive betrachtet werden. Im Gegensatz zu Knochen ist Knorpel ein wesentlich weniger blutdurchströmtes Gewebe, vielleicht sogar vergleichbar mit dem dichten, aber schnell abbaubarem Scaffoldkern. Ein dabei verbleibendes poröses Gerüst, wie z.B. die Polyglycolsäurenetz-Ummantelung, könnte dann die nötige Unterstützung und bessere Perfusionseigenschaften bieten. Zumindest an nicht stark belasteten Stellen können durch eine geringere mechanische Stabilität auch die natürlichen Selbstheilungskapazitäten stimuliert werden. Folglich wird nur die Anwendung bei verschiedenen Knochendefekten in lebenden Organismen ein abschließendes Ergebnis zulassen. Während der Experimente, der Ergebnisauswertung und auch während des Schreibens sind eine Vielzahl and Ideen und Impulsen für die Optimierung und Verbesserung aufgekommen. Diese sind in den Diskussionen, den Zusammenfassungen und Ausblicken der jeweiligen Kapitel der Arbeit eingehend beschrieben.

LITERATURE

1. Laurencin CT, Khan Y. Polymer/calcium phosphate scaffolds for bone tissue engineering. In: Ma PX, Elisseeff JH, eds. Scaffolding in Tissue Engineering. St Lucie Press, 2006: 253-63.
2. Hutmacher DW, Woodruff MA. Design, fabrication, and characterization of scaffolds via solid free-form fabrication techniques. In: Chu PK, Liu X, eds. Biomaterials Fabrication and Processing Handbook. CRC Press, 2008: 45-67.
3. Langer R, Vacanti JP. Tissue engineering. Science 260[5110], 920-926. 1993.
4. Schmelzeisen R, Schimming R, Sittinger M. Making bone: implant insertion into tissue-engineered bone for maxillary sinus floor augmentation-a preliminary report. J Craniomaxillofac Surg 31[1], 34-39. 2003.
5. Boskey AL. Mechanism of mineralization of collagen-based connective tissues. In: Sigel A, Sigel H, Sigel RKO, eds. Biomineralization. From Nature to Application. John Wiley & Sons, 2008: 457-505.
6. Lee JY, Nam SH, Im SY, Park YJ, Lee YM, Seol YJ, Chung CP, Lee SJ. Enhanced bone formation by controlled growth factor delivery from chitosan – based biomaterials. J Control Release 78, 187-97. 2002.
7. Liu H, Webster TJ. Nanomedicine for implants: A review of studies and necessary experimental tools. Biomaterials 28[2], 354-369. 2006.
8. Li J, Chen Y, Yin Y, Yao F, Yao K. Modulation of nano-hydroxyapatite size via formation on chitosan-gelatin network film in situ. Biomaterials 28[5], 781-790. 2006.
9. Cui FZ, Li Y, Ge J. Self-assembly of mineralized collagen composites. Mater Sci Eng R Rep 57[1-6], 1-27. 2007.
10. Burger EH, Klein-Nulend J, Smit TH. Bone remodeling. In: Wnek GE, Bowlin GL, eds. Encyclopedia of Biomaterials and Biomedical Engineering. Informa Healthcare, 2008: 206-14.
11. Meyer U, Wiesmann HP. Bone and Cartilage Engineering. Springer, 2006.
12. Palmer LC, Newcomb CJ, Kaltz SR, Spoerke ED, Stupp SI. Biomimetic Systems for Hydroxyapatite Mineralization Inspired By Bone and Enamel. Chem Rev 108[11], 4754-4783. 2008.
13. Rho JY, Kuhn-Spearing L, Zioupos P. Mechanical properties and the hierarchical structure of bone. Med Eng Phys 20[2], 92-102. 1998.
14. Salgado AJ, Oliveira JT, Pedro AJ, Reis RL. Adult stem cells in bone and cartilage tissue engineering. Curr Stem Cell Res Ther 1[3], 345-364. 2006.
15. Lane JM, Suda M, von der MK, Timpl R. Immunofluorescent localization of structural collagen types in endochondral fracture repair. J Orthop Res 4[3], 318-329. 1986.

16. Bukka P, McKee MD, Karaplis AC. Molecular regulation of osteoblast differentiation. In: Bronner F, Farach-Carson MC, eds. Bone Formation. Springer, 2004: 1-17.
17. Stevens MM, Marini RP, Schaefer D, Aronson J, Langer R, Shastri VP. In vivo engineering of organs: The bone bioreactor. Proc Natl Acad Sci U S A 102[32], 11450-11455. 2005.
18. Ko CC, Somerman MJ, An KN. Motion and bone regeneration. In: Bronner F, Farach-Carson MC, Mikos AG, eds. Engineering of Functional Skeletal Tissues. Springer, 2007: 110-28.
19. Oliveira SM, Amaral IF, Barbosa MA, Teixeira CC. Engineering Endochondral Bone: In Vitro Studies. Tissue Eng Part A 15[3], 625-634. 2009.
20. Muschler GF, Nakamoto C, Griffith LG. Engineering principles of clinical cell-based tissue engineering. J Bone Joint Surg Am 86[7], 1541-1558. 2004.
21. Webster TJ, Ergun C, Doremus RH, Siegel RW, Bizios R. Specific proteins mediate enhanced osteoblast adhesion on nanophase ceramics. J Biomed Mater Res 51[3], 475-483. 2000.
22. Geiger M, Li RH, Friess W. Collagen sponges for bone regeneration with rhBMP-2. Adv Drug Deliv Rev 55, 1613-29. 2003.
23. Wei G, Ma PX. Polymer/ceramic composite scaffolds for bone tissue engineering. In: Ma PX, Elisseeff JH, eds. Scaffolding in Tissue Engineering. St Lucie Press, 2006: 241-51.
24. Mooney MP, Siegel MI. Animal Models for Bone Tissue Engineering of Critical-sized Defects (CSDs), Bone Pathologies, and Orthopedic Disease States. In: Hollinger JO, Einhorn TA, Doll BA, Sfeir C, eds. Bone Tissue Engineering. Crc Press, 2005: 217-44.
25. Vasita R, Katti DS. Growth factor–delivery systems for tissue engineering: a materials perspective. Expert Rev Med Devices 3, 29-47. 2006.
26. Sachlos E, Czernuszka JT. Making tissue engineering scaffolds work. Review on the application of solid freeform fabrication technology to the production of tissue engineering scaffolds. Eur Cell Mater 5, 29-40. 2003.
27. Wahl DA, Czernuszka JT. Collagen – hydroxyapatite composites for hard tissue repair. Eur Cell Mater 11, 43-56. 2006.
28. Sachlos E, Reis N, Ainsley C, Derby B, Czernuszka JT. Novel collagen scaffolds with predefined internal morphology made by solid freeform fabrication. Biomaterials 24, 1487-97. 2003.
29. Supova M. Problem of hydroxyapatite dispersion in polymer matrices: a review. J Mater Sci Mater Med 20[6], 1201-1213. 2009.

30. George J, Kuboki Y, Miyata T. Differentiation of mesenchymal stem cells into osteoblasts on honeycomb collagen scaffolds. Biotechnol Bioeng 95, 404-11. 2006.
31. Friess W. Collagen. Biomaterial for drug delivery. Eur J Pharm Biopharm 45[2], 113-136. 1998.
32. Du C, Cui FZ, de Groot K. Hydroxyapatite/collagen scaffolds. In: Ma PX, Elisseeff JH, eds. Scaffolding in Tissue Engineering. St Lucie Press, 2006: 265-74.
33. Persikov AV, Brodsky B. Unstable molecules form stable tissues. Proc Natl Acad Sci U S A 99[3], 1101-1103. 2002.
34. Davis GE. Affinity of integrins for damaged extracellular matrix: $\alpha_v\beta_3$ binds to denatured collagen type I through RGD sites. Biochem Biophys Res Commun 182[3], 1025-1031. 1992.
35. Kalita SJ, Bhatt HA. Nanocrystalline hydroxyapatite doped with magnesium and zinc: Synthesis and characterization. Mater Sci Eng C Biomim Mater Sens Syst 27[4], 837-848. 2007.
36. Olszta MJ, Cheng X, Jee SS, Kumar R, Kim YY, Kaufman MJ, Douglas EP, Gower LB. Bone structure and formation: A new perspective. Mater Sci Eng R Rep 58, 77-116. 2007.
37. Brandt J, Henning S, Michler G, Schulz M, Bernstein A. Nanocrystalline hydroxyapatite for bone repair. Key Eng Mater 361, 35-38. 2008.
38. Hu Q, Li B, Wang M, Shen J. Preparation and characterization of biodegradable chitosan/hydroxyapatite nanocomposite rods via in situ hybridization: a potential material as internal fixation of bone fracture. Biomaterials 25[5], 779-785. 2004.
39. Chen Q-Z, Boccaccini AR. Bioactive Materials and Scaffolds for Tissue Engineering. In: Wnek GE, Bowlin GL, eds. Encyclopedia of Biomaterials and Biomedical Engineering. Informa Healthcare, 2008: 143-51.
40. Murugan R, Ramakrishna S. Aqueous mediated synthesis of bioresorbable nanocrystalline hydroxyapatite. J Cryst Growth 274, 209-13. 2005.
41. Khor E. Chitin: Fulfilling a Biomaterials Promise. Elsevier, 2001.
42. Elder SH, Nettles DL, Bumgardner JD. Synthesis and characterization of chitosan scaffolds for cartilage-tissue engineering. In: Hollander AP, Hatton PV, eds. Biopolymer Methods in Tissue Engineering. Humana Press, 2004: 41-8.
43. Augsten C, Mäder K. Characterizing molar mass distributions and molecule structures of different chitosans using asymmetrical flow field-flow fractionation combined with multi-angle light scattering. Int J Pharm 351[1], 23-30. 2008.
44. Ogiso B, Hughes FJ, Melcher AH, McCulloch CA. Fibroblasts inhibit mineralised bone nodule formation by rat bone marrow stromal cells in vitro. J Cell Physiol 146[3], 442-450. 1991.

45. Tangsadthakun C, Kanokpanont S, Sanchavanakit N, Pichyangkura R, Banaprasert T, Tabata Y, Damrongsakkul S. The influence of molecular weight of Chitosan on the physical and biological properties of collagen/chitosan scaffolds. J Biomater Sci Polym Ed 18[2], 147-163. 2007.
46. Taravel MN, Domard A. Relation between the physicochemical characteristics of collagen and its interactions with chitosan: I. Biomaterials 14[12], 930-938. 1993.
47. Brey EM, King TW, Johnston C, McIntire L, Reece GP, Patrick CW. A technique for quantitative three-dimensional analysis of microvascular structure. Microvasc Res 63[3], 279-294. 2002.
48. Washburn NR, Weir M, Anderson P, Potter K. Bone formation in polymeric scaffolds evaluated by proton magnetic resonance microscopy and X-ray microtomography. J Biomed Mater Res A 69[4], 738-747. 2004.
49. Peptan IA, Hong L, Xu H, Magin RL. MR assessment of osteogenic differentiation in tissue-engineered constructs. Tissue Eng 12[4], 843-851. 2006.
50. Miyata S, Numano T, Homma K, Tateishi T, Ushida T. Feasibility of noninvasive evaluation of biophysical properties of tissue-engineered cartilage by using quantitative MRI. J Biomech 40[13], 2990-2998. 2007.
51. Potter K, Leapman RD, Basser PJ, Landis WJ. Cartilage calcification studied by proton nuclear magnetic resonance microscopy. J Bone Miner Res 17[4], 652-660. 2002.
52. Heinrich L, Freyria AM, Melin M, Tourneur Y, Maksoud R, Bernengo JC, Hartmann DJ. Confocal laser scanning microscopy using dialkylcarbocyanine dyes for cell tracing in hard and soft biomaterials. J Biomed Mater Res B Appl Biomater 81[1], 153-161. 2007.
53. Licha K, Olbrich C. Optical imaging in drug discovery and diagnostic applications. Adv Drug Deliv Rev 57[8], 1087-1108. 2005.
54. Bulte JWM. Intracellular endosomal magnetic labeling of cells. In: Prasad Pottumarthi V, ed. Magnetic Resonance Imaging: Methods and Biologic Applications. Humana Press, 2006: 419-39.
55. Bulte JWM, Kraitchman DL. Iron oxide MR contrast agents for molecular and cellular imaging. NMR Biomed 17[7], 484-499. 2004.
56. Frank JA, Miller BR, Arbab AS, Zywicke HA, Jordan E Kay, Lewis BK, Bryant LH, Bulte JWM. Clinically applicable labeling of mammalian and stem cells by combining superparamagnetic iron oxides and transfection agents. Radiology 228[2], 480-487. 2003.

57. Hamm J, Pulito R, Benedetto S, Barberis L, Hirsch E, Poli V, Silengo L. Magnetically enriched bone marrow-derived macrophages loaded in vitro with iron oxide can migrate to inflammation sites in mice. NMR Biomed 21[2], 120-128. 2007.
58. Kim D, Hong KS, Song J. The present status of cell tracking methods in animal models using magnetic resonance imaging technology. Mol Cells 23[2], 132-137. 2007.
59. Matuszewski L, Persigehl T, Wall A, Schwindt W, Tombach B, Fobker M, Poremba C, Ebert W, Heindel W, Bremer C. Cell tagging with clinically approved iron oxides: feasibility and effect of lipofection, particle size, and surface coating on labeling efficiency. Radiology 235[1], 155-161. 2005.
60. Rogers WJ, Meyer CH, Kramer CM. Technology insight: in vivo cell tracking by use of MRI. Nat Clin Pract Cardiovasc Med 3[10], 554-562. 2006.
61. Garrido L. Nondestructive evaluation of biodegradable porous matrices for tissue engineering. In: Morgan JR, Yarmush ML, eds. Tissue Engineering Methods and Protocols. Humana Press, 1999: 35-45.
62. Swider P, Conroy M, Pedrono A, Ambard D, Mantell S, Soballe K, Bechtold JE. Use of high-resolution MRI for investigation of fluid flow and global permeability in a material with interconnected porosity. J Biomech 40[9], 2112-2118. 2007.
63. Hartman Ed HM, Pikkemaat JA, Vehof Johan WM, Heerschap A, Jansen JA, Spauwen Paul HM. In vivo magnetic resonance imaging explorative study of ectopic bone formation in the rat. Tissue Eng 8[6], 1029-1036. 2002.
64. Conroy MJ, Pedrono A, Bechtold JE, Soballe K, Ambard D, Swider P. High-resolution magnetic resonance flow imaging in a model of porous bone-implant interface. Magn Reson Imaging 24[5], 657-661. 2006.
65. Neves AA, Medcalf N, Smith M, Brindle KM. Evaluation of engineered meniscal cartilage constructs based on different scaffold geometries using magnetic resonance imaging and spectroscopy. Tissue Eng 12[1], 53-62. 2006.
66. Bashir A, Gray ML, Hartke J, Burstein D. Nondestructive imaging of human cartilage glycosaminoglycan concentration by MRI. Magn Reson Med 41[5], 857-865. 1999.
67. Terrovitis JV, Bulte JWM, Sarvananthan S, Crowe LA, Sarathchandra P, Batten P, Sachlos E, Chester AH, Czernuszka JT, Firmin DN, Taylor PM, Yacoub MH. Magnetic Resonance Imaging of Ferumoxide-Labeled Mesenchymal Stem Cells Seeded on Collagen Scaffolds-Relevance to Tissue Engineering. Tissue Eng 12[10], 2765-2775. 2006.
68. Ittrich H, Lange C, Dahnke H, Zander AR, Adam G, Nolte-Ernsting C. Labeling of mesenchymal stem cells with different superparamagnetic particles of iron oxide and detectability with MRI at 3T. Rofo 177[8], 1151-1163. 2005.

69. Strübing S, Metz H, Mäder K. Characterization of poly(vinyl acetate) based floating matrix tablets. J Control Release 126[2], 149-155. 2008.
70. Metz H, Mäder K. Benchtop-NMR and MRI-A new analytical tool in drug delivery research. Int J Pharm 364[2], 170-175. 2008.
71. Kikuchi M, Ikoma T, Itoh S, Matsumoto HN, Koyama Y, Takakuda K, Shinomiya K, Tanaka J. Biomimetic synthesis of bone-like nanocomposites using the self-organization mechanism of hydroxyapatite and collagen. Compos Sci Technol 64[6], 819-825. 2004.
72. Zhang W, Liao SS, Cui FZ. Hierarchical Self-Assembly of Nano-Fibrils in Mineralized Collagen. Chem Mater 15[16], 3221-3226. 2003.
73. Itoh S, Kikuchi M, Takakuda K, Nagaoka K, Koyama Y, Tanaka J, Shinomiya K. Implantation study of a novel hydroxyapatite/collagen (HAp/Col) composite into weight-bearing sites of dogs. J Biomed Mater Res 63, 507-15. 2002.
74. Kikuchi M, Itoh S, Ichinose S, Shinomiya K, Tanaka J. Self-organization mechanism in a bone-like hydroxyapatite/collagen nanocomposite synthesized in vitro and its biological reaction in vivo. Biomaterials 22, 1705-11. 2001.
75. Hu Y, Zhang C, Zhang S, Xiong Z, Xu J. Development of a porous poly(L-lactic acid)/ hydroxyapatite/collagen scaffold as a BMP delivery system and its use in healing canine segmental bone defect. J Biomed Mater Research A 67, 591-8. 2003.
76. Wang Y, Cui FZ, Hu K, Zhu XD, Fan DD. Bone regeneration by using scaffold based on mineralized recombinant collagen. J Biomed Mater Res B Appl Biomater 86[1], 29-35. 2008.
77. Robinson C, Shore RC, Wood SR, Brookes SJ, Smith DA, Kirkham J. Initiation and modulation of crystal growth in skeletal tissues: role of extracellular matrix. In: Ellingsen JE, Lyngstadaas SP, eds. Bio-Implant Interface: Improving Biomaterials and Tissue Reactions. Crc Press, 2003: 231-45.
78. Andrade AL, Ferreira JMF, Domingues RZ. Zeta potential measurement in bioactive collagen. Materials Research 7[4], 631-634. 2004.
79. de Vos P, de Haan BJ, Kamps JAAM, Faas MM, Kitano T. Zeta-potentials of alginate-PLL capsules: a predictive measure for biocompatibility? J Biomed Mater Res A 80[4], 813-819. 2007.
80. Das KK. Electrokinetics of Mineral Particles. In: Hubbard A, ed. Encyclopedia of Surface and Colloid Science. Marcel Dekker 2002: 1894-906.
81. Russell AE. Effect of pH on thermal stability of collagen in the dispersed and aggregated states. Biochem J 139[1], 277-280. 1974.
82. Jiang F, Hoerber H, Howard J, Mueller DJ. Assembly of collagen into microribbons: effects of pH and electrolytes. J Struct Biol 148[3], 268-278. 2004.

83. Hattori S, Adachi E, Ebihara T, Shirai T, Someki I, Irie S. Alkali-treated collagen retained the triple helical conformation and the ligand activity for the cell adhesion via alpha 2 beta 1 integrin. J Biochem 125[4], 676-684. 1999.
84. Intensive course on the determination of the zeta potential by electrophoretic light scattering in Kirschau, Germany, January 2008, course manual 2008. Malvern Instruments Ltd.
85. Freudenberg U, Behrens SH, Welzel PB, Mueller M, Grimmer M, Salchert K, Taeger T, Schmidt K, Pompe W, Werner C. Electrostatic interactions modulate the conformation of collagen I. Biophys J 92[6], 2108-2119. 2007.
86. Sato K, Kumagai Y, Tanaka J. Inorganic-organic interfacial interactions in hydroxyapatite mineralization processes. Top Curr Chem 270 [Biomineralization I], 127-153. 2007.
87. Taravel MN, Domard A. Collagen and its interactions with chitosan III. Some biological and mechanical properties. Biomaterials 17[4], 451-455. 1996.
88. Taravel MN, Domard A. Collagen and its interaction with chitosan II. Influence of the physicochemical characteristics of collagen. Biomaterials 16[11], 865-871. 1995.
89. Sionkowska A, Wisniewski M, Skopinska J, Kennedy CJ, Wess TJ. Molecular interactions in collagen and chitosan blends. Biomaterials 25[5], 795-801. 2003.
90. Gupta AN, Bohidar HB, Aswal VK. Surface patch binding induced intermolecular complexation and phase separation in aqueous solutions of similarly charged gelatin-chitosan molecules. J Phys Chem B 111[34], 10137-10145. 2007.
91. Eppell SJ, Tong W, Katz JL, Kuhn L, Glimcher MJ. Shape and size of isolated bone mineralites measured using atomic force microscopy. J Orthop Res 19[6], 1027-1034. 2001.
92. Durucan C, Brown PW. Biodegradable hydroxyapatite-polymer composites. Advanced Engineering Materials 3[4], 227-231. 2001.
93. Liao S, Ngiam M, Chan CK, Ramakrishna S. Fabrication of nano-hydroxyapatite/ collagen/osteonectin composites for bone graft applications. Biomed Mater 4[2], 025019-1-025019/8. 2009.
94. Koenig JL. Fourier transform infrared spectroscopy of polymers. In: Frank CW, Koenig JL, von Meerwall ED, eds. Spectroscopy: NMR, Fluroescence, FT- IR. Springer, 1984: 87-154.
95. Ruys AJ, Wei M, Sorrell CC, Dickson MR, Brandwood A, Milthorpe BK. Sintering effects on the strength of hydroxyapatite. Biomaterials 16[5], 409-415. 1995.
96. von Heimburg D, Zachariah S, Kuhling H, Heschel I, Schoof H, Hafemann B, Pallua N. Human preadipocytes seeded on freeze-dried collagen scaffolds investigated in vitro and in vivo. Biomaterials 22[5], 429-438. 2001.

97. Chau DYS, Collighan RJ, Verderio EAM, Addy VL, Griffin M. The cellular response to transglutaminase-cross-linked collagen. Biomaterials 26[33], 6518-6529. 2005.
98. Guo T, Zhao J, Chang J, Ding Z, Hong H, Chen J, Zhang J. Porous chitosan-gelatin scaffold containing plasmid DNA encoding transforming growth factor-β 1 for chondrocytes proliferation. Biomaterials 27, 1095-103. 2006.
99. Zhang Y, Cheng X, Wang J, Wang Y, Shi B, Huang C, Yang X, Liu T. Novel chitosan/ collagen scaffold containing transforming growth factor-β 1 DNA for periodontal tissue engineering. Biochem Biophys Res Commun 344, 362-9. 2006.
100. Ueda H, Nakamura T, Tabata Y, Shimizu Y. Repairing of rabbit skull defect by TGF-ß1-incorporated collagen sponges of different thickness. Biomedical Engineering-Applications, Basis & Communications 15, 1-7. 2003.
101. Marx CK, Hertel TC, Pietzsch M. Soluble expression of a pro-transglutaminase from Streptomyces mobaraensis in Escherichia coli. Enzyme Microb Technol 40[6], 1543-1550. 2007.
102. Marx CK, Hertel TC, Pietzsch M. Purification and activation of a recombinant histidine-tagged pro-transglutaminase after soluble expression in Escherichia coli and partial characterization of the active enzyme. Enzyme Microb Technol 42[7], 568-575. 2008.
103. Marx CK, Hertel TC, Pietzsch M. Random mutagenesis of a recombinant microbial transglutaminase for the generation of thermostable and heat-sensitive variants. J Biotechnol 136, 156-162. 2008.
104. Gelinsky M, Welzel PB, Simon P, Bernhardt A, Koenig U. Porous 3-dimensional scaffolds made of mineralised collagen: Preparation and properties of a biomimetic nanocomposite material for tissue engineering of bone. Chem Eng J 137[1], 84-96. 2008.
105. Pek YS, Gao S, Arshad MSM, Leck KJ, Ying JY. Porous collagen-apatite nanocomposite foams as bone regeneration scaffolds. Biomaterials 29[32], 4300-4305. 2008.
106. Shim IK, Lee SY, Park YJ, Lee MC, Lee SH, Lee JY, Lee SJ. Homogeneous chitosan-PLGA composite fibrous scaffolds for tissue regeneration. J Biomed Mater Res A 84[1], 247-255. 2008.
107. Vert M, Mauduit J, Li S. Biodegradation of PLA/GA polymers: increasing complexity. Biomaterials 15[15], 1209-1213. 1994.
108. Klose D, Siepmann F, Elkharraz K, Siepmann J. PLGA-based drug delivery systems: Importance of the type of drug and device geometry. Int J Pharm 354[1-2], 95-103. 2008.

109. Haugh MG, Jaasma MJ, O´Brien FJ. Dehydrothermal crosslinking of Collagen-GAG scaffolds. Bioengineering in Ireland Conference. January 27-28, 2006, Clybaun Hotel, Galway, Ireland.
110. Griffin M, Casadio R, Bergamini CM. Transglutaminases: Nature's biological glues. Biochem J 368[2], 377-396. 2002.
111. Kaartinen MT, El-Maadawy S, Rasanen NH, McKee MD. Tissue transglutaminase and its substrates in bone. J Bone Miner Res 17[12], 2161-2173. 2002.
112. Ravikumar KM, Hwang W. Region-specific role of water in collagen unwinding and assembly. Proteins 72[4], 1320-1332. 2008.
113. Yang J, Yamato M, Shimizu T, Sekine H, Ohashi K, Kanzaki M, Ohki T, Nishida K, Okano T. Reconstruction of functional tissues with cell sheet engineering. Biomaterials 28[34], 5033-5043. 2007.
114. Nagase K, Kobayashi J, Okano T. Temperature-responsive intelligent interfaces for biomolecular separation and cell sheet engineering. J R Soc Interface 6[Suppl. 3], 293-309. 2009.
115. Landers R, Pfister A, Hübner U, John H, Schmelzeisen R, Mülhaupt R. Fabrication of soft tissue engineering scaffolds by means of rapid prototyping techniques. Journal of Materials Science 37, 3107-16. 2002.
116. Stevens B, Yang Y, Mohandas A, Stucker B, Nguyen KT. A review of materials, fabrication methods, and strategies used to enhance bone regeneration in engineered bone tissues. J Biomed Mater Res B Appl Biomater 85[2], 573-582. 2008.
117. Ang TH, Sultana FSA, Hutmacher DW, Wong YS, Fuh JYH, Mo XM, Loh HT, Burdet E, Teoh SH. Fabrication of 3D chitosan-hydroxyapatite scaffolds using a robotic dispensing system. Mater Sci Eng C Biomim Mater Sens Syst 20, 35-42. 2002.
118. Herklotz M, Melamed M, Trautmann C, Nitschke M, Pompe T, Gast FU, Howitz F, Werner C. Non-contact printing of proteins on reactive polymer surfaces: A novel route towards structured and graded cell culture carriers. Microfluid Nanofluidics 3[5], 629-633. 2007.
119. Lee W, Debasitis JC, Lee VK, Lee J, Fischer K, Edminster K, Park J, Yoo S. Multi-layered culture of human skin fibroblasts and keratinocytes through three-dimensional freeform fabrication. Biomaterials 30[8], 1587-1595. 2009.
120. Isobe M, Yamazaki Y, Oida Si, Ishihara K, Nakabayashi N, Amagasa T. Bone morphogenetic protein encapsulated with a biodegradable and biocompatible polymer. J Biomed Mater Res 32[3], 433-438. 1996.
121. Murua A, Portero A, Orive G, Hernandez RM, de Castro M, Pedraz JL. Cell microencapsulation technology: Towards clinical application. J Control Release 132[2], 76-83. 2008.

122. Siperko LM, Landis WJ. Aspects of Mineral Structure in Normally Calcifying Avian Tendon. J Struct Biol 135[3], 313-320. 2001.
123. Fratzl P, Schreiber S, Klaushofer K. Bone mineralization as studied by small-angle x-ray scattering. Connect Tissue Res 34[4], 247-254. 1996.
124. Kinney JH, Pople JA, Marshall GW, Marshall SJ. Collagen orientation and crystallite size in human dentin: a small angle X-ray scattering study. Calcif Tissue Int 69[1], 31-37. 2001.
125. Spurr AR. A low-viscosity epoxy resin embedding medium for electron microscopy. J Ultrastruct Res 26[1-2], 31-43. 1969.
126. Wang PE, Chaki TK. Sintering behavior and mechanical properties of hydroxyapatite and dicalcium phosphate. J Mater Sci Mater Med 4[2], 150-158. 1993.
127. Zhao C, Pan Y, He C, Guo Z, Sun L. Determination of EDTA species in water by second-derivative square-wave voltammetry using a chitosan-coated glassy carbon electrode. Anal Sci 19[4], 607-609. 2003.
128. Podrazky V, Sedmerova V. Densities of collagen dehydrated by some organic solvents. Experientia 22[12], 792. 1966.
129. Henkelman RM, Watts JF, Kucharczyk W. High signal intensity in MR images of calcified brain tissue. Radiology 179[1], 199-206. 1991.
130. Davis CA, Genant HK, Dunham JS. The effects of bone on proton NMR relaxation times of surrounding liquids. Invest Radiol 21[6], 472-477. 1986.
131. Nitzsche H, Lochmann A, Metz H, Hauser A, Syrowatka F, Hempel E, Müller T, Thurn-Albrecht T, Mäder K. Fabrication and characterization of a biomimetic composite scaffold for bone defect repair. J Biomed Mater Res A . 2010. DOI: 10.1002/jbm.a.32703
132. Bignon A, Chouteau J, Chevalier J, Fantozzi G, Carret J-P, Chavassieux P, Boivin G, Melin M, Hartmann D. Effect of micro- and macroporosity of bone substitutes on their mechanical properties and cellular response. J Mater Sci Mater Med 14[12], 1089-1097. 2003.
133. Park H, Temenoff JS, Mikos AG. Biodegradable orthopedic implants. In: Bronner F, Farach-Carson MC, Mikos AG, eds. Engineering of Functional Skeletal Tissues. Springer, 2007: 55-68.
134. Rehfeldt F, Engler AJ, Eckhardt A, Ahmed F, Discher DE. Cell responses to the mechanochemical microenvironment-Implications for regenerative medicine and drug delivery. Adv Drug Deliv Rev 59[13], 1329-1339. 2007.
135. Hacker M, Tessmar J, Neubauer M, Blaimer A, Blunk T, Göpferich A, Schulz MB. Towards biomimetic scaffolds: anhydrous scaffold fabrication from biodegradable amine-reactive diblock copolymers. Biomaterials 24[24], 4459-4473. 2003.

136. DIN 53421 "Testing of rigid cellular plastics; compression test". 1984. Beuth Verlag
137. DIN EN ISO 1798 "Flexible cellular polymeric materials - Determination of tensile strength and elongation at break". 2008. Beuth Verlag
138. Keller TS, Liebschner MAK. Tensile and Compression Testing of Bone. In: An YH, Draughn RA, eds. Mechanical Testing of Bone and the Bone-Implant Interface. Crc Press, 2000: 175-205.
139. Besheer AIH. Dissertation: Nanomedicines based on modified hydroxyethyl starch. Martin-Luther-Universität Halle-Wittenberg. 2008
140. Cullinane DM, Salisbury KT. Biomechanics. In: Hollinger JO, Einhorn TA, Doll BA, Sfeir C, eds. Bone Tissue Engineering. Crc Press, 2005: 245-74.
141. An YH, Barfield WR, Draughn RA. Basic Concepts of Mechanical Property Measurement and Bone Biomechanics. In: An YH, Draughn RA, eds. Mechanical Testing of Bone and the Bone-Implant Interface. Crc Press, 2000: 24-40.
142. Lee JH, Kisiday J, Grodzinsky AJ. Tissue-engineered versus native cartilage: linkage between cellular mechano-transduction and biomechanical properties. Bock G, Goode J. Novartis Foundation Symposium 249, 52-69. 2003.
143. Levental I, Georges PC, Janmey PA. Soft biological materials and their impact on cell function. Soft Matter 3[3], 299-306. 2007.
144. Kasahara Y, Iwasaki N, Yamane S, Igarashi T, Majima T, Nonaka S, Harada K, Nishimura SI, Minami A. Development of mature cartilage constructs using novel three-dimensional porous scaffolds for enhanced repair of osteochondral defects. J Biomed Mater Res A 86[1], 127-136. 2008.
145. Leon EJ, Verma N, Zhang S, Lauffenburger DA, Kamm RD. Mechanical properties of a self-assembling oligopeptide matrix. In: Shoichet MS, Hubbell JA, eds. Polymers for Tissue Engineering. VSP, 1998: 3-18.
146. Wen F, Chang S, Toh YC, Teoh SH, Yu H. Development of poly (lactic-co-glycolic acid)-collagen scaffolds for tissue engineering. Mater Sci Eng C Biomim Mater Sens Syst 27[2], 285-292. 2007.
147. Eslaminejad MB, Mirzadeh H, Mohamadi Y, Nickmanzar A. Bone differentiation of marrow-derived mesenchymal stem cells using β-tricalcium phosphate-alginate-gelatin hybrid scaffolds. J Tissue Eng Regener Med 1[6], 417-424. 2007.
148. Kisiday J, Kerin A, Grodzinsky A. Mechanical testing of cell-material constructs: a review. In: Hollander AP, Hatton PV, eds. Biopolymer Methods in Tissue Engineering. Humana Press, 2004: 239-54.
149. Cowin SC. Bone poroelasticity. J Biomech 32[3], 217-238. 1999.
150. Biot MA. General theory of three-dimensional consolidation. J Appl Phys 12, 155-164. 1941.

151. Biot MA. Theory of elasticity and consolidation for a porous anisotropic solid. J Appl Phys 26, 182-185. 1955.
152. Kang HG, Lee SB, Lee YM. Novel preparative method for porous hydrogels using overrun process. Polym Int 54, 537-43. 2005.
153. Garcia Y, Collighan R, Griffin M, Pandit A. Assessment of cell viability in a three-dimensional enzymatically cross-linked collagen scaffold. J Mater Sci Mater Med 18[10], 1991-2001. 2007.
154. Clover J, Gowen M. Are MG-63 and HOS TE85 human osteosarcoma cell lines representative models of the osteoblastic phenotype? Bone 15[6], 585-591. 1994.
155. Margaret CH-L, Wallis C, Shou Z, Farhat WA. Quantifying angiogenesis in VEGF-enhanced tissue-engineered bladder constructs by dynamic contrast-enhanced MRI using contrast agents of different molecular weights. J Magn Reson Imaging 25[1], 137-145. 2007.
156. Neu CP, Arastu HF, Curtiss S, Reddi AH. Characterization of engineered tissue construct mechanical function by magnetic resonance imaging. J Tissue Eng Regen Med 3[6], 477-485. 2009.
157. Bumgardner JD, Vasquez-Lee M, Fulzele KS, Smith DH, Branch KD, Christian SI, Williams DL. Biocompatibility testing. In: Wnek GE, Bowlin GL, eds. Encyclopedia of Biomaterials and Biomedical Engineering. Informa Healthcare, 2008: 169-78.
158. Dell'Accio F, De Bari C, Luyten FP. Molecular markers predictive of the capacity of expanded human articular chondrocytes to form stable cartilage in vivo. Arthritis Rheum 44[7], 1608-1619. 2001.
159. Schulze-Tanzil G, de Souza P, Villegas Castrejon H, John T, Merker HJ, Scheid A, Shakibaei M. Redifferentiation of dedifferentiated human chondrocytes in high-density cultures. Cell Tissue Res 308[3], 371-379. 2002.
160. Doherty PJ. Cell culture assays. In: Wnek GE, Bowlin GL, eds. Encyclopedia of Biomaterials and Biomedical Engineering. Informa Healthcare, 2008: 561-7.
161. Frank JA, Anderson SA, Arbab AS. Methods for labeling nonphagocytic cells with MR contrast agents. In: Modo MMJ, Bulte JWM, eds. Molecular and Cellular MR Imaging. Taylor & Francis, 2007: 295-324.
162. Daldrup-Link HE, Meier R, Rudelius M, Piontek G, Piert M, Metz S, Settles M, Uherek C, Wels W, Schlegel J, Rummeny EJ. In vivo tracking of genetically engineered, anti-HER2/neu directed natural killer cells to HER2/neu positive mammary tumors with magnetic resonance imaging. Eur Radiol 15[1], 4-13. 2005.
163. Pinkernelle J, Teichgraeber U, Neumann F, Lehmkuhl L, Ricke J, Scholz R, Jordan A, Bruhn H. Imaging of single human carcinoma cells in vitro using a clinical whole-body magnetic resonances scanner at 3.0 T. Magn Reson Med 53[5], 1187-1192. 2005.

164. Schaefer R, Kehlbach R, Wiskirchen J, Bantleon R, Pintaske J, Brehm BR, Gerber A, Wolburg H, Claussen CD, Northoff H. Transferrin receptor upregulation: in vitro labeling of rat mesenchymal stem cells with superparamagnetic iron oxide. Radiology 244[2], 514-523. 2007.
165. Arbab AS, Wilson LB, Ashari P, Jordan EK, Lewis BK, Frank JA. A model of lysosomal metabolism of dextran coated superparamagnetic iron oxide (SPIO) nanoparticles: implications for cellular magnetic resonance imaging. NMR Biomed 18[6], 383-389. 2005.
166. Vunjak-Novakovic G, Radisic M. Cell seeding of polymer scaffolds. In: Hollander AP, Hatton PV, eds. Biopolymer Methods in Tissue Engineering. Humana Press, 2004: 131-45.
167. Halbleib M, Skurk T, de LC, von HD, Hauner H. Tissue engineering of white adipose tissue using hyaluronic acid-based scaffolds. I: in vitro differentiation of human adipocyte precursor cells on scaffolds. Biomaterials 24[18], 3125-3132. 2003.
168. Rotman B, Papermaster BW. Membrane properties of living mammalian cells as studied by enzymic hydrolysis of fluorogenic esters. Proc Natl Acad Sci U S A 55[1], 134-141. 1966.
169. Armour AD, Powell HM, Boyce ST. Fluorescein diacetate for determination of cell viability in tissue-engineered skin. Tissue Eng Part C Methods 14[1], 89-96. 2008.
170. Li G, Cui Y, McILmurray L, Allen WE, Wang H. rhBMP-2, rhVEGF165, rhPTN and thrombin-related peptide, TP508 induce chemotaxis of human osteoblasts and microvascular endothelial cells. J Orthop Res 23[3], 680-685. 2005.
171. Nitzsche H, Metz H, Lochmann A, Bernstein A, Hause G, Groth T, Mäder K. Characterization of Scaffolds for Tissue Engineering by Benchtop-Magnetic Resonance Imaging. Tissue Eng Part C Methods 15[3], 513-521. 2009.
172. Ishiyama M, Shiga M, Sasamoto K, Mizoguchi M, He PG. A new sulfonated tetrazolium salt that produces a highly water-soluble formazan dye. Chem Pharm Bull 41[6], 1118-1122. 1993.
173. Claassen H, Kampen WU. Localization of collagens and alkaline phosphatase activity during mineralization and ossification of human first rib cartilage. Histochem Cell Biol 105[3], 213-219. 1996.
174. Schoen I, Rahne T, Markwart A, Neumann K, Berghaus A, Roepke E. Cartilage replacement by use of hybrid systems of autologous cells and polyethylene: an experimental study. J Mater Sci Mater Med 20[10], 2145-2154. 2009.
175. Hine IF. Block staining of mammalian tissues with hematoxylin and eosin. Stain Technol 56[2], 119-123. 1981.

176. Lendrum AC, Slidders W, Fraser DS. Renal hyalin. A study of amyloidosis and diabetic fibrinous vasculosis with new staining methods. J Clin Pathol 25[5], 373-396. 1972.
177. Miller RR, McDevitt CA. A quantitative microwell assay for chondrocyte cell adhesion. Anal Biochem 192[2], 380-383. 1991.
178. van Blitterswijk CA, Stamatialis D, Unandhar H, Papenburg B, Rouwkema J, Truckenmuller R, van Apeldoorn A, Wessling M, de Boer J. Materiomics: Dealing with Complexity in Tissue Engineering. Tissue Eng Part A 14[5], 796. 2008.
179. van Blitterswijk CA, Stamatialis D, Unandhar H, Papenburg B, Rouwkema J, Truckenmuller R, van Apeldoorn A, Wessling M, de Boer J. Materiomics: Dealing with Complexity in Tissue Engineering. Book of Abstracts: 2008 E-MRS Fall Meeting & Exhibit. 2009: 251.
180. Seo YK, Yoon HH, Park YS, Song KY, Lee WS, Park JK. Correlation between scaffold in vivo biocompatibility and in vitro cell compatibility using mesenchymal and mononuclear cell cultures. Cell Biol Toxicol 25[5], 513-522. 2009.
181. Kaiser ML, Karam AM, Sepehr A, Wong H, Liaw Lih-Huei L, Vokes DE, Wong BJ. Cartilage regeneration in the rabbit nasal septum. Laryngoscope 116[10], 1730-1734. 2006.
182. Simsa S, Ornan EM. Endochondral ossification process of the Turkey (Meleagris gallopavo) during embryonic and juvenile development. Poult Sci 86[3], 565-571. 2007.
183. Naumann A, Dennis JE, Awadallah A, Carrino DA, Mansour JM, Kastenbauer E, Caplan AI. Immunochemical and mechanical characterization of cartilage subtypes in rabbit. J Histochem Cytochem 50[8], 1049-1058. 2002.
184. Rosenberg L. Chemical basis for the histological use of safranin 0 in the study of articular cartilage. J Bone Joint Surg 53[1], 69-82. 1971.
185. Tallheden T, Dennis JE, Lennon DP, Sjogren-Jansson E, Caplan A, I, Lindahl A. Phenotypic plasticity of human articular chondrocytes. J Bone Joint Surg 85[Suppl 2], 93-100. 2003.

APPENDIX

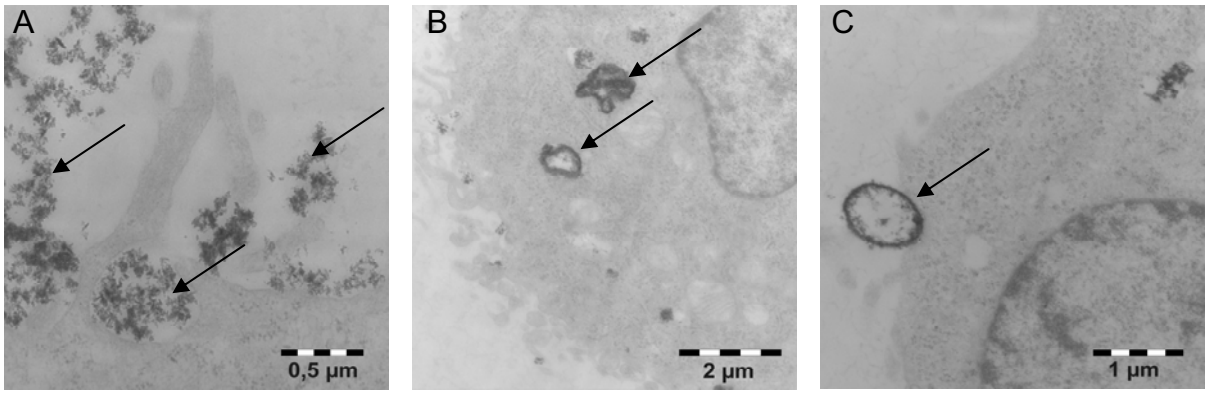

Fig. 5.1 TEM images of MG63 cells obtained under the same experimental conditions as used for the evaluation of the labeling efficiency (see 7.2.5), arrows indicate the iron depositions. An endocytotic process is apparent to be responsible for the uptake of SPIO´s by the cells. The SPIO´s are visible as being engulfed by cellular structures (A). It should be noted that during this stage the SPIO´s appear quite dispersed in the culture medium. After the uptake they are enclosed inside vesicular structures. It seems as if the SPIO´s were accumulated on the surface of these vesicles (B). Such vesicles were also found to be expelled from the cell (C).

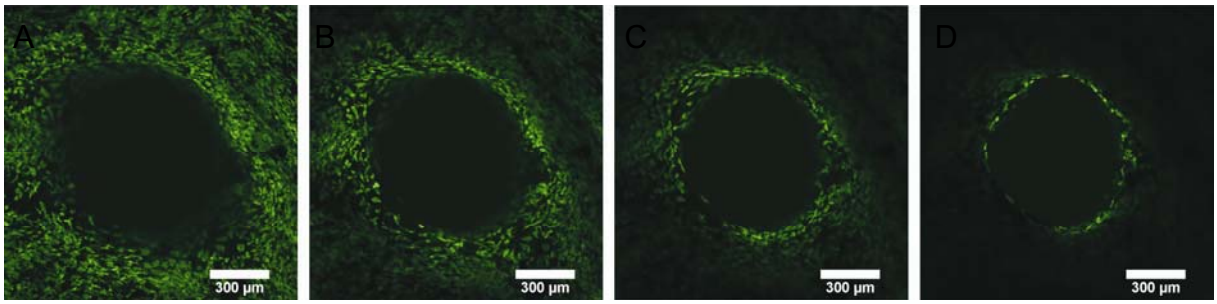

Fig. 5.2 CLSM images of fluorescein diacetate-stained cells growing on a perforated cylindrical hydroxyapatite-collagen-chitosan scaffold. This scaffold modification is described in chapter 6 (Fig. 3.9).On the surface a quite confluent cell growth around the perforation is visible (A). The following images (B-D) represent optical slices obtained during stepwise focusing deeper into the scaffold. It is obvious that the farther the distance is to the surface the less viable cells were found. At around 130 µm deep inside the construct almost no viable cell was found except in direct proximity of the perforation (D).

ACKNOWLEDGEMENT

So many people have supported me directly or indirectly, knowingly or unconsciously. They are too much to mention all of them by name. Almost all of them did it in an unconditional way. I really feel deeply indebted for so much support without those this work would have never been possible. This acknowledgement is not at all enough to balance the support, encouragement, assistance and sponsorship I found during this way, but it takes at least a small part of the sense of indebtedness I am bearing these days.

Notably, it is a deep wish and emphatic pleasure for me to thank my supervisor Professor Karsten Mäder. I want to express my hearty gratitude to him, especially, for the professional guidance combined with a grant of conceivably much liberty and for being like a fountain of creativity and motivation. Additionally, I want to thank him for enabling possibilities to present parts of this work on impressive scientific meetings so far away from the place of work.

As second, I want to acknowledge Dr. Hendrik Metz and Alexander Lochmann. Both were amicable and reliable companions on the travels related to this work. I express my gratitude to Dr. Metz especially for the help with the accomplishment and evaluation of all MRI experiments and also for several inspiring discussions about various other parts of this work. My friend and colleague Alex, I thank for the intense and enduring support in so much scientific, linguistic, organisational and private issues.

My thanks also go to Professor Thomas Groth and his coworkers, especially Dieter Peschel and Dr. Jürgen Vogel for giving me the possibility to do the cell culture experiments in their lab, the support during its completion and assessment and for the assistance during the CLSM observation.

Furthermore, I express my gratitude to Dr. Ilona Schön and her coworkers for the active contribution on the cell compatibility evaluation of the coated polyglycolic acid meshes with primary chondrocytes and osteoblasts.

Dr. Anke Bernstein and her coworkers, especially Mrs. Vetter I want to thank for the help before and during all experiments concerned with the light microscopic evaluation of the SPIO labelled MG63 cells.

I also would like to acknowledge Professor Thomas Thurn-Albrecht and Dr. Elke Hempel for giving me guidance during the SAXS measurements and that they repeatedly took the time for discussions about the results.

I want to express my gratefulness to Professor Michaela Schulz-Siegmund and her coworkers, namely Kristina Ambrosch and Dr. Michael Hacker for providing the PLGA scaffolds. Maja Porodec shall be acknowledged for experiments on the osteogenic properties of the composite material which are not mentioned in the thesis.

My thanks for guidance, support and conversation are directed to Dr. Gerd Hause regarding the TEM investigation, to Dr. Anton Hauser regarding the AFM measurements, to Frank Syrowatka for the ESEM examination and to Dr. Thomas Müller for the XRD analysis.

My thanks also go to Dr. Stefan Schwan, Benjamin Jost and Professor Andreas Heilmann for the help in all fields regarding the characterization of mechanical properties and to Dr. Steffen Howitz and Thomas Wegener from GeSiM mbh for the support during the experiments with the Nano-Plotter™.

I acknowledge Professor Markus Pietzsch and his coworkers, especially Katja Patzsch for providing the enzyme for the collagen crosslinking and the information regarding its application.

Moreover, I thank Dr. Rolf Nitzsche from Malvern Instruments GmbH for enabling zeta potential measurements in combination with titrations and for the support in the related result interpretation.

I also want to express my gratitude to Gabriele Weber, Lutz Buchheister and Gerald Kunt from Porex Technologies GmbH for the courtesy of the mercury intrusion porosimetry experiments and for the help and explanation during its accomplishment.

Furthermore, I thank Dr. Ahmed Besheer for the allocation of Gd-DTPA-HES and several inspiring conversations.

Additionally, I acknowledge Kerstin Schwarz for the help with TGA, Heidi Pötzsch for the assistance regarding the lyophilisation, Dieter Reese, Andreas Nietzschmann and their coworkers for involvement and technical support in the development and optimization of an imaging vessel for fixation and incubation of the scaffolds during the MRI.

Special thanks I want to direct to some students, namely Andreas Noack, Camargo Oliveira, Carina Morgenstern and Michael Pfau, who assisted me in different practical issues of this work. Beside the manpower, it was especially their interest and critical scrutinising that initiated challenging ideas.

I want to express my gratitude to all other members of the Pharmaceutical Technology Group of the Martin-Luther-University, who were not personally mentioned here, for so much help during the time I was working there and for the comfortable working atmosphere.

For financial support, I acknowledge the “Graduiertenförderung des Landes Sachsen-Anhalt” and the Martin-Luther-University of Halle.

Particular gratitude is directed to my parents. Their love, empathy, encouragement and frankness on the one hand and their strictness and orders on the other hand are one main reason for me accomplishing this work.

For invaluable mental support I thank my girlfriend Sabrina, my brother Henning and all my chummy friends.

Last, but by no means least, I thank mother earth and father sky.

PUBLICATIONS

Research papers:

Nitzsche, H., Metz, H., Lochmann, A., Bernstein, A., Hause, G., Groth, T., Mäder, K. Characterization of Scaffolds for Tissue Engineering by Benchtop-Magnetic Resonance Imaging. Tissue Engineering Part C: Methods; 15[3], 513-521. 2009

Nitzsche, H., Lochmann, A., Metz, H., Hauser, A., Syrowatka, F., Hempel, E., Müller, T., Thurn-Albrecht, T., Mäder, K.
Fabrication and Characterization of a Biomimetic Composite Scaffold for Bone Defect Repair. Journal of Biomedical Materials Research Part A; DOI: 10.1002/jbm.a.32703

Oral Presentations:

Nitzsche, H., Mäder, K.
ESR Spectroscopy and Benchtop MRI for Investigation of Hydroxyapatite Loaded Collagen Chitosan Scaffolds; Controlled Release Society, German Chapter Annual Meeting, Freiburg, March 2007

Nitzsche, H., Mäder, K.
Development and Characterization of Scaffolds Facilitating Bone Regeneration; Pharmaceutical Technology Meeting at Bayer Bitterfeld GmbH, Bitterfeld, November 2007

Nitzsche, H., Mäder, K.
Different Strategies for Production and Characterisation of Collagen-Chitosan-Scaffolds; International Symposium Bio meets Nano and IT, Halle, Dezember 2007

Nitzsche, H., Mäder, K.
Development & Characterization of a nano-Hydroxyapatite – Collagen – Chitosan Scaffold for Bone Regeneration; Controlled Release Society, German Chapter Annual Meeting, Halle, March 2009

Poster Presentations:

Nitzsche, H., Metz, H., Peschel, D., Vogel, J., Groth, T., Mäder, K.
Development and characterisation of hydroxyapatite/collagen/chitosan scaffolds for facilitated bone regeneration; Fraunhofer Life Science Symposium, Leipzig, October 2006

Nitzsche, H., Metz, H., Besheer, A., Kempe, S., Peschel, D., Vogel, J., Groth, T., Mäder, K.
Hydroxyapatite/collagen/chitosan scaffolds for enhanced bone regeneration - development and characterisation; 2. Wiener Biomaterialsymposium, Wien, November 2006

Nitzsche, H., Metz, H., Besheer, A., Peschel, D., Vogel, J., Hause, G., Groth, T., Mäder, K.
Non-Invasive Characterization of Hydroxyapatite-loaded Collagen-Chitosan-Scaffolds for Bone Regeneration by Benchtop-MRI; 34th Annual Meeting and Exposition of the Controlled Release Society, Long Beach, July 2007

Nitzsche, H., Wegener, T., Metz, H., Peschel, D., Hause, G., Howitz, S., Groth, T., Mäder, K.
Different Strategies for Production and Characterisation of Collagen-Chitosan-Scaffolds; 3rd World Congress on Regenerative Medicine, Leipzig, October 2007

Nitzsche, H., Noack, A., Lochmann, A., Oliveira, C., Besheer, A., Metz, H., Hause, G., Bernstein, A., Groth, T., Mäder, K.
Scaffold Properties and Interaction with Cells Investigated by Magnetic Resonance Methods; Tissue Engineering and Regenerative Medicine International Society - European Annual Meeting, Porto, June 2008

CURRICULUM VITAE

Personal Information

Name	Hagen Nitzsche
Date of birth	28.09.1980
Place of birth	Bautzen, Saxony, Germany
Nationality	German

Education & work experience

Since December 2009	Teacher for galenics and for physical measurements in a private professional school, Medical profession academy, Naumburg
July 2008 - September 2009	Research assistant in the department of pharmaceutical technology, Institute of Pharmacy, Martin Luther University, Halle
April 2006 - June 2008	PhD Student with postgraduate scholarship in the department of pharmaceutical technology, Institute of Pharmacy, Martin Luther University, Halle
September 2005 - February 2006	Student apprentice in a pharmacy, Ostapotheke, Kamenz
December 2004 - July 2005	Diploma thesis at the Institute of pharmaceutical biology, Ernst Moritz Arndt University, Greifswald
October 2000 - October 2004	Faculty of Pharmacy, Ernst Moritz Arndt University of Greifswald
September 1999 - August 2000	Civilian service in an orthopaedic clinic, Asclepios Orthopädische Klinik, Hohwald
August 1992 - July 1999	Academic prep school, Wilthen

EPILOGUE

9.3 English version

Beyond the scientific enthusiasm one should look a bit further. As so often in life, what shines so bright has its dark side, too. To the author's opinion, Tissue Engineering makes no exception, it is a double-edged sword as well. To get back to the introduction, it seems reasonable to find a comparison for the costs of such therapies. One InductOs® Kit costs around 3800 €. The average income of an African person per year is around 550 €. Therefore, it is quite improbable that the broad populace will benefit from these developments. Certainly, constructs precultivated with cells will be much more expensive. Even for European or US American circumstances it seems that only a few individuals will be able to afford such medical care. Hence, it appears that by Tissue Engineering opportunities appear which provide a considerable lifetime prolongation for a very small group of wealthy individuals. For sure, the costs are justified because of very high amounts of source materials, energy and effort needed for development and supply. But in times where the restricted resources of livelihood become more and more obvious, this appears quite disputable. Notionally, lifetime prolongation for one person will most likely come along with deprivation of livelihood for more than one other person.

Many people run for career, consumer products, money, and short-term satisfaction. But is there a final point in this run? Is there a higher probability to achieve such aims even with prolonged lifetime? To the authors opinion there is no need to artificially prolong the live of somebody just running for non-achievable aims, especially, as long as children die from hunger. This may sound very heartless and cold-blooded, but we should think about our relation to death. Probably, there is a wrong relation between the individual in our community and the conception of death. In former, so-called "uncivilized" communities, there was a different relation to the end of life. We squeezed the native people on so many places on earth, to finally become a cancer like entity on our planet.

In this regard, the humanitarian highlighted field of Tissue Engineering might provide a shady side on the sociality of mankind. In the broader sense, a eugenic like benefit for wealthy people could even disclose a new impact on the evolution of the human race.

"We are on the verge of global transformation. All we need is the right major crisis and the nations will accept the new world order." David Rockefeller

9.4 German version

Jenseits des wissenschaftlichen Enthusiasmus sollte man ein bisschen weiter schauen. Wie es oft im Leben ist, hat alles, was so hell scheint, auch seine Schattenseiten. Nach Ansicht des Autors macht Tissue Engineering da keine Ausnahme, es ist genauso ein zweischneidiges Schwert. Um auf die Einleitung zurückzukommen, erscheint es sinnvoll, einen Vergleich zu den Kosten für derartige Therapien zu finden. Ein InductOs® Kit kostet ungefähr 3800 €. Das durchschnittliche Jahreseinkommen einer afrikanischen Person liegt bei etwa 550 €. Somit ist es ziemlich unwahrscheinlich, dass die breite Bevölkerung von diesen Entwicklungen profitieren wird. Sicher werden Konstrukte noch sehr viel teurer sein, wenn sie mit Zellen vorkultiviert wurden. Es scheint so, als ob sich selbst unter europäischen oder US amerikanischen Verhältnissen nur ein geringer Teil der Patienten eine solche medizinische Versorgung leisten kann. Demzufolge macht es fast den Anschein, als ob durch Tissue Engineering Möglichkeiten aufkommen, die einer sehr kleinen Gruppe von wohlhabenden Individuen eine beachtliche Lebenszeitverlängerung verschafft. Sicher sind die Kosten gerechtfertigt durch die große Menge an Materialien, Energie und Arbeitsaufwand für Entwicklung und Bereitstellung. Dies erscheint aber etwas fragwürdig in Zeiten, in denen die eingeschränkte Verfügbarkeit von Rohstoffen als Existenzgrundlage sich immer deutlicher abzeichnet. Theoretisch geht dadurch sogar die Lebenszeitverlängerung einer einzigen Person mit dem Entzug der Existenzgrundlage von mehreren anderen Personen einher.

Viele Leute streben nach Karriere, Konsumgütern, Geld und kurzzeitiger Befriedigung. Aber gibt es für dieses Streben einen Endpunkt? Ist die Wahrscheinlichkeit höher, ein solches Ziel durch eine Lebenszeitverlängerung zu erreichen? Nach Ansicht des Autors gibt es keinen Grund für eine künstliche Lebenszeitverlängerung für jemanden, der nach unerreichbaren Zielen strebt, besonders, solange zur gleichen Zeit Kinder verhungern. Dies mag herzlos und kaltblütig klingen, aber vielleicht sollten wir unsere Beziehung zum Tod überdenken. Vielleicht ist das Verhältnis zwischen den einzelnen Individuen in unserer Gesellschaft und der Vorstellung vom Tod verkehrt. In früheren, sogenannten „unzivilisierten“ Gesellschaften, gab es andere Beziehungen zum Ende des Lebens. An sehr vielen Orten auf der Erde haben wir die eingeborene Bevölkerung vertrieben, um letztlich wie eine krebsartige Entität auf unserem Planeten zu werden.

In diesem Zusammenhang scheint das humanitäre Glanzlicht des Tissue Engineering auch einen Schatten auf die Sozialität der Menschheit zu werfen. Im weiteren Sinne könnte ein eugenikartiger Benefit für wohlhabende Leute sogar einen neuen Einfluss auf die Evolution der menschlichen Rasse darstellen.

„Wir stehen an der Schwelle einer globalen Transformation. Alles was wir brauchen, ist die richtige Krise und die Nationen werden die Neue Weltordnung akzeptieren.“

David Rockefeller

„Nicht dem Leben mehr Tage hinzufügen, sondern den Tagen mehr Leben geben.“

Cicely Saunders

SELBSTÄNDIGKEITSERKLÄRUNG

Hiermit erkläre ich, dass ich die Ergebnisse der vorliegenden Dissertationsarbeit

"Development and Characterization of
Nano-Hydroxyapatite - Collagen - Chitosan Scaffolds
for Bone Regeneration"

an der Martin-Luther-Universität Halle-Wittenberg unter Anleitung von Herrn Professor Dr. Karsten Mäder selbständig erarbeitet bzw. im Rahmen der angegebenen Kooperationen erhalten und die Dissertation ohne fremde Hilfe angefertigt habe.

Dazu habe ich keine anderen als die angegebenen Quellen und Hilfsmittel benutzt und die den verwendeten Werken wörtlich oder inhaltlich entnommenen Stellen als solche kenntlich gemacht.

Weiterhin erkläre ich, dass ich mich mit der vorliegenden Arbeit erstmals um die Erlangung eines Doktorgrades bewerbe.

Halle (Saale), April 2010

Hagen Nitzsche